# IMPACTS OF LOW LAND USE ON A TROPICAL MONTANE CLOUD FOREST UNDER A CHANGING COASTAL CLIMATE

by

Isaac Gregorio Torres Díaz

A thesis submitted in partial fulfillment of the requirements for the degree of

MASTER OF SCIENCE
in
MECHANICAL ENGINEERING

UNIVERSITY OF PUERTO RICO
MAYAGÜEZ CAMPUS
2007

Approved by:

| | |
|---|---|
| _____ | _____ |
| Nellore S. Venkataraman, PhD<br>Member, Graduate Committee | Date |
| _____ | _____ |
| Nazario Ramírez, PhD<br>Member, Graduate Committee | Date |
| _____ | _____ |
| R. Vikram Raj Pandya, PhD<br>President, Graduate Committee | Date |
| _____ | _____ |
| Eric Harmsen, PhD<br>Representative of Graduate Studies | Date |
| _____ | _____ |
| Paul Sundaram, PhD<br>Chairperson of the Department | Date |

# ABSTRACT

Tropical Montane Cloud Forests (TMCF) are a primary source of fresh water in tropical locations and are highly sensitive to climate changes. Climatic analysis for El Yunque Rain Forest, a TMCF, located in North Eastern of the Island of Puerto Rico 40km south-east of the coastal city of San Juan, reflects changes in the regional meteorology reflected by increasing surface air temperatures in certain regions within this forest. This TMCF is the main water resource of San Juan, one of the largest cities in the Caribbean, and it is surrounded by increasing urban sprawl in the lower elevations; these changes in the low lands have affected atmospheric and surface variables such as sensible heat flux, surface albedo and surface roughness, and the overall energy budget within the forest. It is also hypothesized that increases in sea surface temperatures are also influencing the climate of the forest. The focus of the present research is to quantify the impacts of changes in land use close to coastal TMCFs, characterized by the case of El Yunque in the north-eastern coast of Puerto Rico during the dry season.

A climatological and numerical analysis is presented to characterize these land use processes under a changing coastal climate. The research makes use of a high resolution visible imagery from the NASA ATLAS sensor to characterize the current land use conditions of the area. Surface parameters such as albedo and land classes were introduced into a Mesoscale Model RAMS (Regional Atmospheric Modeling System). The atmospheric model was

calibrated favorably against a high density network of surface temperature sensors located in and around the TMCF. The coupled and decoupled effects of land use changes and global warming (GW represented by SSTs) are investigated in detail by organizing an ensemble of simulation runs that include reconstructed past land-use, present land use, reconstructed average past atmospheric variables and present climate conditions.

Results indicate significant impacts due to GW effects with increasing SSTs, which are highly reflected on a TMCF environment, generating variations in its sensitive variables such as cloud base, cloud cover, air temperature and precipitation. Contrary, Land use changes generate local affects, which are less pronounced than GW, generating variations in physical variables close to the land. The variables that most influence the TMCF fresh water productivity are the GW effects.

# RESUMEN

Un Bosque Nublado Tropical Montañoso (TMCF), por sus siglas en ingles, es una fuente primaria de agua en zonas tropicales y es altamente sensitivo a los cambios climáticos. El análisis climatológico de El Yunque, un TMCF, localizado al Noreste de la Isla de Puerto Rico, a 40 Km. al Suroeste de la ciudad costera de San Juan, refleja cambios en su meteorología regional, reflejada en el incremento de la temperatura del aire en diversas áreas de este Bosque. Este TMCF es la fuente hídrica más importante de San Juan, una de las ciudades más grandes de El Caribe, y está rodeado por un creciente desparramiento urbano en las zonas de baja elevación; estos cambios en las zonas bajas afectan las variables atmosféricas y superficiales tales como los flux de calor sensible, el albedo superficial, la rugosidad superficial, y el balance total de energía en el bosque. Se establece la hipótesis que el clima del bosque es igualmente afectado por el incremento en la temperatura superficial del océano.

La presente investigación se centra en cuantificar los impactos del cambio en uso de tierras en un TCMF costero, caracterizado por el caso de El Yunque en la costa Noreste de Puerto Rico durante la temporada seca. Se presenta un análisis climatológico y numérico para caracterizar el efecto de uso de terrenos sobre un clima costero cambiante. La investigación hace uso de imágenes visibles de alta resolución del sensor NASA ATLAS para caracterizar

el uso de terreno actual en el área de interés. Algunos parámetros de superficie tales como el albedo y clases de terrenos fueron introducidos in el modelo de Mesoscala de RAMS (Sistema Regional de Modelado Atmosférico). El modelo atmosférico fue calibrado con el apoyo de una red refinada de sensores de temperatura localizados dentro y en los alrededores del TMCF. Los efectos directos e indirectos acoplados del uso de terreno y del Calentamiento Global (CG, representados por temperaturas del océano) son investigados en detalle mediante una organización de simulaciones matemáticas que incluyen la reconstrucción de uso de terrenos en el pasado, el uso de terrenos en el presente, variables atmosféricas reconstruidas y el clima presente. Los resultados indican impactos significativos debido a los efectos de CG con incrementos en temperaturas del oceano, los cuales son reflejados sobre el TMCF, generando variaciones en sus variables sensitivas, tales come Base de Nube, Cubierta de Nube, Temperatura del aire y Lluvia. De otra manera el cambio en uso de terrenos genera efectos locales, los cuales son menores comparados con los producidos por los efectos de CG, generando solo variaciones en las variables cercanas a la superficie del terreno. Consecuentemente, se implica que la variable mas influyente en la productividad de un TMCF son debido principalmente a CG.

*To my wife, for her important*
*support and strength*
*in the development of our*
*life's main objectives.*

*To my family, because they were always*
*with me from a distance.*

*And finally, with no less importance,*
*to **GOD**, helping and being always with us.*

# ACKNOWLEDGEMENTS

I express my sincere thanks to the Mechanical Engineering Department - University of Puerto Rico at Mayaguez and its faculty and staff, special remarks to Dr. Nellore Venkataraman and Dr. Vikram Pandya who play an important role in my Master Degree. It is necessary to add and recognize the support of NASA-EPSCoR Program which sponsored a big part of my research. Additional considerations to Dr. Jorge Gonzalez, who played an important role in the development of this research. Thanks to Dr. Jeff Luvall who provides data from the ATLAS sensors. Thanks to Dr. Eric Harmsen for helpful suggestions to improve the final version of the thesis. Thanks to Dr. Nazario Ramirez and Daniel Comarazamy whom supported the statistical analysis and modeling, respectively. Thanks to Pieter Van der Meer for his continued aid and collaboration, to Luis Lopez for his important technical support in the Climatemaster server. I recognize the National Center for Research Resources (NCRR), Grand Number P20 RR-016470, where the simulations were made conducted.

# Table of Contents

# Table List

**Tables** **Page**

# Figure List

**Figures** **Page**

## ACRONYMS USED IN THIS STUDY

| | |
|---|---|
| AGL | Above Ground Level. |
| APC | Average Past Conditions. |
| ASL | Above the Sea Level. |
| ATMET | Atmospheric, Meteorological, and Environmental Technology. |
| CBL | Convective Boundary Layer. |
| ENSO | El Nino Southern Oscillation. |
| ERSST | Extended Reconstructed Sea Surface Temperature. |
| FAO | Food and Agricultural Organization of the United Nations. |
| GHE | Green House Effect. |
| GHG | Green House Gases. |
| GHT | Geopotential Height. |
| GRADS | Grid Analysis and Display System. |
| GW | Global Warming. |
| IPCC | Intergovernmental Panel of Climate Change. |
| LAI | Leaf Area Index. |
| LEAF | Land Ecosystem-Atmosphere Feedback. |
| LEF | Luquillo Experimental Forest. |
| LULC | Land Use – Land Cover. |
| NCEP | National Centers for environmental Prediction. |
| RAMS | Regional Atmospheric Modeling System. |

| | |
|---|---|
| REVU | RAMS/HYPACT Evaluation and Visualization Utilities. |
| RH | Relative Humidity. |
| RH | Relative Humidity. |
| RT | Reference Time. |
| SJMA | San Juan Metropolitan Area. |
| SJMA | San Juan Metropolitan Area. |
| SST | Sea Surface Temperature. |
| SSTA | Sea Surface Temperature Anomaly. |
| TMCF | Tropical Montane Cloud Forest. |
| UHI | Urban Heat Island. |
| Vfrac | Vegetation Fraction. |
| Zo | Surface Roughness. |

# 1 INTRODUCTION

The atmosphere plays an important role in the energy budget of the world, transporting heat, momentum and mass, i.e. water vapor, gases and different aggregates present inside it. Both, water vapor and Carbon Dioxide ($CO_2$) are the most important Green House Gases (GHG) present in the atmosphere. Their presence increase the absorption and return of long wave radiation back to the earth surface, known as the Green House Effect (GHE).

The Intergovernmental Panel on Climate Change (IPCC) – Four Assessment Report [1], indicate that the "Global concentration of Carbon dioxide, methane and nitrous oxide have increased markedly as a result of human activities", primarily the burning of fossil fuels and to a lesser extent to increases in carbon dioxide related to land-use change. The report asserts that the influence of land-use impact, consequence of surface roughness, albedo and other surface variables, may be lower when compared with the green house gases. However in the tropics, land use may play a larger role in global climate change [2] [3], and in the local climate variables.

Since the atmosphere is a fluid system, the balance of its diverse transport processes is highly influenced by boundary conditions of the system. The bottom boundary is very important in the atmospheric flow balance, because it is in this interface where mass, energy, and momentum are exchanged from and to the atmosphere. In the bottom boundary are immersed

many specific surface variables such as: surface roughness, albedo, emissivity, etc, which are highly related with land-use. Another important property associated with this boundary is Sea Surface Temperature (SST), since the ocean plays an important role in the atmospheric balance, transporting and balancing heat from the low to high latitudes.

A Tropical Montane Cloud Forest (TMCF) is known as an area where the mountains are frequently enveloped by tradewind-derived orographic clouds and mist in combination with convective rainfall [4] [5]. TMCFs are located in many tropical regions including oceanic islands, and can be found in altitudinal ranges as low as 500 meters [1]. Its principal characteristic is the ability to extract water from clouds, collecting humidity directly from the cloud contact, being a main freshwater source of the endemic species and the surrounding communities during the dry period of the year, when the precipitation is diminished.

TMCFs have a great importance in the Tropical regions especially during the dry season. For this reason many of these ecosystems are policy protected by governments, attempting to conserve their natural conditions. However, TMCFs are being stressed by both global warming (GW) and lowland use changes which cause changes in atmospheric conditions, generating lower cloud formation, higher minimum temperatures, increasing accumulated precipitation during the dry periods, which promote the migration of animal species to higher elevations.

The magnitude and/or the individual effects of GW and land use changes on a TMCF are unknown. This research has the main objective of implementing a methodology to separate and quantify the individual effects of GW and land use changes on the atmospheric variables of a TMCF.

For this purpose, El Yunque which is a TMCF located in the northeastern part of Puerto Rico, in the Caribbean Region, has been selected as a reference case. El Yunque appears to have been influenced by both GW and lowland urban development during the past decades. This forest is also a well study site which makes ideal for this type research.

This thesis is organized as follows: A detailed review of past research in the field is presented in Chapter 2, showing previous analyses for GW and land use change influences at three different scales: Synoptic Scale, Regional Scale and Local Scale. The methodology followed during this research to quantify the coupled and decoupled effects is presented in Chapter 3, including a description and analysis for the region and case selected here, which is El Yunque Rain Forest. In Chapter 4 it is presented the characteristic variables used to quantify the variation of the dry season in recent years. It is also presented the analysis of the variables within El Yunque during the time selected for the study, and the quantification and significant change analysis. In Chapter 5 are presented the results of the regional model. The first section of this chapter describes the validation of the simulation selected as the study case under present conditions, the following sections show the results of the separated effects in the mean and extreme atmospheric variables including those that affect the productivity of

the TMCF. Additionally it is included and described the methodology to quantify the Cloud Base Height, which is a variable of great importance in a Cloud Forest. The final chapter includes the conclusions and recommendations from the results and analysis. Additional information used during this research has been included in the appendices.

# 2 LITERATURE REVIEW

## 2.1 Climate Change Indicators

### *2.1.1 Synoptic Influences*

The Intergovernmental Panel of Climate Change (IPCC) [1] has reported that $CO_2$ is the most important anthropogenic GHG, which has elevated concentrations due to fossil fuel use and land-use change. The warming of the atmosphere is evident from increases in global average air temperatures and ocean temperatures, where the Ocean has been absorbing more than 80% of the heat added to the climate system. Additionally, the IPCC in previous reports [7] expressed that from 1850 to 1998 approximate 33% of the total Carbon emitted into the atmosphere as Carbon Dioxide ($CO_2$) was a result of land use change, principally from the forest ecosystems. Between 1980 and 1989 there is an annual average trend of 1.7±0.8 Gt C $yr^{-1}$, and between 1989 and 1998 this trend is reduced to 1.6±0.8 Gt C $yr^{-1}$. Whereas the present trends for emissions from fossil fuel combustion indicate higher values, 5.5±0.5 Gt C $yr^{-1}$ between 1980 and 1989, and and 6.3±0.6 Gt C $yr^{-1}$ between 1989 and 1998. It should also be considered that methane ($CH_4$) and Nitrous Oxide ($N_2O$) are also influenced by the land use change and forestry activities.

On the other hand, Polcher & Laval [8] considered deforested scenario in tropical zones to understand the effect of deforestation on larger areas on the tropical climate, such as Africa and the Amazon Region. They integrated the coupled equations for vegetation models and the general circulation models (GCMs) for one year of simulation, replacing the tropical

forests in the Amazon, Africa and Indonesia with grassland, considering two cases for analysis, namely, (1) partial deforestation and (2) total deforestation. Results showed that in each case, sensible heat flux is increased, as the soil temperature, changed the outgoing long wave radiation.

Several assessments in the analysis of GHGs were developed at the global and synoptic scale, Still et al. [5] compared the simulation effects produced by doubling Carbon Dioxide ($CO_2$) concentration compared with the conditions of the last Glacial Maximum. They observed that the Global Climate Model (GCM) driven by an increasing SST reproduces the observed tropospheric warming between 1970 and 1992. Additionally, it was observed that the specific humidity and air temperature increased with increasing SSTs, associated with the increasing $CO_2$ concentration; but the relation of cloud formation, which depends on the relative humidity (RH) was not proportional. Through the simulation it was concluded that increasing evapotranspiration caused the altitude at which any given absolute humidity surface would occur to rise by approximately 300m.

### *2.1.2 Regional Influences*

The global scale influences of global warming (GW) and land use change can be expected to be different at the regional and lower scales. For this reason several investigations have been conducted to determine the influences of the land use change at the regional scale. Karl et al. [9] used data from the United States Historical Climate Network to analyze the urban bias in

the first eighty years of the twenty century, concluding that it is essential to consider the impact of urbanization on long-term temperature trends.

For this reason the influence of the major coastal cities were analyzed, presenting precipitation and temperature differences with the surrounding areas. Shepherd et al. [10] presented an analysis of the rainfall anomalies in the surroundings of an extensively urbanized major coastal city (Houston). Their results revealed anomalies in the annual and warm season downwind of the urban area, and refer that the possible mechanisms which generated the urban induced precipitation in this area are: a convergence zone created by the Urban Heat Island (UHI) and the sea breeze front, a convergence zone generated by the increased surface roughness in the large urban areas, thermal perturbation of the boundary layer induced by the UHI, which was translated to downstream areas, generating convective clouds. Additionally they mention the possibility that aerosols generated within the urban area may provide nuclei for cloud condensation (i.e. a cloud microphysics influence), which affects the mean state of the convective atmosphere in three primary ways [11]: profiles of the temperature and water vapor mixing ratio are affected by the coupling between convection and surface processes; the sedimentation rate of cloud and precipitation particles influence profiles of condensate mixing ratios inside clouds and residence time of cloud and precipitation particles. Although urbanization may have an important influence on regional precipitation, the IPCC [1] has stated that the UHI has negligible effects on the total global changes.

Similarly, in other major coastal city, San Juan Metropolitan Area (Puerto Rico), increasing urban area (population trends) [12] has resulted in air temperature differences between the urban and rural areas [13], with warmer air temperatures within the urban area. To analyze this phenomena's influence, Velazquez-Lozada et al. [13] configured land use classes of the Regional Atmospheric Modeling System (RAMS) under three different scenarios, one with the present land use and two potential scenarios, one in the past without the presence of the urban areas and only forested zones, and a third configuration in the future with the increasing urban areas based on projected demographic growth by the year 2050. Results show that there is significant increase in the surface sensible heat fluxes and in the low turbulent-kinetic energy over the urbanized area.

From measured data from a high density built-up city (Mexico City) [14], the results indicate that during the dry season daytime there is a greater Bowen ratio (sensible > latent heat fluxes), which generates a reduced convective heating of the atmosphere, and consequently reduced urban mixing layer and magnitude of the urban heat island. Showing that during the Dry season the convective heating is reduced to 38%, consequently reducing the precipitation induced downstream of large urban cities.

### *2.1.3 Tropical Montane Cloud Forests*

Further analysis is centered in TMCFs, since the importance of their role develops during the dry season in most Tropical regions. In the area of Costa Rica, a study was conducted of the cloud field pattern of a Cloud Forest [15], as influenced by deforestation in the surrounding

areas. The analysis was conducted using RAMS in simulations with a time domain of 12 hours and initialized with homogeneous radiosonde data. Results showed that the land use change (from forested to pasture) generated significant impacts than the effect of SST variation on cloud formation, increasing the cloud base height under the deforested and pasture conditions.

Analyzing the same region in Costa Rica, Nair et al. [16] suggested that the cumulus cloud formation over deforested regions is lower compared with the forested areas, during the morning hours. Using regional atmospheric simulations (with an unrealistic flat topography) the cloud base height had greater values in pasture than forest simulations, where the mean difference reached a maximum value around 750 meters. It was suggested that reduced latent heat flux over deforested areas and enhanced sensible heat flux reduced the cloud field on deforested areas, however the cloud top height difference was not significant.

In a related work, Deepak et al [17] showed that the cloud base height increased as a function of the level of deforestation on the upwind (pre mountain) areas in a TMCF in Costa Rica, showing that the air temperatures rise over deforested areas as a consequence of the increase in the surface fluxes (sensible). Increases of air temperature were between 1 – 5 ºC range in deforested regions.

On the other hand, in the eastern area of Puerto Rico, in a closely related work Van der Molen [3] reported on a regional analysis in Puerto Rico using RAMS, in which he replaced

land use in the island with pasture and forest respectively. He concludes that deforested areas generated decreasing cloud base height during the dry season at around 200 meters, as consequence of the lower evaporation and greater sensible heat fluxes in forested areas.

## 2.2 SST influences in the Caribbean Region

The ocean and the Sea Surface Temperature (SST) are variables that influence the Tropical Regions [18], such as the Caribbean Basin, and are important in the energy balance of the atmosphere, absorbing more than 80% of the heat added to the climate system [1].

In the Topical regions, between 30ºS to 30ºN, there is a nonlinear correlation and dependence of rainfall with SST [18]. There is no dependence of rainfall with SST for SSTs between 19 and 26ºC. However, greater values in SST (between 26 and 29ºC) generate rapid increase in rainfall. Further increases in SST values generate drastic reductions in rainfall. This nonlinear dependence of precipitation and SST in the tropics is shown in convective mass with SST increases. “Convective mass is a measure of the mass in the convective boundary layer (CBL) thermodynamically able to participate in deep convection by virtue of its positive Convective Available Potential Energy” [18].

However, the North Atlantic Ocean exhibits a high degree of variability in the time lag [19], which generates difficulties in the stabilization of the correlation analysis, assuming that the lag time is constant from event to event, where there is suggested that the Atlantic regions are remotely influenced by the Pacific Ocean [19].

Recent studies indicate that the SST variability in the Pacific Ocean, related with El Niño Southern Oscillation (ENSO) [20], present a linked correlation with SST variability and convective movements in the Main Developed Region (MDR), which encloses the Caribbean Region, between 10 ºN and 20ºN. Chikamoto & Tanimoto [21] state that the response of the Caribbean SST under the ENSO influence in the Pacific Ocean, represented by the ENSO Index 3, influence climatologically the Caribbean region two months later in the warm events and one month later during the cold events. In the warm events (positive Niño 3 Index), this is reflected in the increasing SST in the Caribbean region, which is related with increasing latent heat flux anomalies (heat added to the Ocean) in this region.

## 2.3 Indicators of Change in Eastern Puerto Rico

Puerto Rico is located in the north-eastern Caribbean, east of the Dominican Republic and west of the Virgin Islands; approximately 1,280 miles (2,000 km) off the coast of Florida, in the contour that limits the Atlantic Ocean and the Caribbean Sea, between 18º - 18.5º N, and 65.30º 67.25º W (around 177 Km long by 56 Km wide) [22]. The island has a large area covered by mountains (Figure 2-1), which have an influential role on the climate in both, mountains and surroundings areas, as is the case of El Yunque Rain Forest (hereafter referred to as El Yunque), also known as Luquillo Experimental Forest (LEF), which is a protected area located in the north-eastern part of the Island with elevations from about 100 m to 1075 m above mean sea level [22]. El Yunque is located in Northeastern Puerto Rico, around 40 Km South-east of San Juan city (Puerto Rico). It has a complex topography with a rapid

elevation to around 1000 meters in less than 15 km. In this mountainous area four ecosystems can be clearly differentiated: [23] Tabonuco Forest (<600m 70% LEF), Colorado Forest (>600m 17% LEF), Elfin Forest (>750m 2% LEF) and Palm Forest (11% LEF) in limited areas of all elevations. El Yunque is a TMCF, and is a freshwater resource of the surrounding urban areas [1], and the biodiversity habitat of the important endemic species in Puerto Rico, such as Coquí.

### *2.3.1 Atmospheric Variations*

The Eastern part of Puerto Rico has a similar monthly accumulated precipitation and mean temperature climatology behavior, as depicted in Figure 2-2, where there is a climatologic time interval in which the monthly accumulated precipitation is continuously less than other months of the year, and the mean temperature is minimum during these months. Climatologically speaking this period is known as the dry season (January to March).

Puerto Rico has conditions of a tropical rainforest climate [25] [23] and a warm and humid subtropical maritime climate [26] with an increasing rainfall with elevation; where the mean air temperature in El Yunque has a lapse rate of 5.58ºC per kilometer increase in elevation [4]. The climate in the Luquillo Mountains (Puerto Rico) is characterized by both local convective storms and mesoscale atmospheric disturbances [27]. Where the principal weather systems affecting the level of the moist layer in Puerto Rico are: 1) easterly waves, 2) polar troughs, 3) shear lines, and 4) tropical storms.

A climate classification in Puerto Rico is presented under different assessments, where the interpolation of measured data between 1963 and 1995 in Puerto Rico [28], with a finer grid resolution of about ~450 meters, shows that in the boundary layer the minimum temperature slope is -3 ºC/km, and in the free atmosphere -4.5 to -5 ºC/km throughout the year. In the same manner based in an Artificial Neural analysis [29], considering thirty years starting at 1960, at 18 stations dispersed around the island (none inside of El Yunque), resulted in climatic characteristics of El Yunque which underestimated precipitation and overestimated mean, maximum and minimum temperatures, with respect to the measured results.

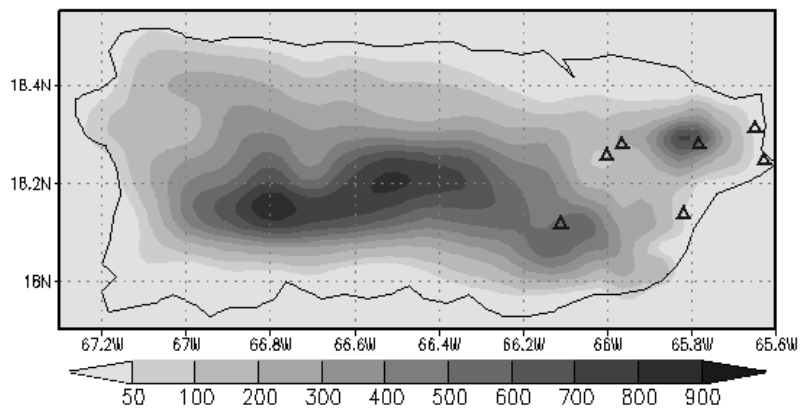


**Figure 2-1 Puerto Rico elevation map (meters). Marks represent location of the stations depicted in Figure 2-2.**

Puerto Rico presents a clear reduction in the accumulated annual precipitation trends in the sparse located stations around the island (including El Yunque), varying between – 0.73 and –4.9 (check this value) mm $yr^{-1}$ [3]. Additionally, in the eastern Puerto Rico, there is air temperature variability in El Yunque, which presents to have certain correlation with the Atlantic SST variability [30]. In this region it is clear the larger temperature difference

between the SJMA and its surrounding rural areas, probably increased by the land use change [30].

Cloud cover is an important variable which is reflected in the productivity of El Yunque, where the probability of cloud cover in El Yunque is lower during the dry season than the wet season, without considering other effects than the topography [31]. Additionally, in El Yunque the probability of cloud cover increases with elevation and is higher during the night hours, and has minimum values during the first hours in the afternoon [31].

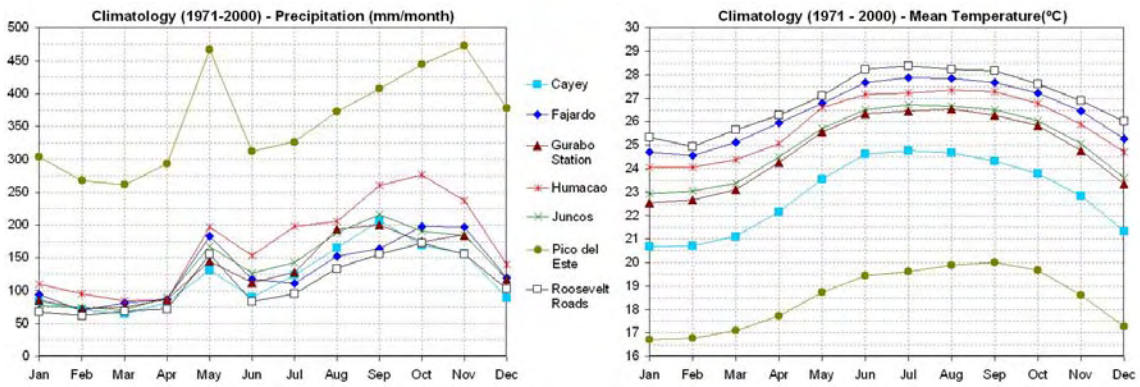


**Figure 2-2 Climatology of Monthly accumulated precipitation in mm/month (left) and Surface temperature (right) Climatology of some stations of Puerto Rico. The location of the stations is shown in Figure 2-1.**

### *2.3.2 Land Use Changes*

There is significant urban development in the surrounding areas to El Yunque. Between 1988 and 1993 [32], in the Luquillo municipality (north-eastern of Puerto Rico), there was a reduction of rural landscape and an increase in urban area, where 5% of the vegetated areas were changed to urbanized areas. Additionally, there was an increased urban development

close to the forested areas, increasing the urban sprawl around El Yunque, rather than in high density residential areas.

The urban development in Puerto Rico is also influenced by the urban sprawl, described as "peripheral growth that expands in the unlimited and non-contiguous way outward from the solid build-up core of a metropolitan area" [33]. Based on the Census data and in the remote sensing imagery information, Martinuzzi et al. [33] concluded that the urban development tendency decreased with increasing slope; opposite behavior occurred in the low-density urban areas, which predominate in the hills and mountains around El Yunque.

Additionally, there is an emerging forest naturally occurring on abandoned land areas previously covered to agriculture, which combined with the native tree species, generates new landscape characteristics of the Island [34]. Birdsey & Weaver [35] showed that in Puerto Rico the forest areas are increasing at a rate of 4000 ha $yr^{-1}$, where the highest percentage of the forest is growing in the abandoned pasture and coffee shade. That is consistent with the study of Del Mar Lopez et al. [36], showing that in 1994 there was an increase in the urban areas of 27.4% with respect to 1977; where 41.6% of urban areas sit on soils suitable for agriculture in Puerto Rico.

In the same manner, the Food and Agricultural Organization of the United Nations (FAO) [12], reported that land use (Figure 2-3) and population (Figure 2-4) long term data for the last 40 years indicate that the agricultural areas are decreasing and urban areas (population

trends) are increasing. Figure 2-3 reflects the clear land use change in Puerto Rico in the last decades.

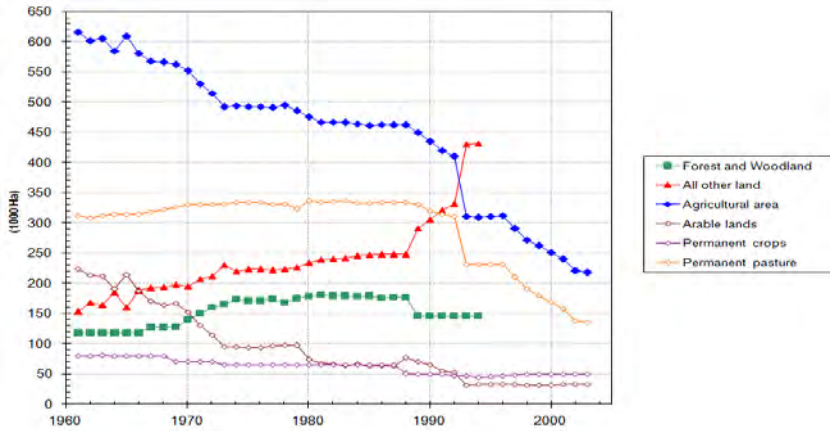


**Figure 2-3: Historical land use in Puerto Rico. Data available in: http://faostat.fao.org.**

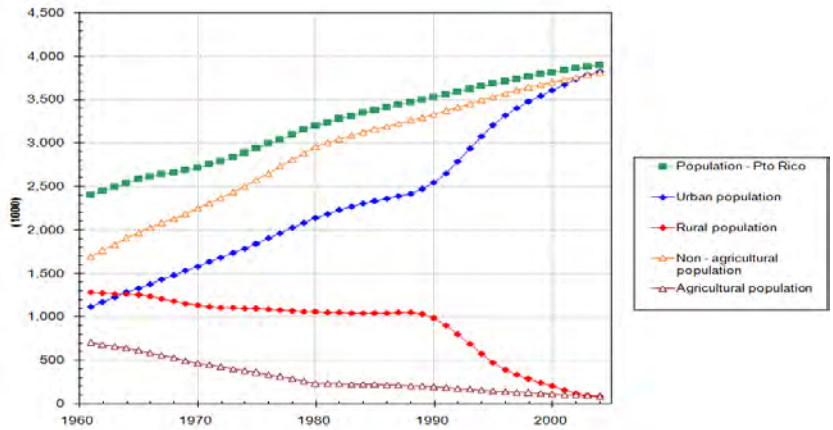


**Figure 2-4: Historical Population in Puerto Rico. Data available in: http://faostat.fao.org.**

## 2.4 Research Justification

As expressed in the literature reviewed above, a Tropical Montane Cloud Forests is stressed from both, global warming and lowland use changes, which may be affecting this sensible ecosystem.

There are some assessments in a greater scale only, as the case presented by Polcher and Laval [8] in the Land use change and by Still et al. [5] in the case of global warming effects. However, on a regional scale, the individual impact of each variable is taken into account only as the effect of the Land use change, in the case of the inland TMCF (Costa Rica), and in the case of Coastal TMCF by Van der Molen [3], with extreme deforested and forested cases, which do not quantify the real tendencies of the Land use trends. But, the quantification of the influence of each variable in the TMCF is unknown. There is no reported clear methodologies which quantify the separated effects and their influence in the coupled or total effects.

Thus, for both variables, global warming and land use changes, there is need to quantify the individual and coupled effects on a regional scale, to understand at a finer resolution the mean effects which influence this sensitive ecosystem.

El Yunque in northeastern Puerto Rico is a Coastal TMCF, which has been stressed by atmospheric warming and by the land use changes, with increasing urbanization areas and new forested areas replacing the past agricultural zones. This region will be analyzed as the case study for this research in which the individual separated effects of land use and global warming will be evaluated.

Global warming has a spatial variation in the global atmosphere, and the land use a local and surface variation. Thus, the hypothesis considered here to analyze a TMCF in the Caribbean Region can be posted as follows: “Global Warming has significant and larger influences than lowland use changes on the total environmental impact produced on a TMCF, inducing increases in air temperatures and accumulated precipitation during the dry season.”

Summarizing these paragraphs, this research will try to answer the following general scientific questions:

1. Is it possible to separate the individual and coupled effects of global warming and Land use changes?
2. Which influencing variables have the most significant effect in a Coastal Tropical Montane Cloud Forest?

## 2.5 Objectives

The specific objectives of this research are:

- Obtain a methodology to separate the effects of land use change and global warming in a TMCF.
- Determine the mean impacts of both land use change and global warming on a TMCF, characterized by El Yunque, during the dry season.
- Quantify the influence of both land use change and global warming, as a coupled effect under a TMCF during the dry season.

# 3 METHODOLOGY AND SELECTED CASE

## 3.1 Methodology

To satisfy the objectives of this research, it is proposed the methodology which is presented in Figure 3-1, Figure 3-2 and Figure 3-3, that show total steps in a flow chart format, divided into three most relevant steps: Time domain selection – present time, selection of the average past conditions, and modeling strategy, which will be explained in the next sections of this chapter.

### *3.1.1 Time domain selection – Present Time*

To select the time for the analysis it is considered the analysis of long and short term data for precipitation and air temperature at different stations sparsely located around El Yunque, a TMCF, during the dry season. The long term data is considered during a time interval of 30 years, to take a better assessment of the trends, and climatic behavior in the area. The short term data provide the case of analysis; where the selected time must be similar to the climatology behavior during the dry season. Additionally, it is included in the analysis the SST at a larger spatial scale (in the order of 100s of Kms) than the scale of the TMCF (in the order of a few Kms), during a long term period. The SSTs are analyzed in the same manner as local parameters (precipitation and temperature), obtaining mean values which represent the dry season period.

If the mean atmospheric conditions are similar to climatic behavior during the dry season, the short time is selected as representative of the dry season climatology, and can be used to analyze its average behavior.

### *3.1.2 Selection of the average Past conditions*

Since the present or actual conditions of dry season conditions are set with the considerations discussed in the previous subsection, the next step is to obtain the past conditions, which will be set to by comparing with actual atmospheric conditions. The external variation that influences the Caribbean region is imposed by the ENSO teleconnection [19] [20], which generates increases in heat flux and anomalies in the humidity content in the Caribbean Region, two months later during the warm seasons and one month later during the cold seasons [21]. Taking this lag into account, the ENSO index 3 will influence the dry season in the Caribbean Basin (January - March) between November and January during the warm events, and between December and February during the cold events. Thus, ENSO Index 3 (external variable) will be averaged during the influencing time (November – January).

Starting at each year, it is necessary to find the number of years required to obtain a mean similar ENSO index 3 as in the present time, during the influencing time of the Caribbean dry season, with an absolute maximum difference of 0.05 to present time conditions. If this condition is satisfied, the “Average Atmospheric Past Conditions” (AAPC), with similar ENSO Index 3 conditions are found.

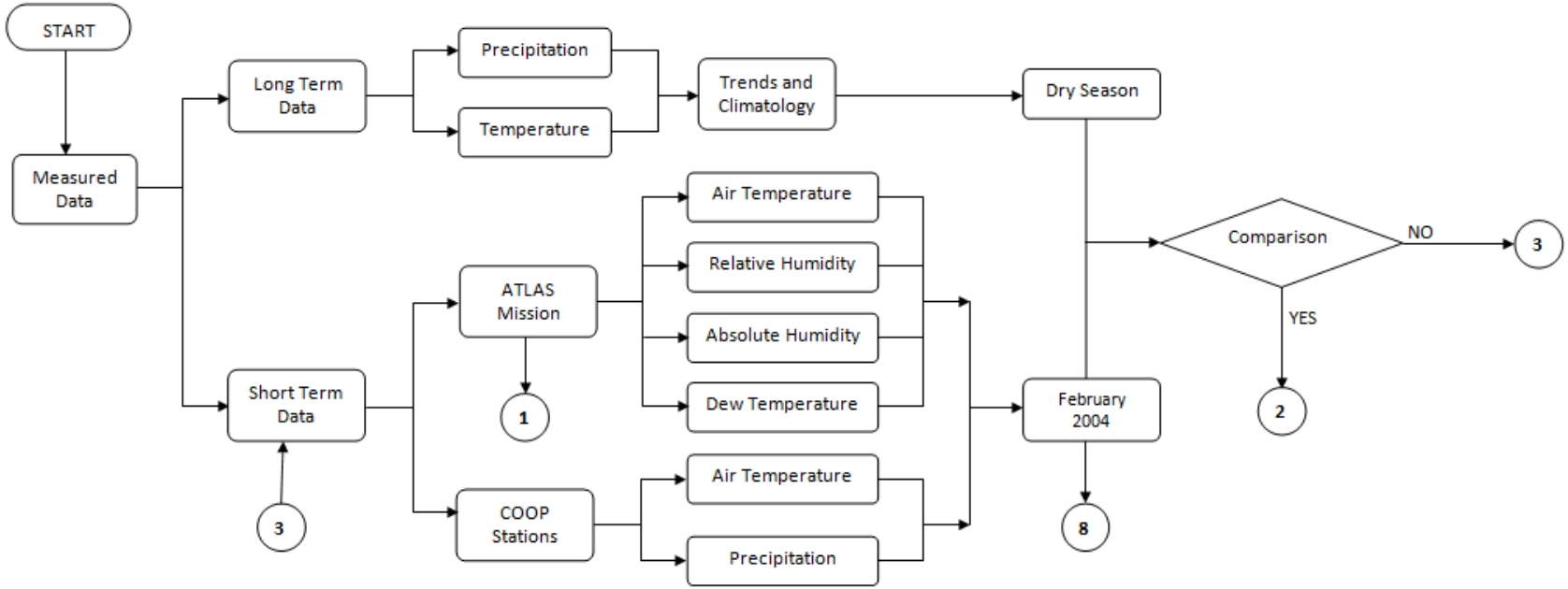


**Figure 3-1: Flow chart showing the methodology for the time domain selection – present time.**

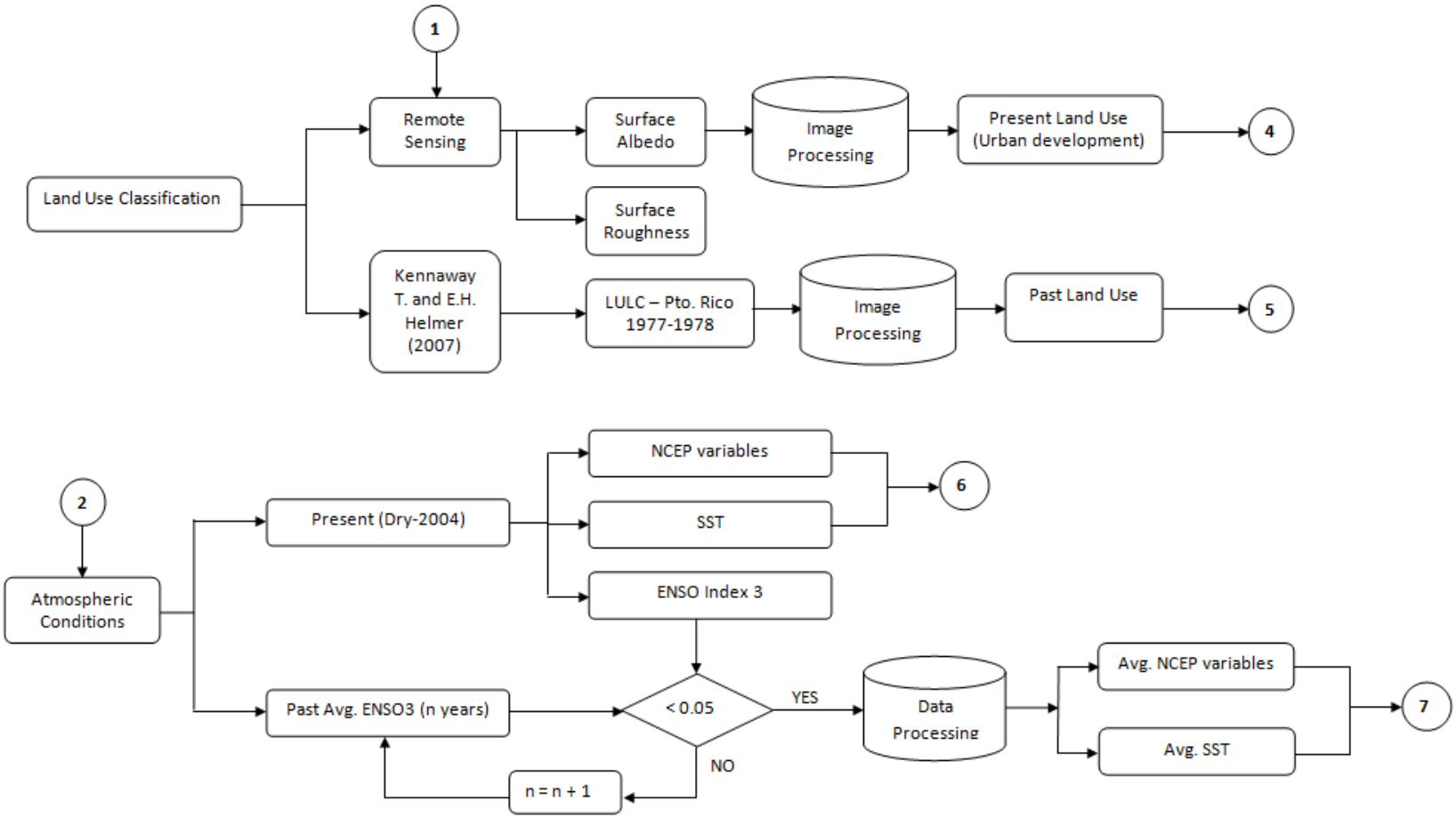


**Figure 3-2: Flow chart showing the methodology to select the average past conditions.**

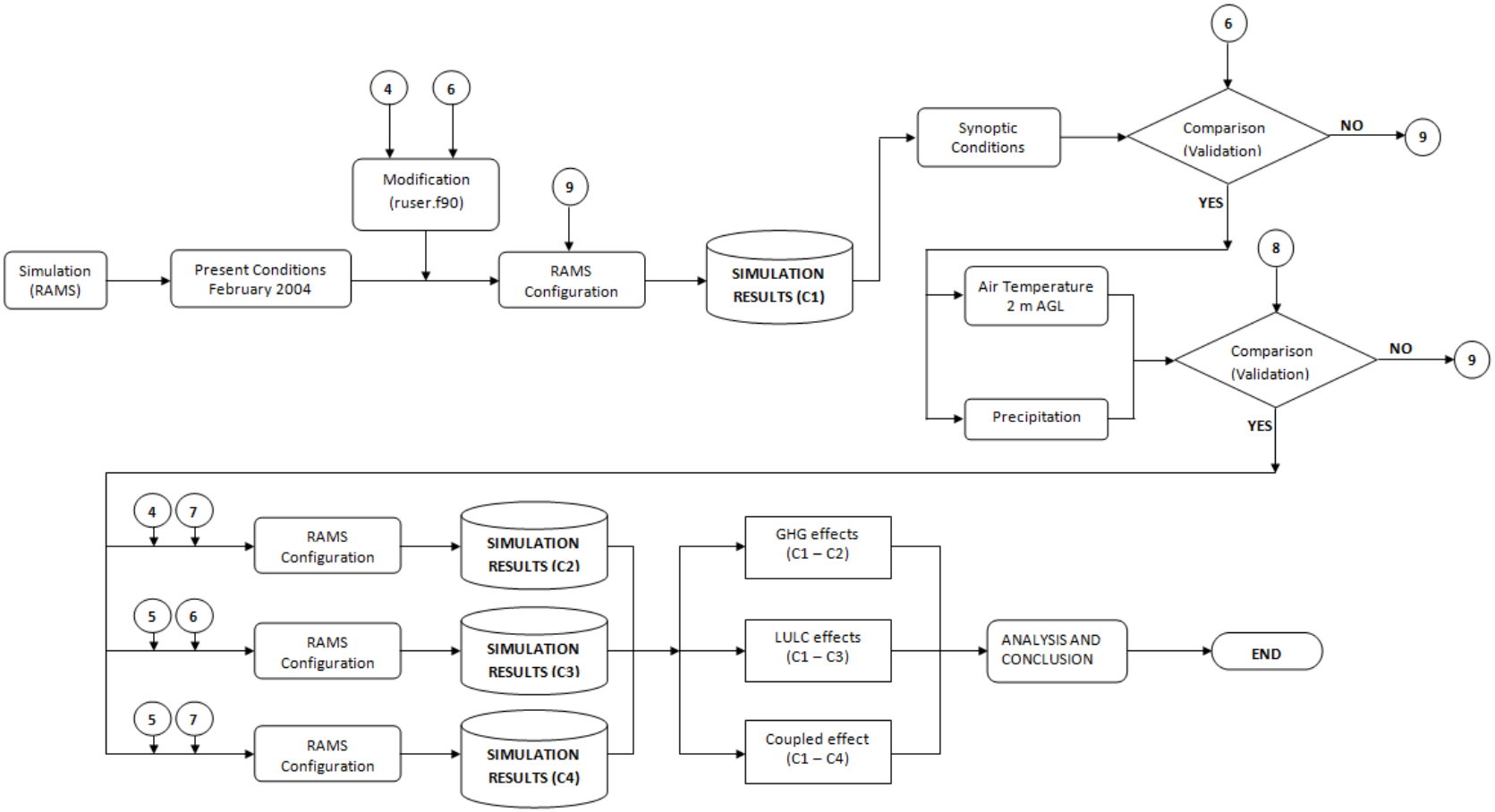


**Figure 3-3: Flow chart showing the methodology in the modeling strategy.**

### *3.1.3 Modeling Strategy*

In the simulations it is considered the variation in the land use classification, under two different scenarios: One at the present conditions, with the present urban areas, and other considering the past land use classification, to compare the impact of the land use change. A similar strategy is followed for the atmospheric conditions (including SST), where present conditions were selected as described in the previous subsection, and average past conditions will be used to quantify the impact at the present time. In summary, there are a total of four different conditions, two for the present conditions and two for the average past conditions (land use classes and atmospheric conditions in each case).

To analyze the land use change effect it is necessary to remove the global warming influence, and in the opposite way, to quantify the global warming effect it is necessary to remove the land use influence on the area. In this way, it is necessary to configure any atmospheric model under four (4) different configurations which provide the present, past and coupled, two by two, land use and global warming effect in the study area. TABLE 3-1 shows these 4 configurations (since there are two influencing variables[1]), where the first one (C1) is used to calibrate the model with the actual conditions, the remaining three configurations are used to obtain the separated effects and the total change by land use change and global warming.

[1] For "n" variables the number of simulations should be ($2^n$)

**TABLE 3-1 Matrix simulations arrangement used to analyze the land use changes and global warming (GW) effects.**

| Index | land use | GW |
|---|---|---|
| C1 | Present | Present |
| C2 | Present | Past |
| C3 | Past | Present |
| C4 | Past | Past |

In order to satisfy the main objectives of the research through the simulations of quantifying the separated effects of global warming and land use changes on a TMCF, the Regional Atmospheric Modeling System (RAMS) is used. RAMS provides is a powerful modeling tools that provides fine spatial and temporal resolutions in a nested grids, capturing the synoptic variability conditions very well; additionally to the great capability to be modified in its subroutines to load input surface and atmospheric parameters.

RAMS is a numerical code that resolves the standard non-hydrostatic Reynolds average equations. These non-hydrostatic equations are: the conservation of momentum (A-1, A-2 and A-3), conservation of heat (A-4), conservation of water (A-5), and mass continuity equation (A-6) [37]. Detailed description of these equations is given in Appendix A.

RAMS presents different capabilities and configuration characteristics for different simulation assessments, such as high resolution cloud scale grids [38], synoptic climate patterns [7], and hemispheric scales; where the nested grid scheme for the analysis at finer resolution phenomena is very important. Additionally, it presents radiation, convection and

other physical features, and model packages such as cloud microphysics and Land Ecosystem-Atmosphere Feedback (LEAF). RAMS can be initialized with different types of spatial and temporal conditions, such as the balloon sounding data or the NCEP reanalysis data. The model provides a high resolution of the vertical axis, a very special capability necessary in the analysis of the planetary boundary layer with complex surface characteristics. Some of the most important RAMS model and physical options are shown in TABLE A-2.

LEAF is a sub-model of RAMS [38], which evaluates the water and energy budget in the atmosphere bottom surface and their interaction with it. LEAF has the ability to represent sub-grid scale (patch) characteristics for the surface parameters, such as vegetation class, soil type, surface roughness, etc. generating a bi-dimensional variability inside each grid. The vegetation classes parameterized in RAMS – LEAF 2 are presented in Table 3-2.

### *3.1.4 Separating the Effects*

To separate the effect of each variable analyzed, the cases shown in TABLE 3-1 are taken into consideration. These simulations will provide results by maintaining any of variables constant (C2 and C3) or varying both variables (C4). For example, to quantify the GW effect is it necessary to maintain the land use change constant in the integration domain. The difference of the first two simulations (C1-C2) will provide the effect produced by GW, without the land use change effect in the area and under similar ENSO index 3 conditions (external influencing variable).

**Table 3-2: LEAF-2 Biophysical parameters by Land use Class number.**

| Albedo | Emissivity | LAI | Vfrac | Zo | LEAF-2 Class | Description |
|---|---|---|---|---|---|---|
| 0.14 | 0.99 | 0.00 | 0.00 | 0.00 | **0** | **Ocean** |
| 0.14 | 0.99 | 0.00 | 0.00 | 0.00 | **1** | **Lakes, rivers, streams (inland water)** |
| 0.40 | 0.82 | 0.00 | 0.00 | 0.01 | **2** | **Ice cap/glacier** |
| 0.10 | 0.97 | 6.00 | 0.80 | 1.00 | **3** | **Evergreen needleleaf tree** |
| 0.10 | 0.95 | 6.00 | 0.80 | 1.00 | **4** | **Deciduous needleleaf tree** |
| 0.20 | 0.95 | 6.00 | 0.80 | 0.80 | **5** | **Deciduous broadleaf tree** |
| 0.15 | 0.95 | 6.00 | 0.90 | 2.00 | **6** | **Evergreen broadleaf tree** |
| 0.26 | 0.96 | 2.00 | 0.80 | 0.02 | **7** | **Short grass** |
| 0.16 | 0.96 | 6.00 | 0.80 | 0.10 | **8** | **Tall grass** |
| 0.30 | 0.86 | 0.00 | 0.00 | 0.05 | **9** | **Desert** |
| 0.25 | 0.96 | 6.00 | 0.10 | 0.10 | **10** | **Semi-desert** |
| 0.20 | 0.95 | 6.00 | 0.60 | 0.04 | **11** | **Tundra** |
| 0.10 | 0.97 | 6.00 | 0.80 | 0.10 | **12** | **Evergreen shrub** |
| 0.20 | 0.97 | 6.00 | 0.80 | 0.10 | **13** | **Deciduous shrub** |
| 0.15 | 0.96 | 6.00 | 0.80 | 0.80 | **14** | **Mixed woodland** |
| 0.20 | 0.95 | 6.00 | 0.85 | 0.06 | **15** | **Crop/mixed farming** |
| 0.18 | 0.95 | 6.00 | 0.80 | 0.06 | **16** | **Irrigated crop** |
| 0.12 | 0.98 | 6.00 | 0.80 | 0.03 | **17** | **Bog or marsh** |
| 0.06 | 0.97 | 6.00 | 0.80 | 0.98 | **18** | **Evergreen needleleaf forest** |
| 0.08 | 0.95 | 6.00 | 0.90 | 2.21 | **19** | **Evergreen broadleaf forest** |
| 0.06 | 0.95 | 6.00 | 0.80 | 0.92 | **20** | **Deciduous needleleaf forest** |
| 0.09 | 0.95 | 6.00 | 0.80 | 0.91 | **21** | **Deciduous broadleaf forest** |
| 0.07 | 0.96 | 6.00 | 0.80 | 0.87 | **22** | **Mixed cover** |
| 0.08 | 0.96 | 5.70 | 0.80 | 0.83 | **23** | **Woodland** |
| 0.18 | 0.96 | 5.00 | 0.80 | 0.51 | **24** | **Wooded grassland** |
| 0.10 | 0.97 | 5.10 | 0.63 | 0.14 | **25** | **Closed shrubland** |
| 0.12 | 0.97 | 6.00 | 0.22 | 0.08 | **26** | **Open shrubland** |
| 0.11 | 0.96 | 2.60 | 0.73 | 0.04 | **27** | **Grassland** |
| 0.10 | 0.95 | 6.00 | 0.84 | 0.11 | **28** | **Cropland** |
| 0.16 | 0.86 | 0.70 | 0.07 | 0.05 | **29** | **Bare ground** |
| 0.15 | 0.90 | 4.80 | 0.74 | 0.80 | **30** | **Urban and built up** |

In the same manner, to quantify the land use change effect in the area the actual atmospheric conditions are maintained constant in the domain; thus the difference (C1-C3) will provide the separated land use change effects under the same atmospheric conditions, i.e. without GW effect.

## 3.2 Selected Case

The focus of the analysis is to quantify the coupled and decoupled effects of GW and LULC change on a TMCF in a maritime location, such as El Yunque, located in northeastern Puerto Rico. February of 2004 is selected as the reference present time for the analysis and the dry season during the same year. The analysis of atmospheric conditions and parameters which characterize this time are presented and described in Chapter 4.

### *3.2.1 Present Atmospheric Conditions*

For the actual atmospheric conditions during the dry season, February 2004 is considered for various reasons but more important because there is a wealth of available measured air data which provide the spatial trends in El Yunque at this time. Additionally, it is available visible and infrared imagery provided by the NASA ATLAS sensor. Thus, this data provide the information necessary to characterize the eastern area of Puerto Rico, i.e. El Yunque and its surroundings.

To characterize the synoptic atmospheric conditions during February 2004 it is considered NCEP Reanalysis data at 17 pressure levels for the following variables: air temperature, geopotential height, relative humidity, horizontal velocity components (data available at: http://nomad3.ncep.noaa.gov/pub/reanalysis-2/). Additionally, SST in the Caribbean Region for this month are taken from the Extended Reconstructed Sea Surface Temperature data [40]

[41], available at: http://www.ncdc.noaa.gov/oa/climate/research/sst/ersstv2.php, which has long term monthly data, starting in January 1854 at a 2 degrees of grid resolution.

### *3.2.2 Average Atmospheric Past Conditions*

To characterize the average past conditions it is necessary to find the following dry season conditions:

1. GHG concentration must be less than the actual conditions.
2. SSTs lower than the present time.
3. Similar actual ENSO conditions.

It is a challenging task to find any specific dry season at any year that meets these criteria. Then, averaging the dry season conditions to specific number of years (calculated) should result in similar actual atmospheric conditions.

Considering that the first condition is easy to satisfy, since $CO_2$ concentration (a GHG) is increasing over time, generating an average global increasing trend of 5.5±0.5 Gt C $yr^{-1}$ between 1950 and 1998, as a consequence of fossil fuel combustion [7], additionally the Global average of Carbon dioxide (available at: http://www.esrl.noaa.gov/gmd/webdata/ccgg/trends/co2_mm_gl.dat) presents an increasing tendency (Figure 3-4), in the same figure is depicted (as reference) data from the station in Mauna Loa – Hawaii (http://www.esrl.noaa.gov/gmd/webdata/ccgg/trends/co2_mm_mlo.dat),

which provide extended data than the global average (Figure 3-4). Thus as depicted in Figure 3-4 at any time, $CO_2$ concentration is a monotonically increasing function during the dry season, then any time interval will produce $CO_2$ concentration lower than the actual conditions, i.e. the first condition is absolutely satisfied at any time.

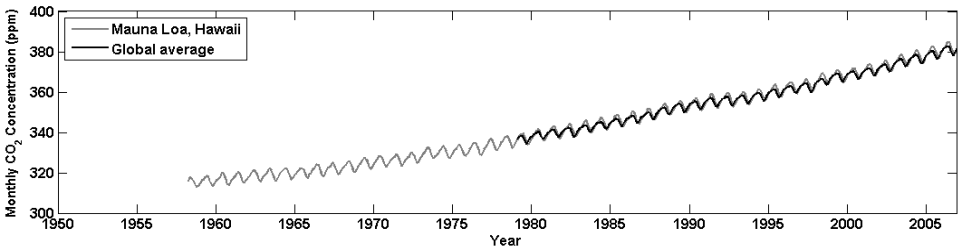


**Figure 3-4 Monthly mean concentration of the atmospheric CO2, Global average and Mauna Loa, Hawaii (Data at: http://www.esrl.noaa.gov/gmd/webdata/ccgg/trends/).**

Monthly SST anomalies (SSTA) are calculated removing mean patterns of the total period in analysis (1950-2006). Averaged grid data between 76º W - 56º W and 10º N - 26º N was obtained of representative monthly and average dry season SST anomaly (Jan. – Mar.) values around Puerto Rico. Now, as it will depicted in Chapter 3, the SSTA during dry season 2004 has one of the largest values since 1950; thus similar increase function to the GHG are presented; any time interval will produce average SST lower than actual time (2nd condition).

The third condition, the monthly ENSO Index 3 anomaly, since 1950 are taken into account, during the mean influencing time under the Caribbean dry season (November – January), considering the fact that it appears two months before [21] in the Pacific Ocean during the complete period of time (ENSO anomalies index data are from **http://wwww.cpc.ncep.noaa.gov/data/indices/sstoi.indices**). As it will be depicted in

Chapter 3, ENSO has a high variability, and does not have the same behavior as GHG and SSTs. Given the fact that ENSO is a variable that influences significantly the atmospheric conditions in the Caribbean during the dry season, it will be the variable selected as reference to meet the established criteria, of the atmospheric average past conditions.

Following these conditions, and under the same ENSO index, the GW and LULC effects in the Caribbean may be quantified. Figure 3-5 shows the number of years required to have similar ENSO index (minus 0.05) as in the dry season of 2004. ENSO Index 1+2 is depicted only as reference to insure that in the past conditions there are similar conditions, but it is only used as reference, since this variable does not influence in the Caribbean region during the dry season.

It can be noted that there are few number of average ENSO which satisfy the condition of similar ENSO index 3 as the present time. However, there are only two average conditions which meet the criteria of similar Index 3, and additionally similar Indexes 1+2, the first one with average of 3 years (starting at 1958), and the second with 8 years (starting at 1976). Since the initial condition takes into account the influence of ENSO Index 3 [21], the average of 8 years starting at 1976 is selected, i.e. the mean dry season (January - March) between 1976 and 1983, is selected as characteristic of past climate. It is noticed that ENSO Index 1+2 for this period does not vary very much from the average of the dry season 2004 (~ 0.1).

Since the present atmospheric conditions during February 2004 is considered as "Reference Time", will be compared with similar past ENSO conditions, i.e. the second month of the average dry season past conditions which will be referred as "Average Past Conditions."

**TABLE 3-3 Comparison between average past ENSO dry season (1976-1983) and the dry season actual conditions. Value of ENSO 1+2 in brackets means the average for 10 years, number of years to satisfy the condition.**

| Dry season | 2004 | 1976 -1983 |
|---|---|---|
| ENSO 3 | 0.4067 | 0.40167 |
| ENSO 1+2 | 0.1700 | 0.27543 (0.18800) |

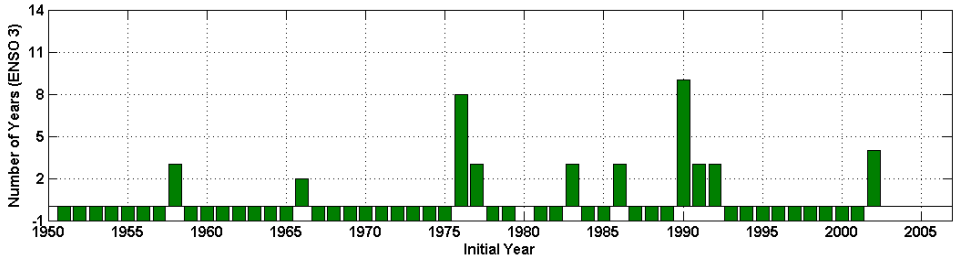


(a)

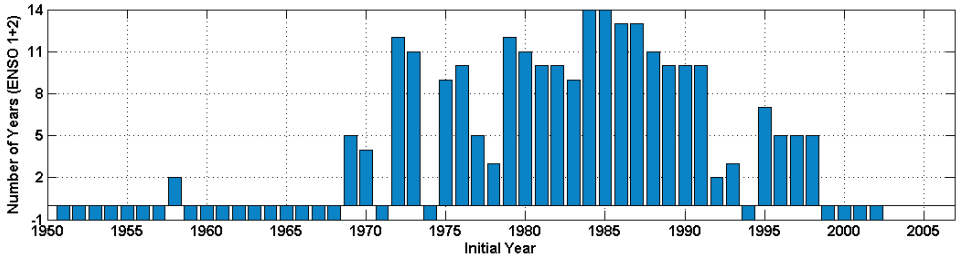


(b)

**Figure 3-5 Number of years (starting at depicted year) necessaries to obtain (with absolute difference less 0.05) similar dry season Condition to 2004, for ENSO (a) 3 and (b) 1+2. (Processed from: http://wwww.cpc.ncep.noaa.gov/data/indices/sstoi.indices).**

## 3.3 Model Configuration - RAMS

The Regional Atmospheric Modeling System (RAMS), is a versatile numerical code developed by Colorado State University and the *ASTER division of Mission Research Corporation, and currently by the company Atmospheric, Meteorological, and Environmental Technology (ATMET). Initially developed in 1983, RAMS since has gained many different characteristics including the Message Passing Interface (MPI) capability [22] [23].

The ensemble configurations C1 to C4 presented in TABLE 3-1, consist of 3 nested grids of integration, with a coarse parent grid of 20 km with an extension of 2000 km x 2000 km enclosing the Caribbean region (Figure 3-6(a)), second grid with 5 km resolution and an extension of 310 km x 310 km, enclosing Puerto Rico island (Figure 3-6(b)), and finer nested grid with 1 km resolution on the eastern part of the island, centered on El Yunque and enclosing its surroundings (Figure 3-6(c)). The model was configured with terrain following high resolution vertical levels, with grid spacing stretched at a constant ratio of 1.1 until 1000 meters maximum, to obtain finer resolution near to the surface, especially above complex topography areas, such as El Yunque. Soil moisture and temperature initial condition profiles were considered uniform in the complete non water domain, since there is no spatial data available to the island. For the soil temperature it was considered as reference the average profile pattern provided by C.B. Briscoe [42] in areas of Cape San Juan, El Yunque and Juncos, where temperature profile includes 4 under and 7 above the ground surface, between -0.25 and 4.0 m.

Models were initialized with atmospheric data at 17 pressure levels, with 2.5º resolution of National Center of Environmental Prediction (NCEP) Reanalysis II [43]. For present atmospheric conditions (C1 and C3) and average past conditions (C2 and C4), input data is considered with 12 hours of time interval. Reynolds Smith Extended Reconstructed SST (ERSST) with 2.5º resolution was used for the model.

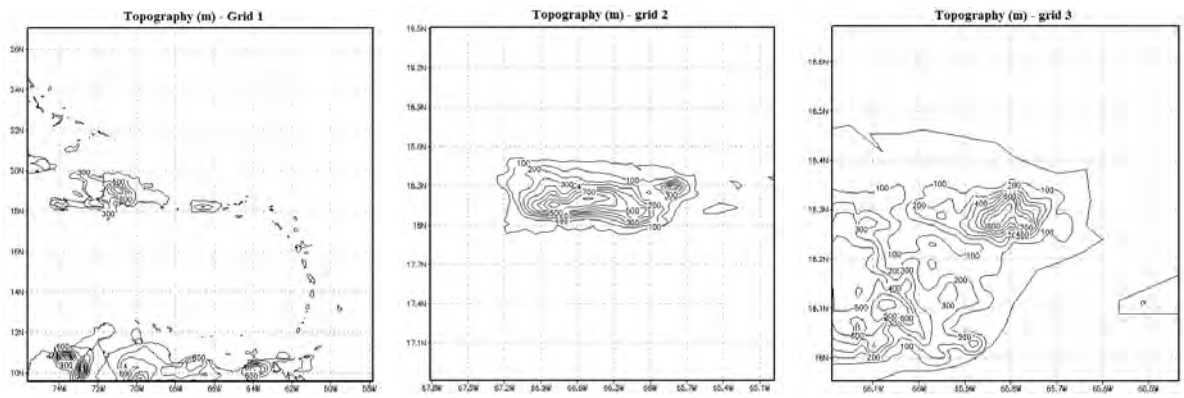


(a) (b) (c)

**Figure 3-6 Topography (m) of three grids configured in RAMS. (a) Parent Grid. (b) Second Grid. (c) Finer Grid.**

Since the objective of this research include quantification of global warming effects, for short and long wave radiation it is considered the scheme of Mahrer and Pielke, which takes into accounts scattering by oxygen, ozone, carbon dioxide and water vapor [37]. For lateral boundary conditions it is considered Klemp and Lilly scheme, which quantifies the phase velocity “c” as an average in vertical direction of Orlanski phase velocity [37]. Since the horizontal grid spacing is larger than vertical grid variation, near to the surface, the model is

configured to resolve turbulent closure by the Mellor and Yamada scheme, which resolve vertical transport with parameterized transport [37]. It was considered total prognostic microphysics scheme, however considering the location in analysis, it will be needed only the warm microphysics scheme.

Each configuration considers a complete month for the simulation time, similar to February 2004, to capture total atmospheric month interaction. The principal flags used to configure the model in the RAMSIN file are presented in Appendix B.

### *3.3.1 Present Land Use Classification*

LULC suffered changes in the last decades in the eastern of Puerto Rico, and this may be a source of local impacts. Thus it is necessary to configure the RAMS model under two Land use classifications (TABLE 3-1), one considering the actual and a second one considering past land use classification.

From the ATLAS sensor imagery was developed a urban density and a finer land use classification for the eastern part of Puerto Rico during February 2004. This was accomplished through modification of FORTRAN 90 standard subroutine (ruser.f90) of RAMS and loading the physical parameters with 4 patches per resolution grid, obtaining a new land use classification for this area that represents the present time. Figure 3-7 depicts

the predominant land use class in the eastern Puerto Rico as of February 2004, which corresponds to the third grid configured in RAMS.

### *3.3.2 Past Land Use Classification*

Past land use classification at the time interval of interest (1976 - 1983), in eastern Puerto Rico is available for the years of 1977-1978 [44] [45] with grass land and agriculture areas around El Yunque and less urban development than the current LULC. Similarly, the past land use for Puerto Rico was loaded into RAMS model by modifying FORTRAN 90 standard subroutine (ruser.f90) to allow reading the land use files for the eastern Puerto Rico from the external source in each configured grid, under 4 patches configured for each grid. Figure 3-8 presents the resulting predominant land use class for the average past conditions, which correspond to the third grid configured in RAMS model.

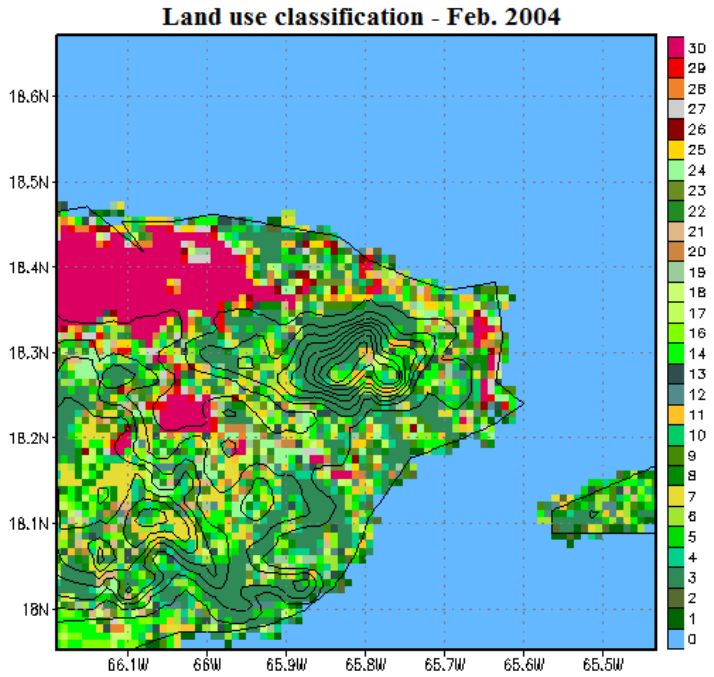


**Figure 3-7 Predominant land use classification in RAMS for the present (2004). Index description and parameterization appear in Table 3-2.**

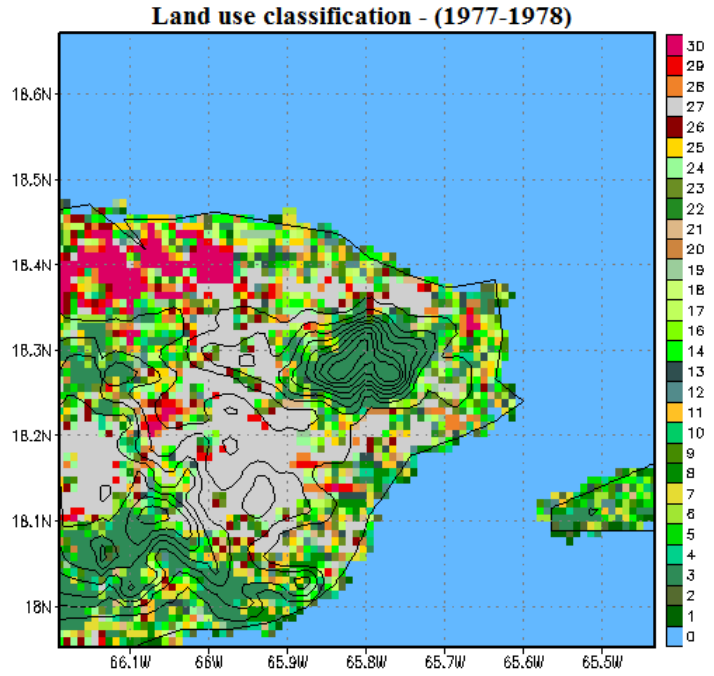


**Figure 3-8 Predominant land use classification in RAMS for the average past conditions (1977-1978). Index description and parameterization appear in Table 3-2.**

# 4 CARIBBEAN DRY SEASON AND EL YUNQUE

Climatology behavior in the eastern Puerto Rico has the same pattern, as shown in Figure 2-2, where the dry season time interval is between January and March, during this time interval there are characteristic variables which affect the climatic behavior in the Caribbean region (and Puerto Rico). In this section presented the long term data analysis of these variables is presented which affect the area of analysis and their corresponding physical behavioral characteristics which will be basis for the analysis in the simulations.

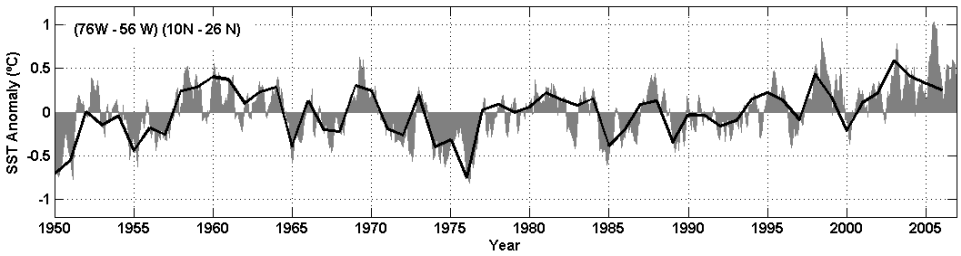


**Figure 4-1 Monthly SST anomaly around Puerto Rico [76ºW - 56ºW and 10ºN - 26ºN], black line represents the mean value for the dry season (Jan - Mar). Data processed from http://www.ncdc.noaa.gov/oa/climate/research/sst/ersstv2.php.**

## 4.1 SST around Puerto Rico

For the analysis of SST in the Caribbean and particularly around Puerto Rico, Extended Reconstructed SST version 2 [40] [41] data was selected. Monthly SSTA and its average dry season (Jan. – Mar.) anomaly values are depicted in Figure 4-1, where it is clearly an increasing trend in during this period (0.0059 ± 4e-06 ºC $yr^{-1}$), which is 95% significant. Time interval around 1960s, have similar anomaly mean values than the present time. Thus,

by removing the years around sixties, SSTA can be considered as monotonically increasing function may be attributed to global warming.

El Niño Southern Oscillation (ENSO) is a factor that affects the Atlantic Ocean and the Caribbean Sea [46], and appears two months later in warm events and one month later in cold events, based on ENSO 3 index [21]. Figure 4-2 and Figure 4-3 show the monthly ENSO 3 and ENSO 1+2 anomalies (http://wwww.cpc.ncep.noaa.gov/data/indices/sstoi.indices), respectively, during the same period of time. Black line represents the mean value for the months between November and January, considering the fact that ENSO appears two months before [21] in the Pacific Ocean during the complete time interval of analysis (1950 – 2006). There is a clear correlation between the ENSO and the Caribbean SSTs during the dry season (Figure 4-4). But, in recent years the SSTs have increased by an external factor, where the presumption is this trend is due to global warming (driven may be by GHG) [5] which has an increasing tendency (Figure 3-4). Thus, the assumption is that global warming effects are reflected in increasing SSTs in the Caribbean.

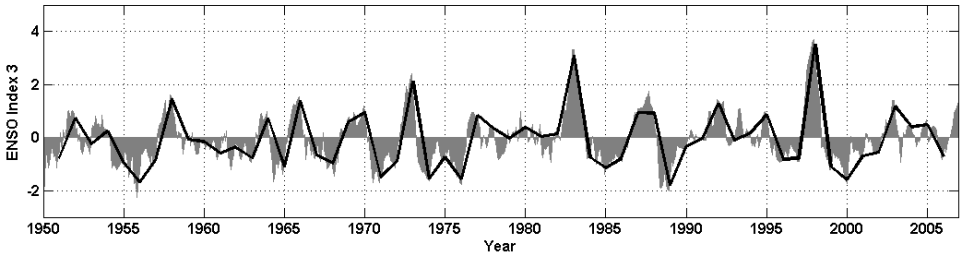


**Figure 4-2 Monthly ENSO anomaly Niño 3, black line represents the mean value between November and January months (time interval which affect the Caribbean Dry**

**season during warm events). Data processed from: http://wwww.cpc.ncep.noaa.gov/data/indices/sstoi.indices.**

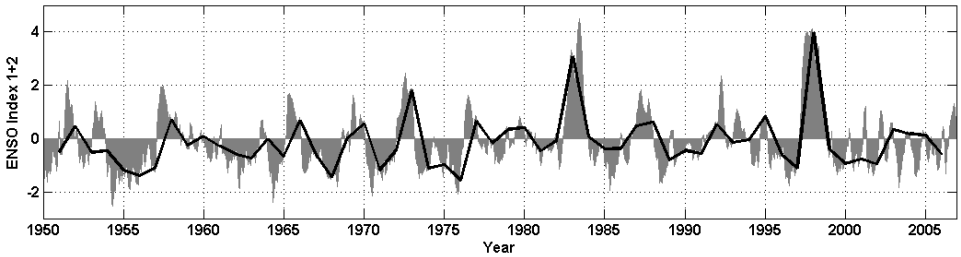


**Figure 4-3 Same as Figure 4-2, for Niño 1+2.**

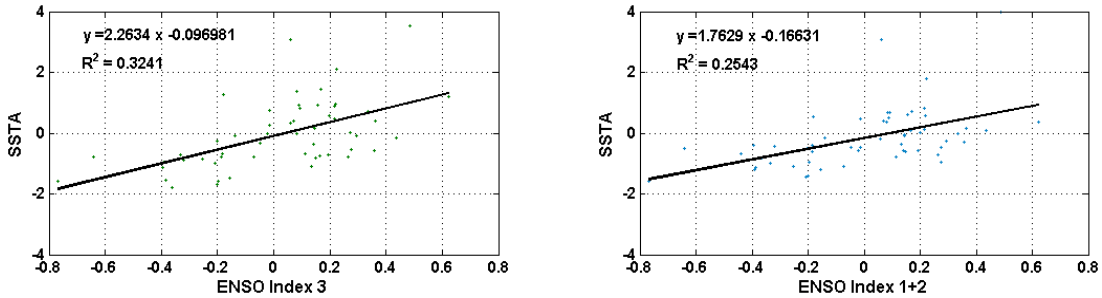


(a) (b)

**Figure 4-4 Scatter diagram for the ENSO vs. SST anomalies, for Niño (a) 3 and (b) 1+2.**

## 4.2 Temperature and Precipitation

A total of eight stations located around El Yunque, which contain precipitation and air temperature data for the last thirty years were analyzed averaging the mean, maximum and minimum air temperature during three months of the dry season; additionally averages were calculated of total accumulated precipitation during the dry season; in this manner the two mean variables which describe the mean conditions of this period for each year were quantified.

Figure 4-5 andFigure **4-6** present the time series of these variables, maximum and minimum air temperature and precipitation, respectively. These stations present no significant trends [47] at each location. However, by averaging all selected stations the average precipitation and temperature trend behavior in the area (eastern Puerto Rico) were obtained; these results presents that minimum temperature trend (0.0466 ±0.0737 ºC $yr^{-1}$) presents a 95% significant change. However,, mean temperature (0.0357 ± 1.3830 ºC $yr^{-1}$), maximum temperature (0.0378 ± 1.9480 ºC $yr^{-1}$) and average precipitation (0.2458 ± 1154.9 mm $yr^{-1}$) do not present a significant change.

However, during the dry season in Puerto Rico, there is variability in average maximum and minimum temperatures trends in the surrounding areas of El Yunque (Figure 4-5). In Pico del Este there is a decreasing tendency in the maximum temperatures and an increasing tendency in the minimum temperatures, i.e. most uniform temperature conditions at this location. In El Verde there is an increasing tendency of maximum temperatures. Figure 4-6 shows the dry season accumulated precipitation with an increasing tendency in El Yunque and a decreasing tendency in the eastern area.

Thus, around El Yunque there is an increasing tendency in precipitation during the dry season, but there is an asymmetric tendency of the temperature trends in the northern and southern areas, where the El Verde area (north) presents increasing tendencies and in the south the opposite tendencies.

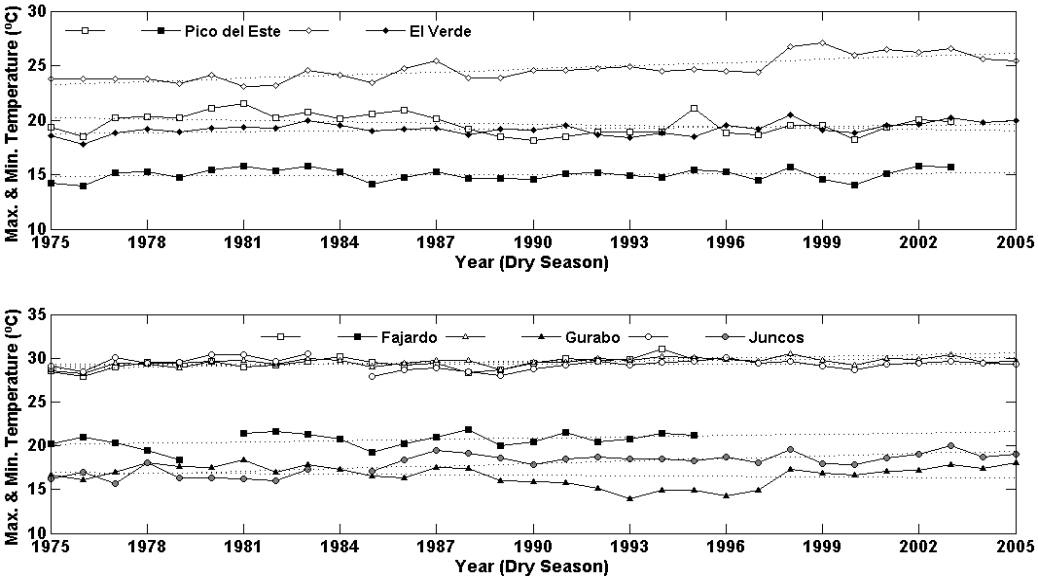


**Figure 4-5 Mean maximum and minimum temperature (ºC) around El Yunque during dry season (Jan - Mar).**

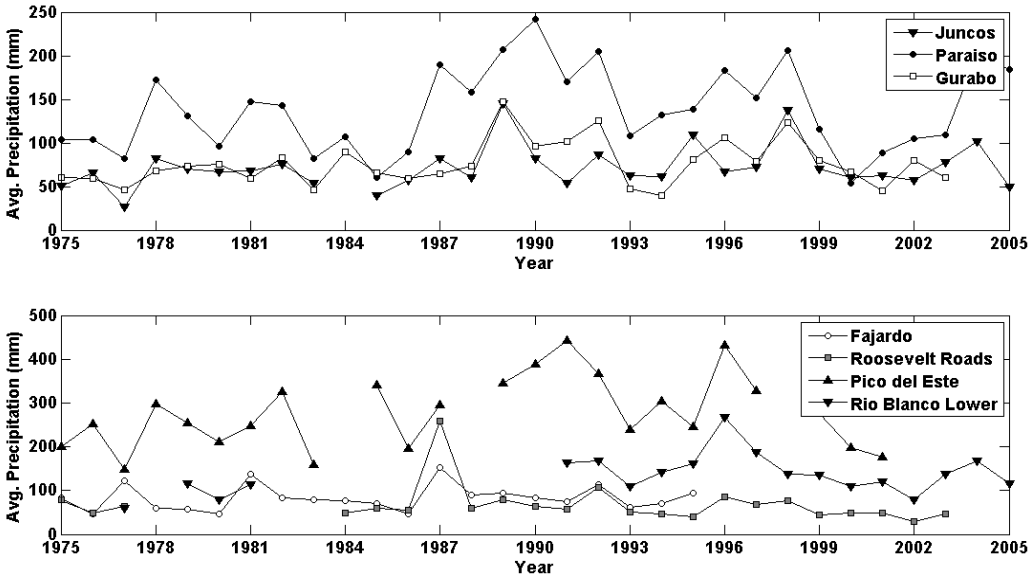


**Figure 4-6 Total accumulated precipitation (mm) during dry season.**

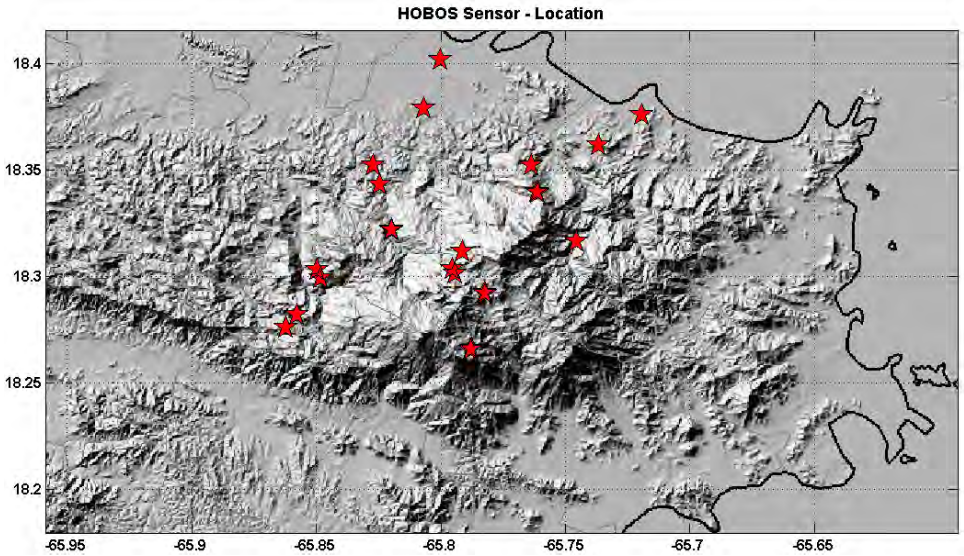


**Figure 4-7 Location of the HOBOS sensors data logger during ATLAS mission campaign.**

## 4.3 ATLAS Mission Campaign

The Atlas Mission Campaign was conducted between 11 and 16 February of 2004 and consisted of an onboard remote sensor of 15 multi spectral radiation channels between the thermal, infrared and visual bands [47]. Part of this mission covered the areas of El Yunque and SJMA (Figure 4-10), with a resolution of 10 meters. Additionally, around this month, a measured air field campaign around El Yunque, in the direction of the easterly tradewinds took place to obtain data profiles of the following variables: air temperature, dew temperature, relative humidity and absolute humidity. A total of 45 HOBOS sensors were placed around El Yunque, filtering the total common time interval of February 2004, with 5 minutes time step, the number of HOBOS sensors analyzed was reduced to 24 stations around El Yunque. The locations of these stations is summarized in TABLE 4-1 and depicted in Figure 4-7.

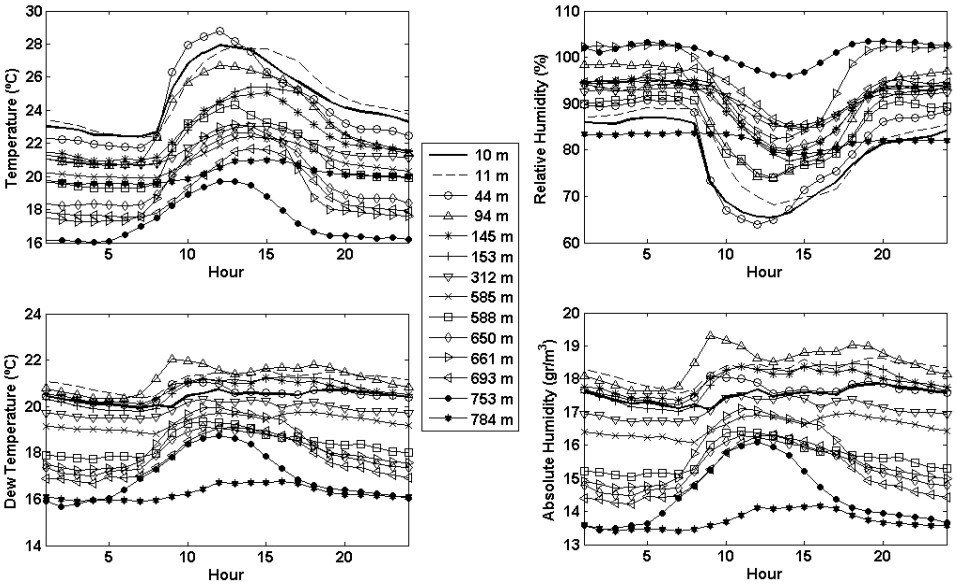


**Figure 4-8 Hourly average of the variables measured by HOBOS during February 2004 - ATLAS mission campaign.**

The mean hourly profile for the complete month in the analysis was obtained, and shown in Figure 4-8. In this figure it was remarked the HOBOS at extreme elevations (minimums and maximum) in El Yunque. It is visible that in the highest elevation the temperature along with the other variables present an anomaly, departing from its behavior as function of elevation.

Since there are a high number of stations in the analysis for each of the 4 measured variables, as depicted in Figure 4-7 and Figure **4-8**, a field (three dimensional) interpolation was performed, with a grid enclosing the El Yunque mountain area, i.e. measured stations with an extension of 15 km by 20 km and 1 km resolution (Figure 4-9).

**TABLE 4-1 Geographic Coordinates of the HOBOS sensor during the ATLAS mission campaign.**

| | | | Geographic | | Date | |
|---|---|---|---|---|---|---|
| | Sensor | Location | Longitude | Latitude | Up | Down |
| 1 | 274253 | 191 Landslide RB2 shade | -65.78782 | 18.26572 | 1/8/04 | 2/16/04 |
| 2 | 471786 | 191 Landslide RB2 sun | -65.78772 | 18.26578 | 2/16/04 | 3/13/04 |
| 3 | 258109 | Bisley Tower 12m | -65.74534 | 18.31635 | 1/8/04 | 3/3/04 |
| 4 | 262316 | Bisley Tower 18m | -65.74534 | 18.31635 | 1/8/04 | 3/3/04 |
| 5 | 262319 | Bisley Tower top | -65.74534 | 18.31635 | 1/8/04 | 3/3/04 |
| 6 | 262386 | Bisley Tower 2m | -65.74534 | 18.31635 | 1/8/04 | 3/3/04 |
| 7 | 274250 | Bisley Tower 6m | -65.74534 | 18.31635 | 1/8/04 | 3/3/04 |
| 8 | 258104 | Catalina shade | -65.76085 | 18.33933 | 1/8/04 | 3/3/04 |
| 9 | 262474 | Catalina sun | -65.76132 | 18.33952 | 1/8/04 | 3/13/04 |
| 10 | 274265 | Coco Beach shade | -65.80012 | 18.40197 | 1/8/04 | 3/13/04 |
| 11 | 274251 | Coco Beach sun | -65.80682 | 18.37890 | 1/8/04 | 2/16/04 |
| 12 | 249808 | Cubuy east house shade | -65.84819 | 18.29914 | 1/8/04 | 3/3/04 |
| 13 | 258108 | Cubuy east house sun | -65.84819 | 18.29914 | 1/8/04 | 3/13/04 |
| 14 | 262452 | Cubuy west shade | -65.86228 | 18.27586 | 1/8/04 | 3/3/04 |
| 15 | 485475 | Cubuy west sun | -65.86228 | 18.27586 | 1/8/04 | 3/3/04 |
| 16 | 249801 | El Verde field station porch | -65.81974 | 18.32220 | 1/8/04 | 2/16/04 |
| 17 | 485442 | El Verde Sonodora Bridge sun | ----- | ----- | 1/8/04 | 2/16/04 |
| 18 | 262318 | El Verde Tower 12m | -65.81992 | 18.32175 | 1/8/04 | 3/3/04 |
| 19 | 274252 | El Verde Tower 18m | -65.81992 | 18.32175 | 1/8/04 | 2/16/04 |
| 20 | 262475 | El Verde Tower top | -65.81992 | 18.32175 | 1/8/04 | 3/3/04 |
| 21 | 274262 | El Verde Tower 2m | -65.81992 | 18.32175 | 1/8/04 | 3/3/04 |
| 22 | 258106 | El Verde Tower 6m | -65.81992 | 18.32175 | 1/8/04 | 3/3/04 |
| 23 | 262388 | El Verde trail shade | ----- | ----- | 1/8/04 | 2/16/04 |
| 24 | 262460 | El Verde trail shade | ----- | ----- | 1/8/04 | 3/3/04 |
| 25 | 262477 | El Verde trail shade | ----- | ----- | 1/8/04 | 3/13/04 |
| 26 | 262815 | El Verde trail shade | ----- | ----- | 1/8/04 | 3/3/04 |
| 27 | 258116 | Hwy 956 forest | -65.84958 | 18.30288 | 1/8/04 | 3/3/04 |
| 28 | 274268 | Las Vegas shade | -65.76365 | 18.35221 | 1/8/04 | 3/6/04 |
| 29 | 262453 | Las Vegas sun | -65.76365 | 18.35221 | 1/8/04 | 3/13/04 |
| 30 | 274261 | Mata de Platano shade | -65.73680 | 18.36159 | 1/8/04 | 3/3/04 |
| 31 | 485444 | Mata de Platano sun | -65.73680 | 18.36159 | 1/8/04 | 3/3/04 |
| 32 | 258111 | Luquillo urban partial shade | -65.71928 | 18.37570 | 1/8/04 | 3/3/04 |
| 33 | 262534 | Monte Britton trail shade | -65.79441 | 18.30122 | 1/8/04 | 2/16/04 |
| 34 | 274257 | Pico del Este shade | -65.78225 | 18.29204 | 1/8/04 | 3/13/04 |
| 35 | 258114 | Pico del Este sun | -65.78257 | 18.29224 | 1/8/04 | 3/3/04 |
| 36 | 262317 | Pico del Yunque shade | -65.79129 | 18.31159 | 1/8/04 | 2/16/04 |
| 37 | 274248 | Pico del Yunque sun | -65.79129 | 18.31159 | 1/8/04 | 3/3/04 |
| 38 | 262461 | Rio Grande - Bella Vista shade | -65.82725 | 18.35211 | 1/8/04 | 3/3/04 |
| 39 | 258107 | Rio Grande - Bella Vista sun | -65.82725 | 18.35211 | 1/8/04 | 3/13/04 |
| 40 | 258112 | Road to Pico del Yunque shade | -65.79531 | 18.30342 | 1/8/04 | 2/16/04 |
| 41 | 258117 | Southern Guaynabo shade | -66.12517 | 18.32546 | 1/8/04 | 3/13/04 |
| 42 | 258113 | Stream house shade | -65.82460 | 18.34292 | 1/8/04 | 3/13/04 |
| 43 | 258105 | Stream house sun | -65.82460 | 18.34292 | 1/8/04 | 3/3/04 |
| 44 | 262384 | Tradewinds Trail shade | -65.85772 | 18.28205 | 1/8/04 | 3/3/04 |
| 45 | 262385 | Tradewinds Trail sun | -65.85772 | 18.28205 | 2/16/04 | 3/3/04 |

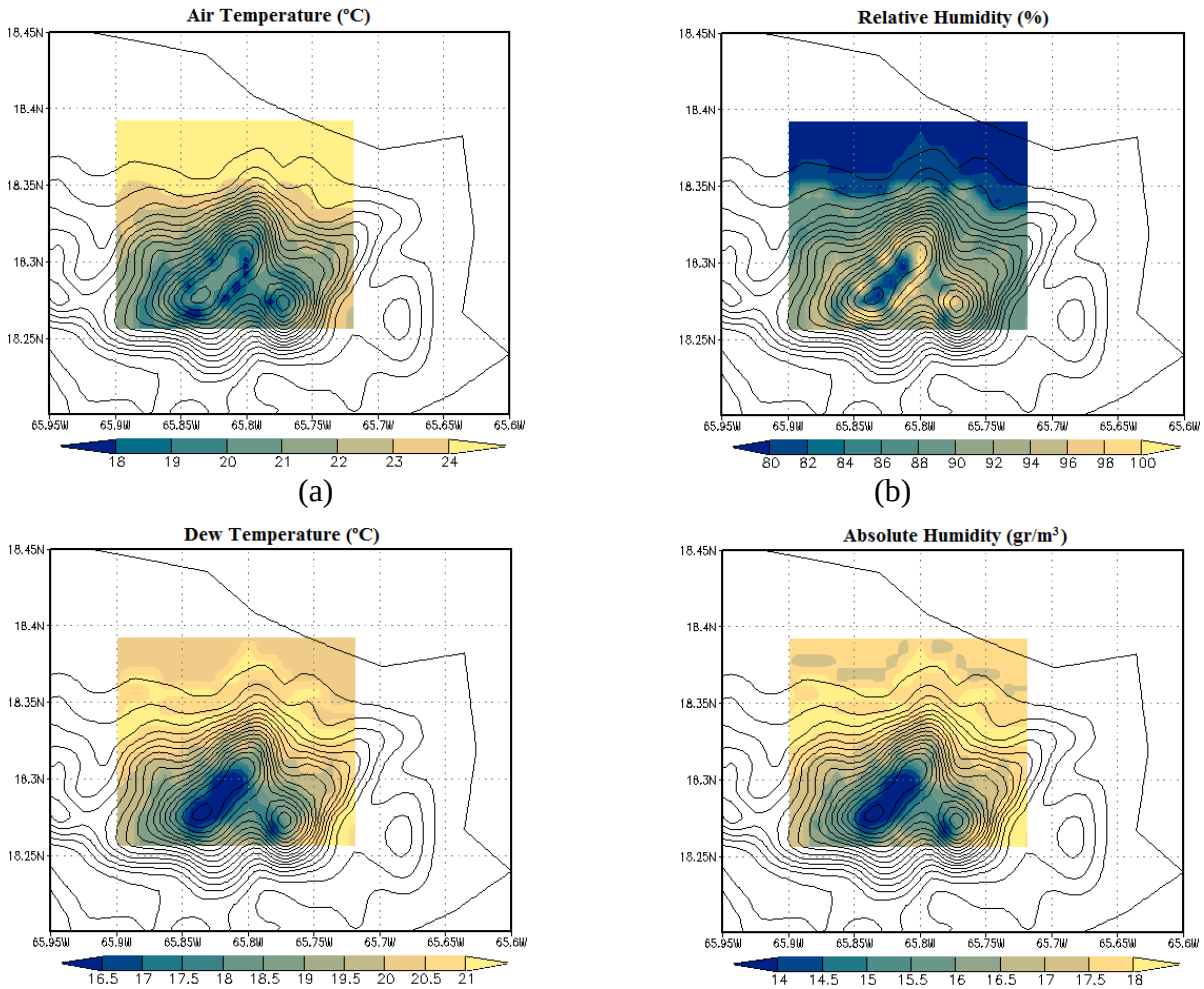


**Figure 4-9 Mean February 2004 HOBOS sensors data field interpolation around El Yunque. (a) temperature (ºC); (b) relative humidity (%); (c) dew temperature (ºC); (d) absolute humidity (g/m$^3$).**

It was noticed that absolute humidity and dew temperature had the same behavior, with maximum values on the lowlands, and decreasing to minimum values on the peaks. Additionally, as it was mentioned in the analysis of Figure 4-8, the plots show that the mean temperatures in the area do not have a complete linear profile in the domain [4], decreasing temperature with elevation, since there are some areas in which the minimum mean

temperatures are not at the mountain peaks. Similar behavior is presented in the relative humidity profile as a consequence of the temperature variation in the peaks resulting in the maximum value of relative humidity (RH) surrounding peaks with a diminished RH at the maximum altitudes.

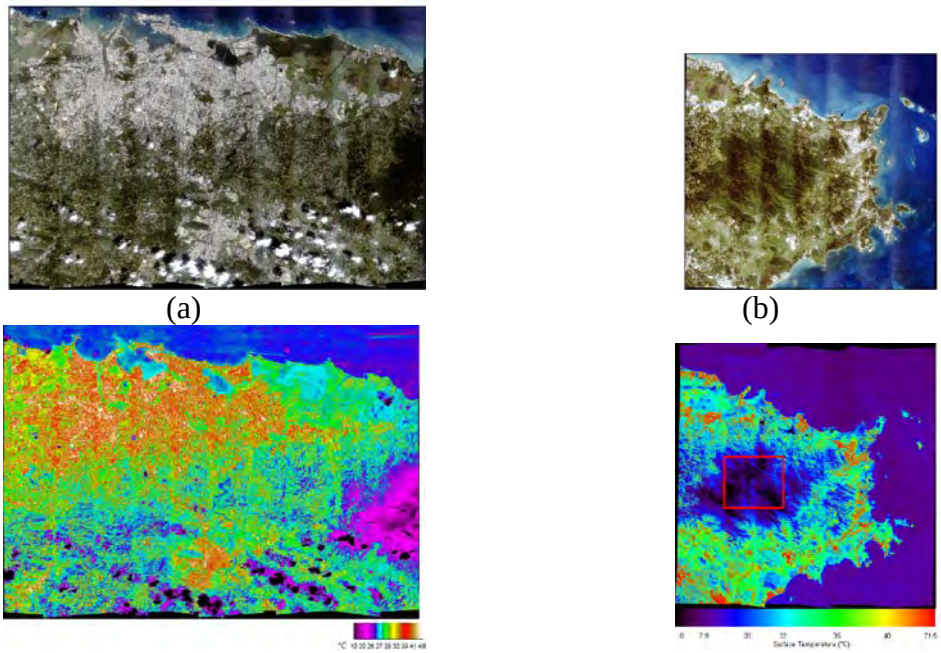

(a) (b)

(c) (d)

**Figure 4-10 ATLAS visual and thermal imagery for the SJMA (a), (c) and El Yunque (b), (d) respectively, during February 2004.**

## 4.4 Urban Development - Land Use 2004

From the Atlas imagery at 10 meters of resolution (Figure 4-10), the urban density with 1 km resolution in the eastern part of Puerto Rico (Figure 4-11) was obtained. Two images were matched and composed to obtain a detailed visual pattern of north eastern Puerto Rico; from which the urban areas were extracted. Further processing was performed using a Matlab

program, to obtain the urban density in each km$^2$ (Figure 4-11), in which the image was fractioned in a bi-dimensional array, where each element has the number of pixels corresponding to 1 km$^2$; the fraction between the number of urban pixels and the total number of pixels in the element results in the urban density.

Urban density (Figure 4-11) in the eastern Puerto Rico presents similar visual patterns of other research projects [33], with a large concentration in the SJMA, but with no uniform pattern, in which areas appear without the presence of urbanization, such as inland water or parks areas. The SJMA in the north-eastern of Puerto Rico appears as an urban core, from where the urbanization density decreases as distance from the center is increasing. But, there is no unique urbanization center in this area, where the area of Caguas (south) appears with highly density, however with smaller horizontal spread. Additionally, there is an increasing urban area, which appears with lower density compared with SJMA or Caguas, known as Urban Sprawl [33], but covering great part of the north-eastern area, surrounding and enclosing El Yunque, where the most notorious is Fajardo (eastern corner).

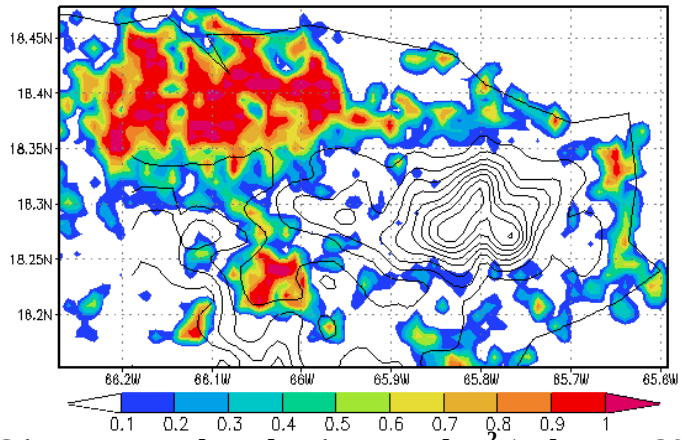


**Figure 4-11 ATLAS imagery - Urban density per 1 km$^2$ (February 2004).**

## 4.5 Caribbean Synoptic Conditions - February 2004

### *4.5.1 ENSO conditions*

As shown in Figure 4-2 and Figure 4-3, average ENSO index is positive during the time of influence on the Caribbean dry season of 2004 (November 2003 - January 2004); the values are summarized in TABLE 4-2. Then, during dry season of 2004, the conditions of ENSO warm event (not an extreme warm event) are presented, so there are positive SST and humidity anomalies in the Caribbean Sea [21].

**TABLE 4-2 ENSO average conditions between November 2003 - January 2004. Data processed from http://wwww.cpc.ncep.noaa.gov/data/indices/sstoi.indices.**

| Average ENSO Index | |
|---|---|
| ENSO 1+2 | 0.1700 |
| ENSO 3 | 0.4067 |

### *4.5.2 Sea Surface Temperature (SST)*

As depicted in Figure 4-12, the SSTs present a variability of 2.5 ºC in the Caribbean, with highest values in the Caribbean Sea reaching the 27.5 ºC. These characteristics in SST lead to positive SSTA in this region during the dry season of 2004, as depicted in Figure 4-1 and summarized in TABLE 4-3, reflecting warming conditions in the Caribbean in recent years, departing off the ENSO influencing behavior.

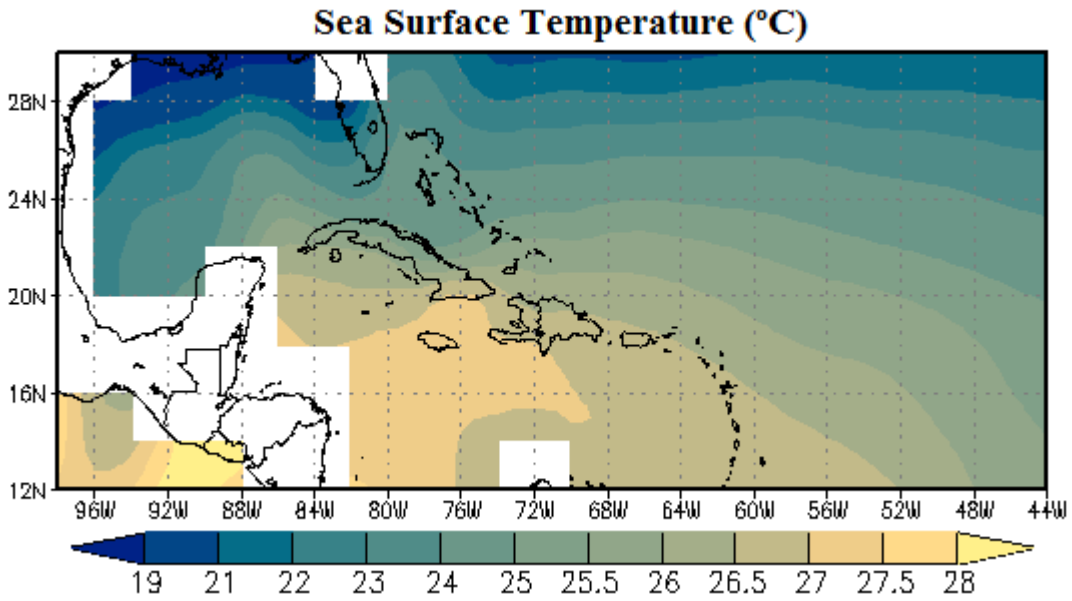


**Figure 4-12 Average Sea Surface Temperature (ºC) during February 2004. Data processed from http://www.ncdc.noaa.gov/oa/climate/research/sst/ersstv2.php.**

**TABLE 4-3 SSTA in the Caribbean Region, around Puerto Rico, during February and dry season 2004. Data processed from http://www.ncdc.noaa.gov/oa/climate/research/sst/ersstv2.php.**

| SSTA around Puerto Rico | |
|---|---|
| February 2004 | 0.46904 |
| Dry season 2004 | 0.39973 |

### *4.5.3 Atmospheric Conditions in El Yunque – February 2004*

To analyze the atmospheric conditions in the eastern Puerto Rico during February of 2004 it is considered air temperature and daily accumulated precipitation, in sparse locations around and inside El Yunque. Additionally, it was considered data obtained from HOBOS stations

(relative humidity, absolute humidity, temperature and dew temperature), during the ATLAS mission campaign.

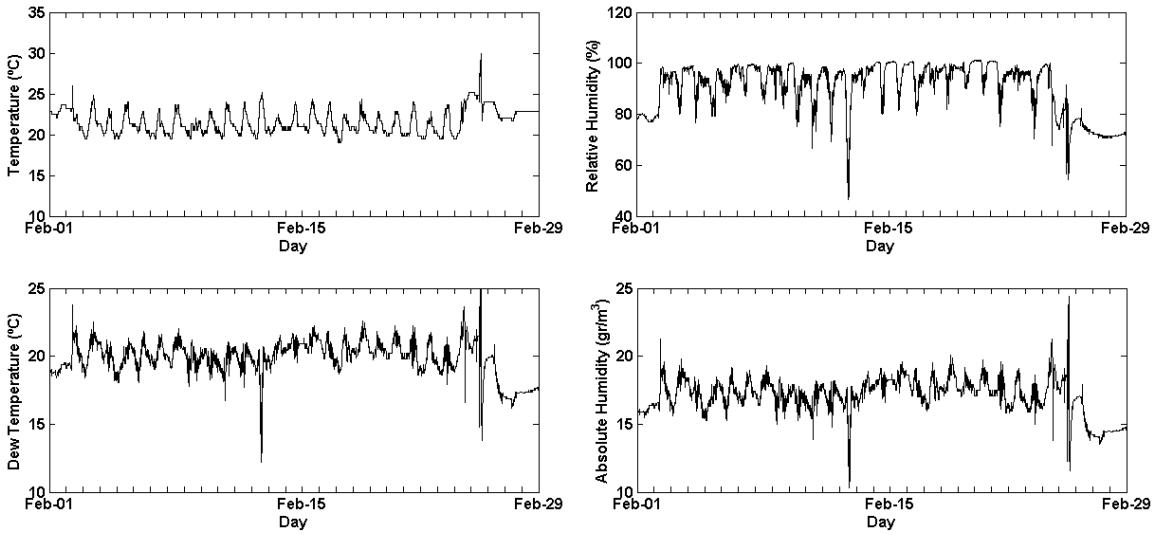


**Figure 4-13 Five minutes time HOBOS data in Bisley tower 2m - measured during the Atlas mission campaign.**

Measured data during ATLAS mission campaign for three selected stations: Bisley, El Verde and Pico del Este are presented in Figure 4-13 through Figure **4-15**, additionally in the same location, there is available accumulated daily precipitation data (Figure 4-16). Both set of data provide a detailed physical description about what is happening along this month, selected as reference time of analysis.

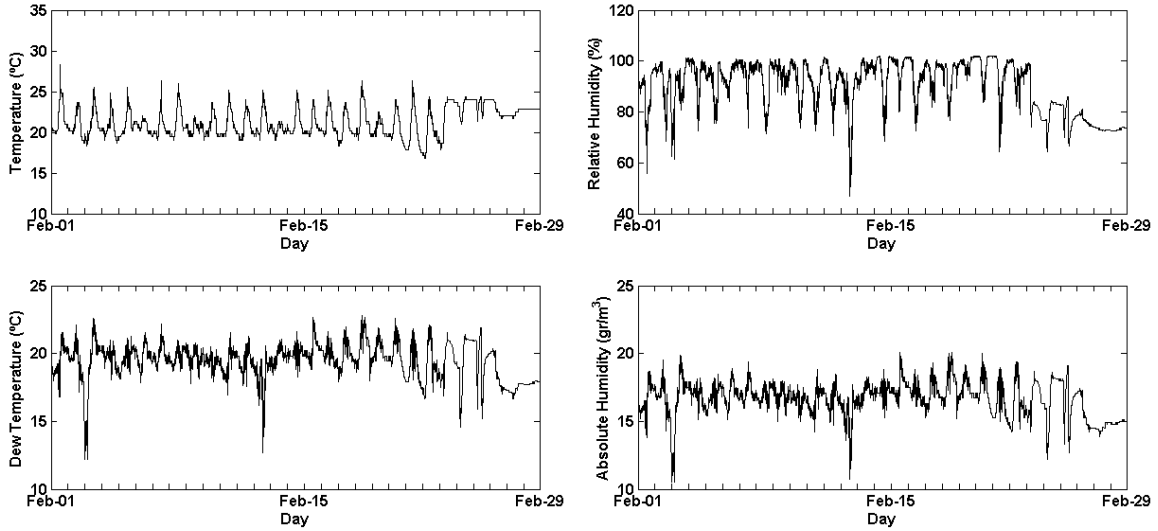


**Figure 4-14 Same as Figure 4-13, for El Verde tower at 2m.**

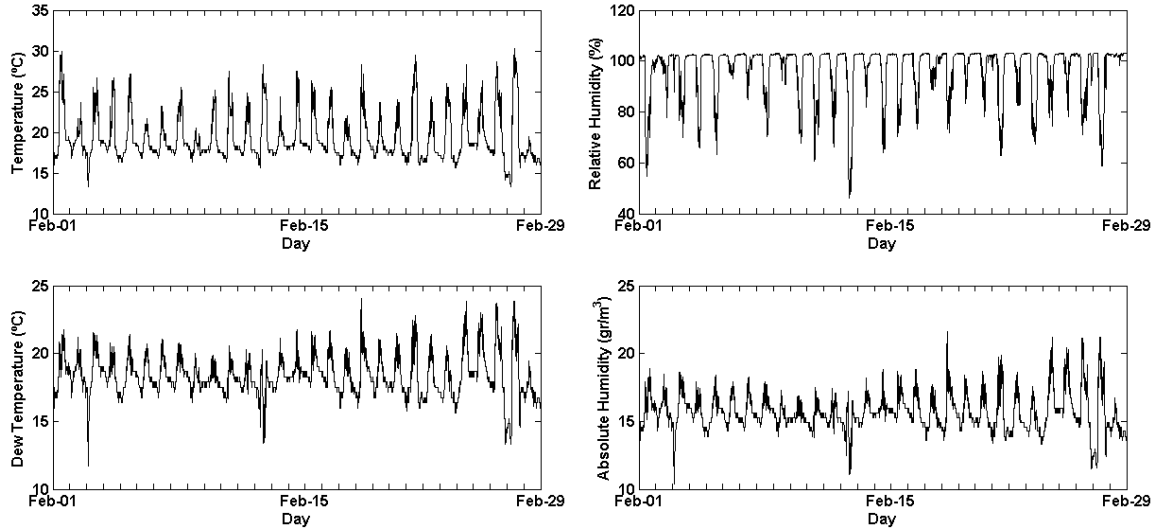


**Figure 4-15 Same as Figure 4-13, for Pico de Este.**

Seeing daily accumulated precipitation data, it is noticed that there are a total of 5 extreme events during February 2004, around sixth – seventh days, fifteenth – seventeenth days, twentieth - twenty first days, twenty fifth - twenty seventh and twenty ninth days. These extreme precipitation events are reflected at local scale by HOBOS sensors, showing a

decreasing of maximum temperatures, which are imposed in the increase of the minimum relative humidity which can suggest that there was a low pressure in the area, with higher humid contents in the air. The most evident event during this time occurred at the last day of the month, which reflects an extreme precipitation event, with reduced air temperatures.

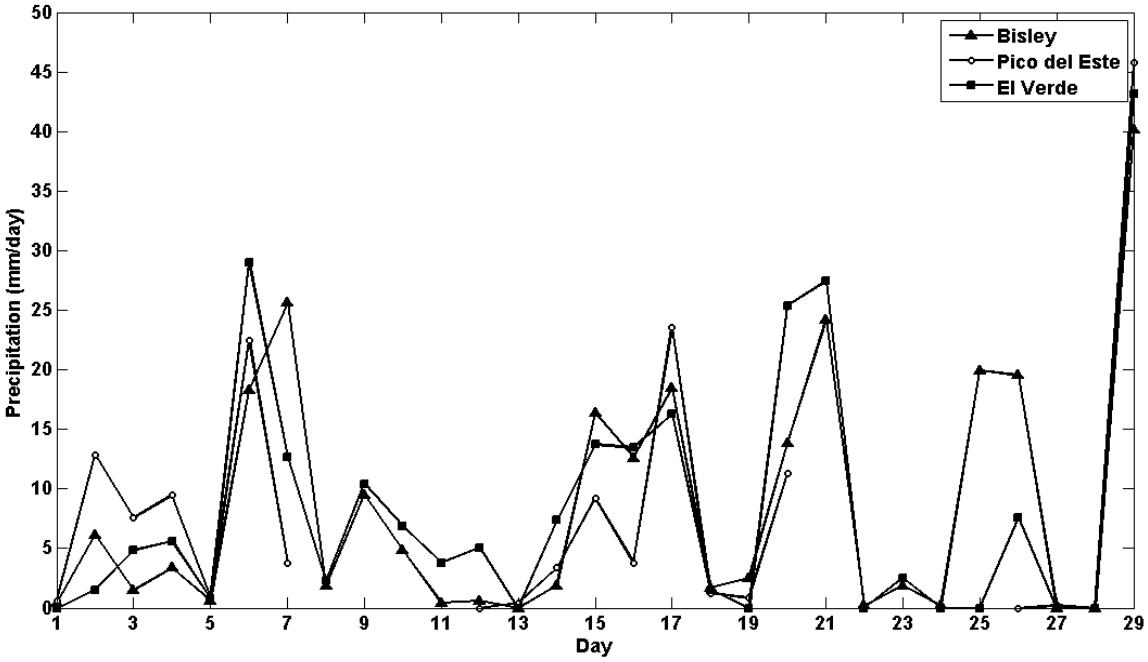


**Figure 4-16 Accumulated daily precipitation (mm) in three stations located in El Yunque.**

### *4.5.4 Synoptic Atmospheric Conditions*

During February 2004 there are average high pressure conditions in the Caribbean region reflected in the north easterly trade winds in the low atmosphere (1000 and 700 mbar). In Figure 4-17 it is depicted the mean air temperature at three atmospheric levels; at 1000 mbar (Figure 4-17(a)) it is depicted that in the Caribbean there is average high pressure, with the

maximum values located in the Atlantic Ocean, which is reflected in the North-easterly Trade winds over the Caribbean region, and Puerto Rico. At this pressure level, there is an average air temperature conditions between 23 and 24ºC over Puerto Rico, with higher values located over the Caribbean Sea; air temperature reflects a difference in about 2ºC between the Sea Surface (Figure 4-12) and this pressure level. The mean behavior presented for the wind direction at 700 mbar (Figure 4-17(b)) reflects also the easterly trade winds behavior in the Caribbean region in the low atmosphere. Relative humidity (Figure 4-18) in the Caribbean region have a similar mean value (0.8 – 0.85%) at 1000 mbar (Figure 4-18(a)), which is reduced in the 700 mbar (Figure 4-18(b)) as consequence of the low vapor content in the area at this pressure level.

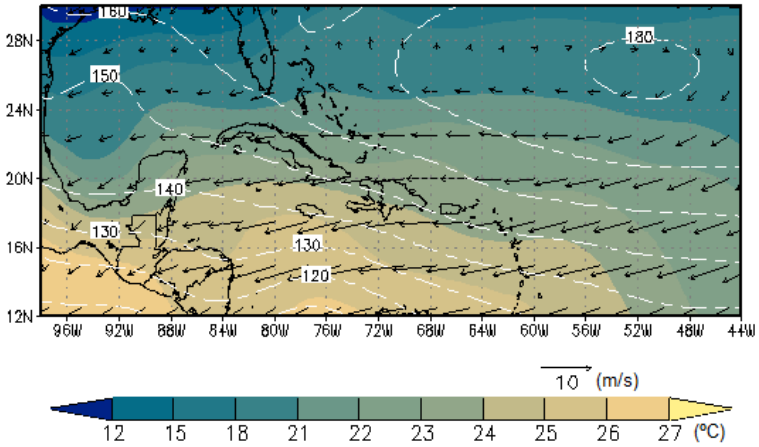


(a)

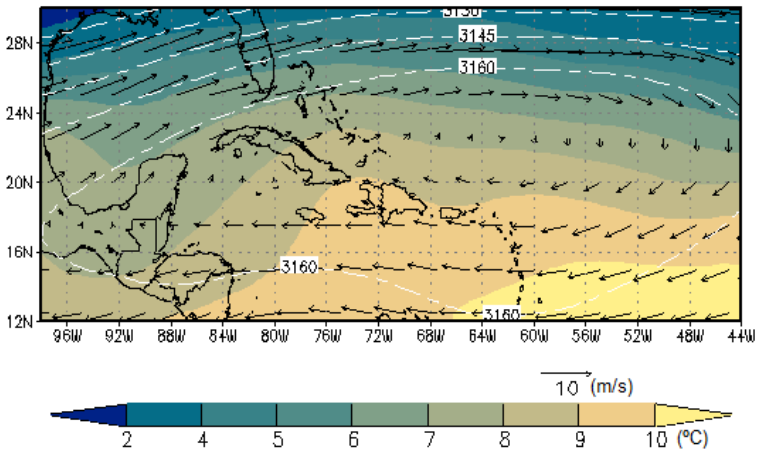


(b)

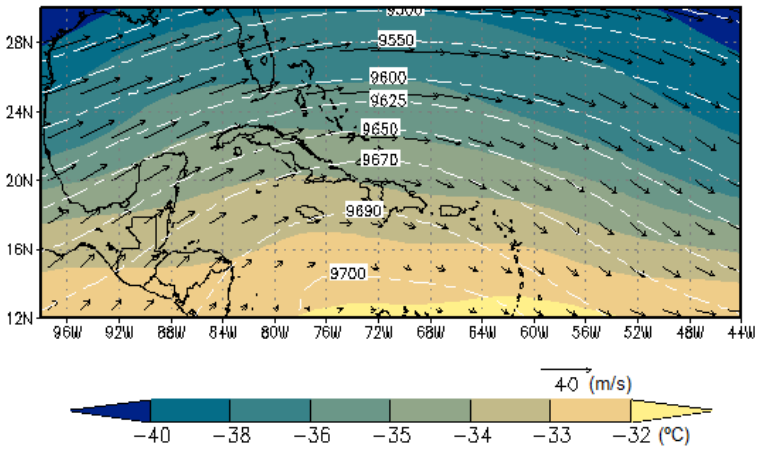


(c)

**Figure 4-17 Average air temperature (ºC); average horizontal wind (m/s); and average GHT (m) during February 2004 (NCEP Reanalysis data) at (a) 1000mb; (b) 700mb; and (c) 300mb.**

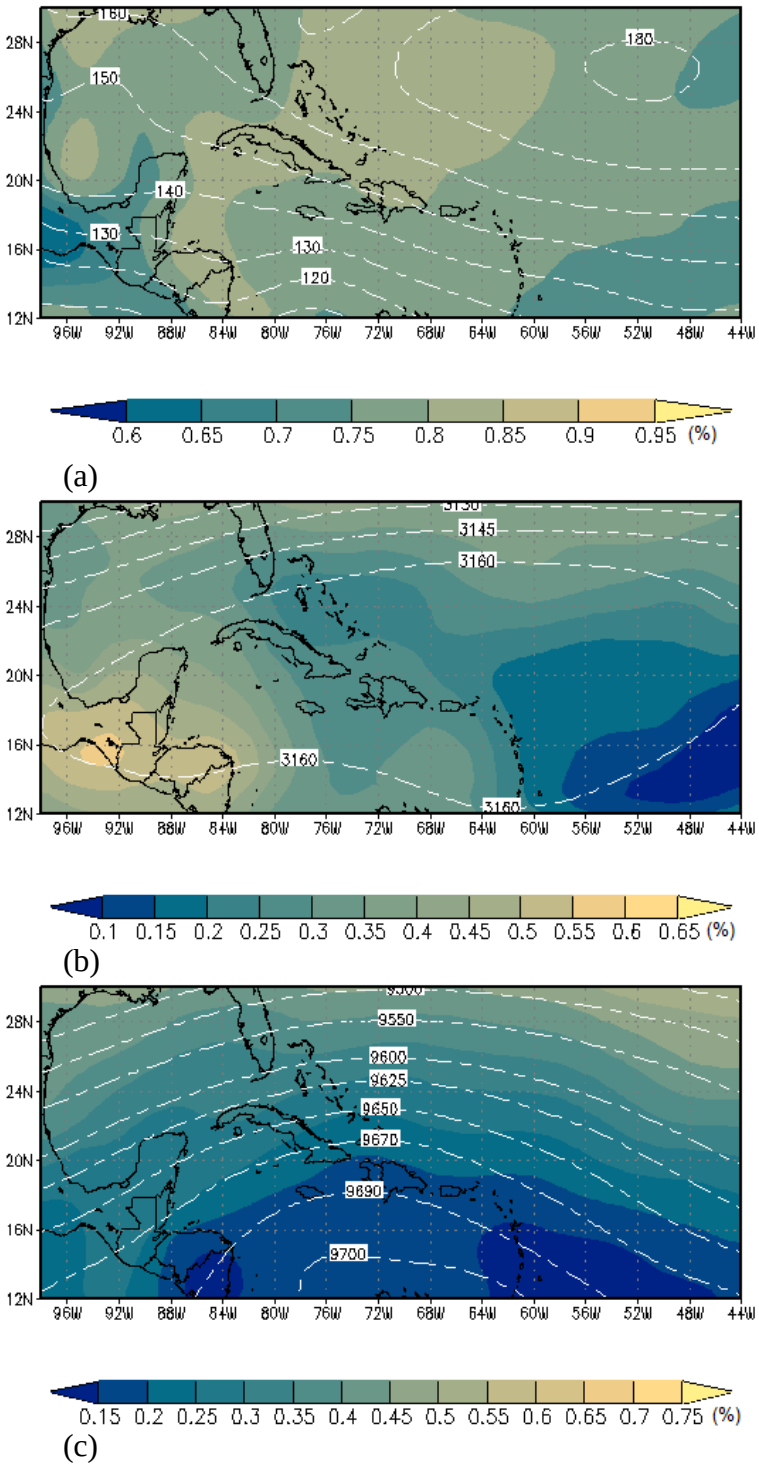


**Figure 4-18 Average relative humidity (%) and average GHT (m) during February 2004 (NCEP Reanalysis data) at (a) 1000mb; (b) 700mb; and (c) 300mb.**

## 4.6 Influences in Caribbean Dry Season - Synoptic Conditions

The atmospheric influences on Caribbean Basin is considered based on differences between February 2004, the reference time, hereafter RT, and similar time conditions in the second month of average past conditions, hereafter APC, during the dry season. Figure 4-19 shows the SST difference between RT and APC, which reflects warmer surface temperatures in the Caribbean Sea at the present time, with larger values in the Atlantic Ocean, closed to 1ºC.

Similarly, Figure 4-20 and Figure **4-21** show the difference in the atmospheric conditions between RT and APC, in which the increase in air temperatures and moisture content in the low atmosphere (1000 and 700 mbar) are visible, as consequence of the increased evaporation from the Ocean. Opposite behavior in air temperature is presented in the high atmosphere (300 mbar) where there is a reduction in moisture content, with an increasing temperature tendency. However, it appears to be an increasing pressure condition in the all Caribbean region at the RT compared with the APC.

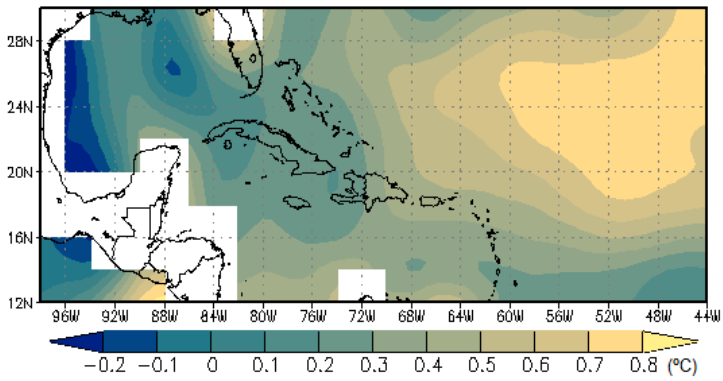


**Figure 4-19 Difference between average SST (ºC) February 2004 and average past conditions.**

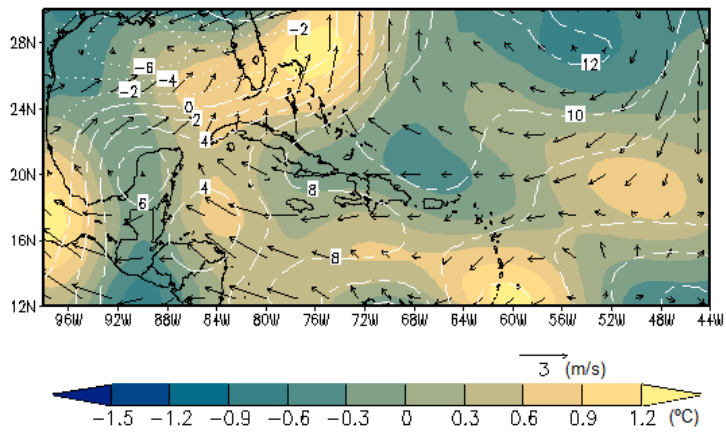


(a)

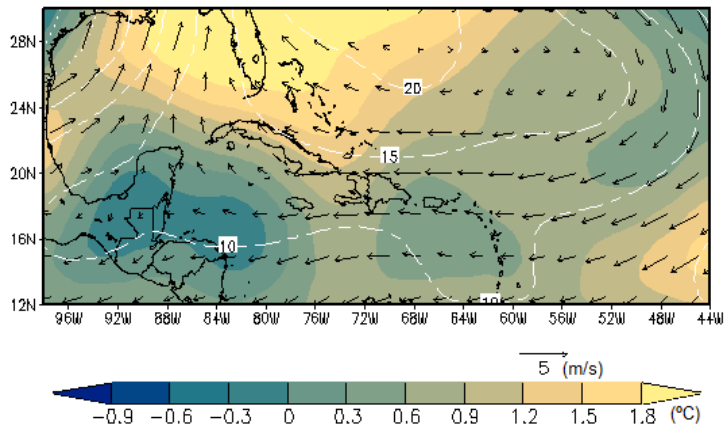


(b)

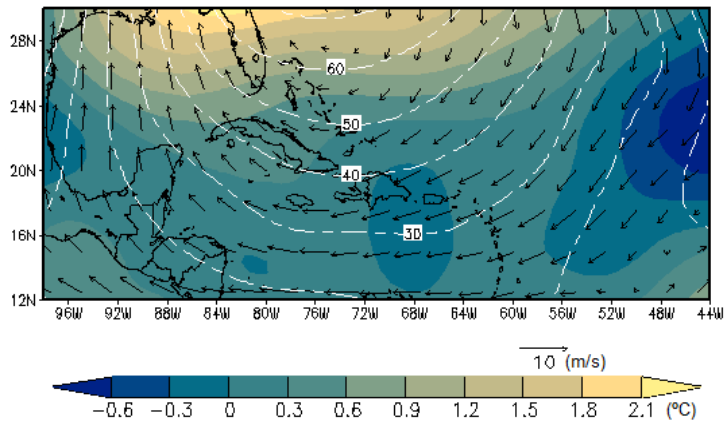


(c)

**Figure 4-20 Difference (NCEP Reanalysis data) between average February 2004 and average past conditions to air temperature (ºC); average horizontal wind (m/s); and average GHT (m) at (a) 1000mb; (b) 700mb; and (c) 300mb.**

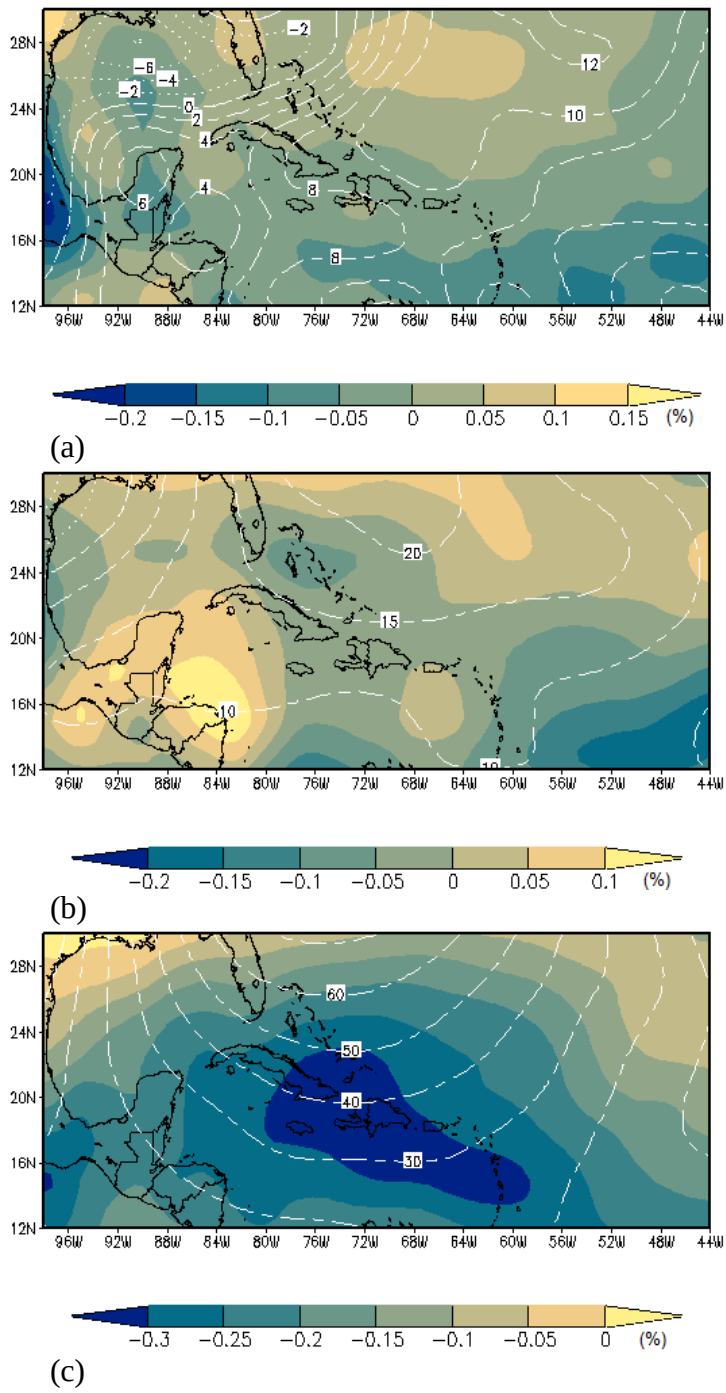


**Figure 4-21 Difference (NCEP Reanalysis data) between average February 2004 and average past conditions to relative humidity (%) and average GHT (m) at (a) 1000mb; (b) 700mb; and (c) 300mb.**

# 5 MODEL RESULTS AND ANALYSIS

The analysis of the results from the atmospheric model will focus in the parent grid, which includes the Caribbean Basin, and third grid (finer one) which is centered in El Yunque and encloses the eastern area of Puerto Rico. In the parent grid it will be analyzed the impact of the global warming since the land use change was configured only for the eastern part of Puerto Rico because the lack of availability of the data for the entire Caribbean domain. However, in the finer grid, where present and past land uses were configured, global warming and land use changes effects will be both analyzed. These analyses are presented in the next sections.

## 5.1 MODEL CALIBRATION

The output variables of the model were calibrated using the average NCEP Reanalysis II [43] data at the synoptic scale and, in the regional scale with the measured air temperature and daily precipitation data around El Yunque. These variables provide the necessary accuracy conditions for the model results.

### *5.1.1 Synoptic Conditions*

For the synoptic conditions, NCEP Reanalysis data with a resolution of 2.5º at 17 pressure levels [43] is used for the model calibration, which is also used as an initial input to RAMS

model. After comparing the model outputs with the data, it is determined how the model is responding to the first spatial grid integration. Considering that model is configured to integrate the equations with a horizontal spatial resolution of 0.18º (10.8'), then spatial comparison must be visual, comparing the time average behavior of measured data (Figures Figure **4-12**, Figure **4-17** and Figure **4-18**) with integrated data (Figures Figure **5-1**, Figure **5-2** and Figure **5-3**), respectively. The average of the first integration grid in RAMS at different vertical pressure levels were comparing with an enclosing grid NCEP Reanalysis data at the same pressure interval, presenting good accuracy in all pressure levels (Figure 5-4) with maximum variations obtained at 600 mbar, since this pressure level is not calculated by the model. Therefore, it is fair to conclude that the RAMS model captures very well mean synoptic conditions in the Caribbean Region for the different analyzed pressure levels.

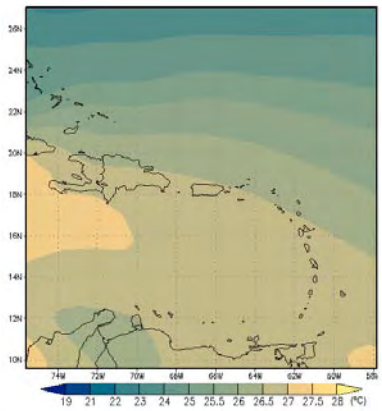


**Figure 5-1 Simulated average Sea Surface Temperature during February 2004.**

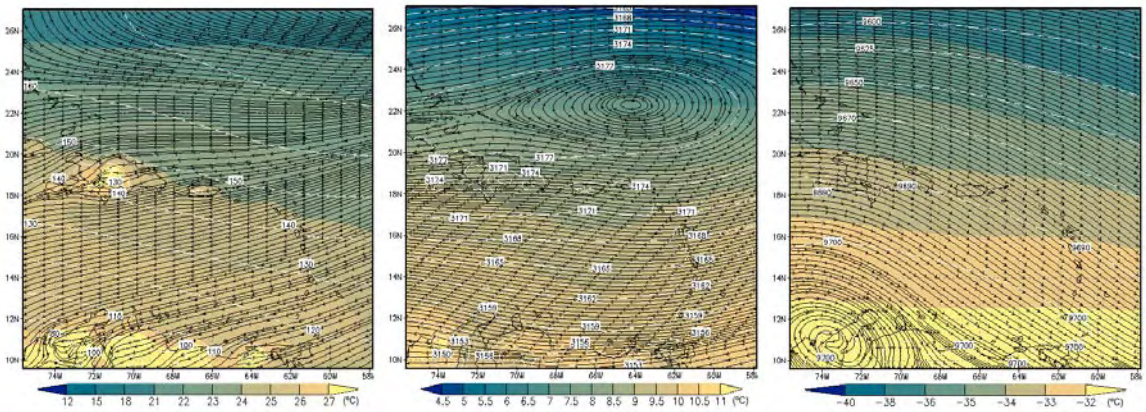

(a) 1000 mbar (b) 700 mbar (c) 300 mbar

**Figure 5-2 Simulated average air temperature (ºC); average horizontal wind streamlines; and average GHT (m) during February 2004 (RAMS model) at (a) 1000mb; (b) 700mb; and (c) 300mb.**

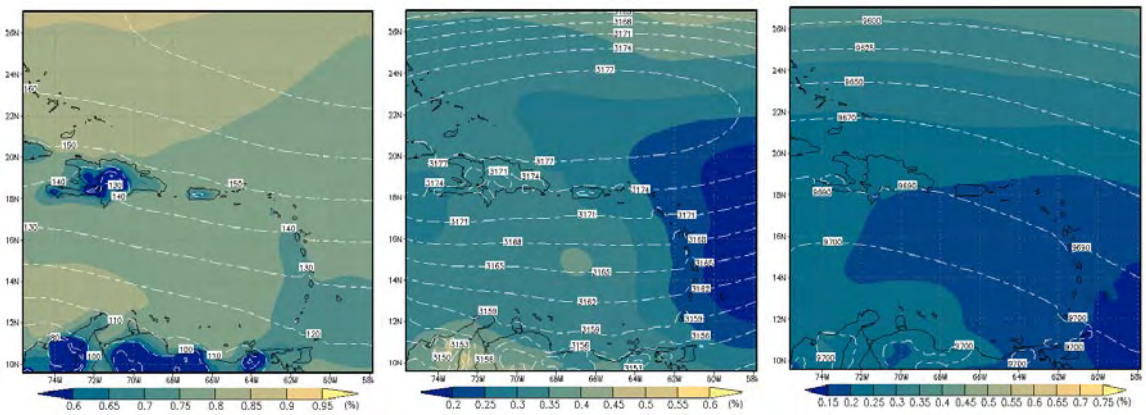

(a) 1000 mbar (b) 700 mbar (c) 300 mbar

**Figure 5-3 Simulated average relative humidity (%) and average GHT (m) during February 2004 (RAMS model).**

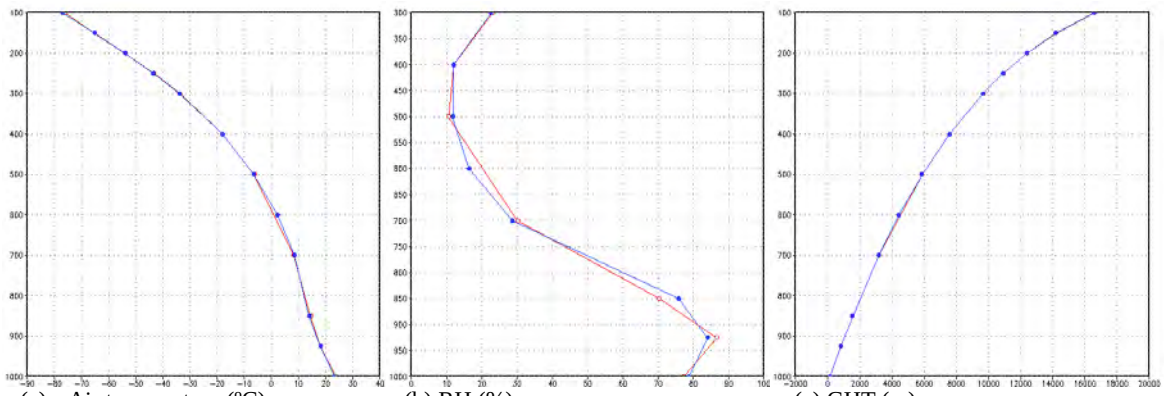

(a) Air temperature (ºC) (b) RH (%) (c) GHT (m)

**Figure 5-4 February average pressure levels profile of the Parent grid in RAMS (red) and the NCEP Reanalysis data (blue).**

### *5.1.2 Air Temperature - February 2004*

To calibrate the finer grid of integration, data from the HOBOS temperature network, shown in Figure 4-7, was used. These data was collected during February 2004 as part of the ATLAS mission campaign. These data were compared with simulated air temperature 2 meters above the surface from the RAMS simulations. Figure 5-5 shows the field confidence interval of the measured temperature data in El Yunque area, obtained from the HOBOS network stations data interpolation in a 20 km by 15 km grid (1 km resolution), with nodes located at the same locations as the third grid nodes of the configured model in RAMS. This plot shows a reduced variability of measured data above 800 meters; maximum variability is found in low land areas, between sea level and 200 meters above sea level (ASL). Between 500 and 700 m ASL there is an increasing data variability compared with the surrounding areas with lower elevations ASL. Maximum values of confidence interval are presented in coastal areas and minimum at the peaks, however the reduction is not linear.

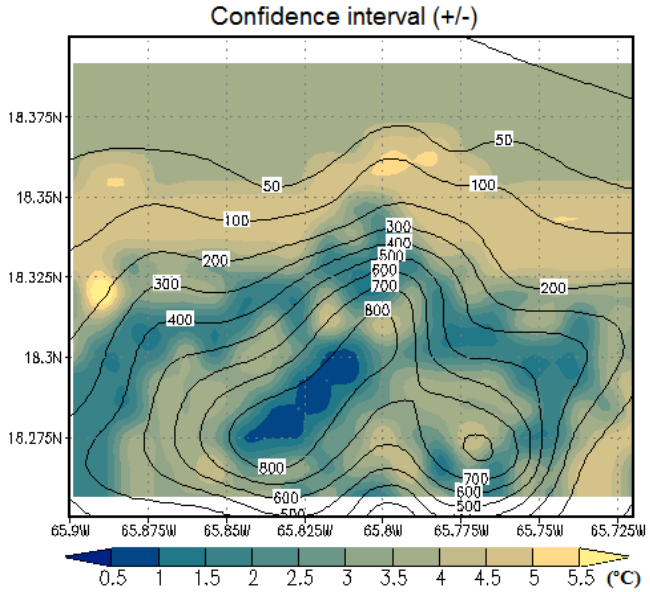


**Figure 5-5 Confidence interval (+/-) of HOBOS monthly mean air temperature measured data (February 2004).**

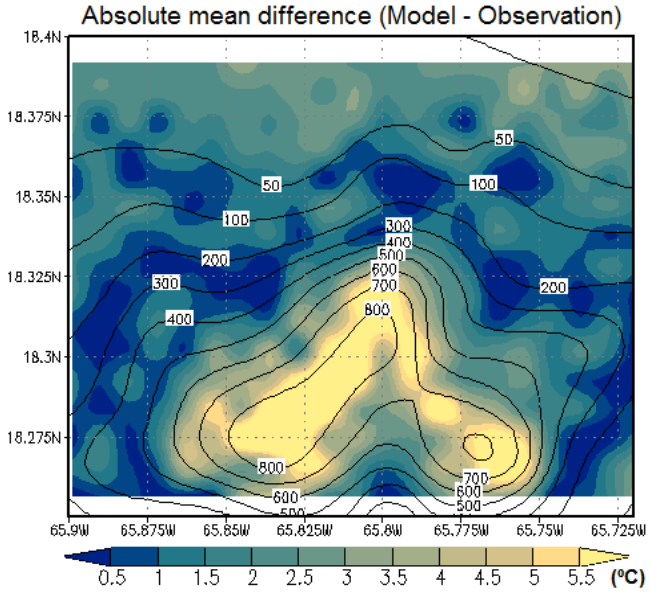


**Figure 5-6 Absolute difference between monthly average 2 meter air temperature RAMS simulated and monthly average HOBOS air temperature data, February 2004.**

Figure 5-6 depicts the absolute difference field value between the monthly average 2 meters air temperature simulated by RAMS and monthly average HOBOS temperature measured data (February 2004). A good accuracy is depicted in most parts of the grid with a maximum difference between 2 and 2.5ºC. A rapid increase of absolute difference is present above the 700 meters, with a maximum value of 6ºC at the peak of el Yunque, above 800 meter ASL, with simulated lower values than reported by measured data, with greater values and less variability in this area. Based on these results, it can be concluded that the simulation captures with reasonable accuracy mean surface atmospheric conditions around El Yunque in February 2004.

### *5.1.3 Daily and Accumulated Precipitation*

Precipitation is a variable which is the result of the spatial interaction between the different integration atmospheric variables and merits analysis in the validation exercise. Considering that precipitation measured data is located at specific location, the model can not capture the total accumulated effect at a determined location, because the model integrate the equations in a discrete domain. For this reason, to compare the model with the measured data the average conditions under an area of 3 km x 3 km is taken, which encloses the location of the considered station.

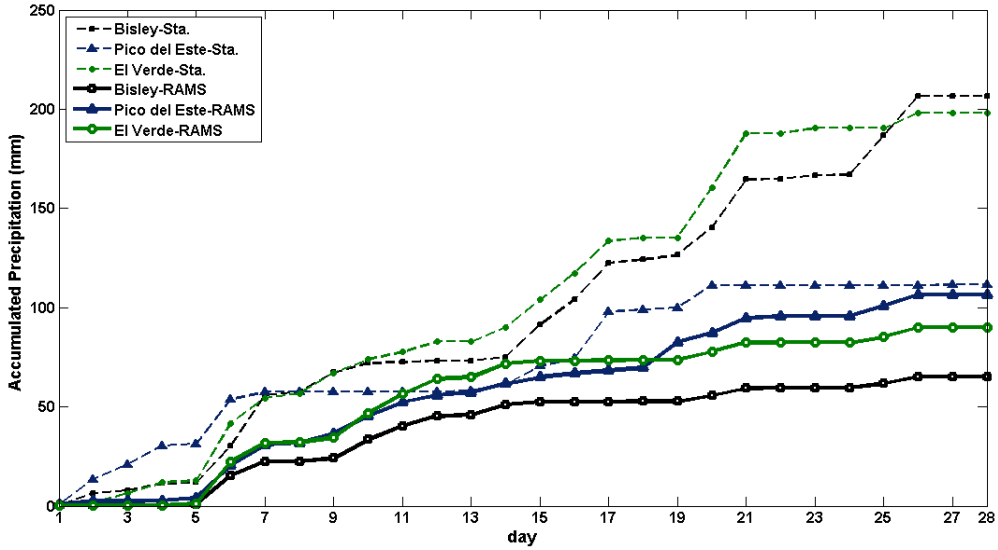


**Figure 5-7 Model comparison for measured accumulated precipitation (mm), in three stations located in El Yunque, February 2004.**

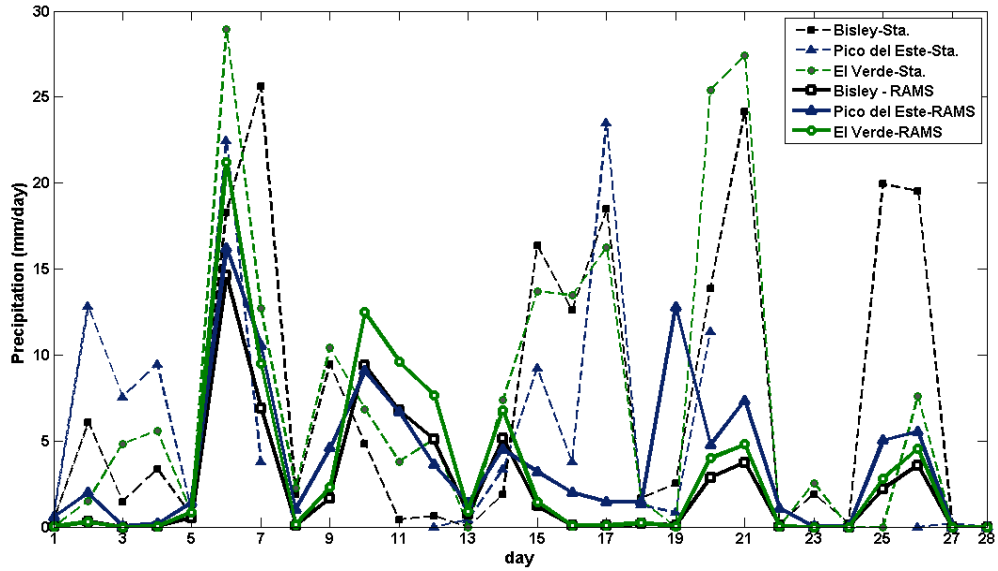


**Figure 5-8 Model comparison for measured daily precipitation (mm), in three stations located in El Yunque, February 2004.**

As depicted in Figure 5-7 the model has a good performance in the region of Pico del Este, capturing very well the accumulated precipitation; however in the north-eastern areas of El

Yunque, the model differs from measured data by factor of about 50% of the total precipitation (Table 5-1). However, Figure 5-8 reflects that the model captures the behavior of daily precipitation during the time of integration, where a better approximation occurs during the sixth-seventh days, and during the ninth and thirteenth days events, obtaining results of accumulated precipitation very close to the reported by measured data. The last two precipitation events (Feb 21$^{st}$ and Feb 27$^{th}$) are partially captured by the model. Prediction for the Bisley station presents a bias for these two events with errors higher than 100%. However, considering that most events were captured, it can be concluded that the simulation captures with reasonable accuracy the general profile of daily accumulated precipitation around El Yunque during February 2004.

## 5.2 RESULTS FOR CLOUD BASE

There are several relevant investigation results which show that there is a variation of cloud base height under the effects of low land use changes, which influences the TMCFs in Costa Rica [15] [16] [17] [49] and Puerto Rico [2] [3]. Spatial field distribution of this variable is very important in the analysis of the effects or influences of any specific variable under this cloud variable, since TMCFs are always in direct interaction with orographic clouds. Thus, increasing or decreasing cloud base should be a good indicator of water productivity of TMCF. For this reason, and because cloud base height is not a standard integration output

from RAMS, it is necessary to generate this variable as a function of cloud mixing ratio (g/Kg), which is a 3D field variable that quantifies the cloud concentration in Kg of dry air.

**Table 5-1 Daily percentage error of the accumulated precipitation between the model and the measured data.**

| | Bisley | | | Pico del Este | | | El Verde | | |
|---|---|---|---|---|---|---|---|---|---|
| Day | Meassured | Model | %error | Meassured | Model | %error | Meassured | Model | %error |
| 1 | 0.42 | 0.018 | -0.956 | 0.63 | 0.559 | -0.113 | 0.00 | 0.007 | |
| 2 | 6.51 | 0.324 | -0.950 | 13.44 | 2.529 | -0.812 | 1.52 | 0.297 | -0.805 |
| 3 | 7.98 | 0.324 | -0.959 | 21.00 | 2.581 | -0.877 | 6.35 | 0.297 | -0.953 |
| 4 | 11.34 | 0.338 | -0.970 | 30.45 | 2.751 | -0.910 | 11.94 | 0.319 | -0.973 |
| 5 | 11.97 | 0.866 | -0.928 | 31.29 | 4.143 | -0.868 | 12.70 | 1.177 | -0.907 |
| 6 | 30.24 | 15.467 | -0.489 | 53.76 | 20.365 | -0.621 | 41.66 | 22.401 | -0.462 |
| 7 | 55.86 | 22.329 | -0.600 | 57.54 | 30.918 | -0.463 | 54.36 | 31.925 | -0.413 |
| 8 | 57.75 | 22.419 | -0.612 | 57.54 | 31.913 | -0.445 | 56.64 | 32.040 | -0.434 |
| 9 | 67.20 | 24.076 | -0.642 | 57.54 | 36.488 | -0.366 | 67.06 | 34.375 | -0.487 |
| 10 | 72.03 | 33.474 | -0.535 | 57.54 | 45.550 | -0.208 | 73.91 | 46.848 | -0.366 |
| 11 | 72.45 | 40.229 | -0.445 | 57.54 | 52.221 | -0.092 | 77.72 | 56.450 | -0.274 |
| 12 | 73.08 | 45.294 | -0.380 | 57.54 | 55.835 | -0.030 | 82.80 | 64.122 | -0.226 |
| 13 | 73.08 | 46.052 | -0.370 | 57.96 | 57.203 | -0.013 | 82.80 | 65.008 | -0.215 |
| 14 | 74.97 | 51.196 | -0.317 | 61.32 | 61.713 | 0.006 | 90.17 | 71.775 | -0.204 |
| 15 | 91.35 | 52.398 | -0.426 | 70.56 | 64.893 | -0.080 | 103.89 | 73.219 | -0.295 |
| 16 | 103.95 | 52.472 | -0.495 | 74.34 | 66.868 | -0.101 | 117.35 | 73.276 | -0.376 |
| 17 | 122.43 | 52.544 | -0.571 | 97.86 | 68.313 | -0.302 | 133.60 | 73.344 | -0.451 |
| 18 | 124.11 | 52.726 | -0.575 | 99.12 | 69.779 | -0.296 | 135.13 | 73.567 | -0.456 |
| 19 | 126.63 | 52.813 | -0.583 | 99.96 | 82.569 | -0.174 | 135.13 | 73.612 | -0.455 |
| 20 | 140.49 | 55.681 | -0.604 | 111.30 | 87.340 | -0.215 | 160.53 | 77.597 | -0.517 |
| 21 | 164.64 | 59.432 | -0.639 | 111.30 | 94.688 | -0.149 | 187.96 | 82.389 | -0.562 |
| 22 | 164.85 | 59.477 | -0.639 | 111.30 | 95.757 | -0.140 | 187.96 | 82.414 | -0.562 |
| 23 | 166.74 | 59.477 | -0.643 | 111.30 | 95.759 | -0.140 | 190.50 | 82.414 | -0.567 |
| 24 | 166.95 | 59.477 | -0.644 | 111.30 | 95.766 | -0.140 | 190.50 | 82.414 | -0.567 |
| 25 | 186.90 | 61.681 | -0.670 | 111.30 | 100.802 | -0.094 | 190.50 | 85.231 | -0.553 |
| 26 | 206.43 | 65.265 | -0.684 | 111.30 | 106.338 | -0.045 | 198.12 | 89.771 | -0.547 |
| 27 | 206.43 | 65.265 | -0.684 | 111.51 | 106.338 | -0.046 | 198.12 | 89.771 | -0.547 |
| 28 | 206.43 | 65.265 | -0.684 | 111.51 | 106.338 | -0.046 | 198.12 | 89.771 | -0.547 |

### *5.2.1 Definition of Cloud Base*

The calculation of cloud base is based on cloud mixing ratio, which is a scalar field with (x,y,z) as independent variables at each time. Cloud base is a scalar variable which depends on (x,y) at each time. Thus, at each time it is necessary calculate in all surface nodes location (x,y) where a first value greater than zero of cloud mixing ratio is found, following the z positive direction. If the scalar value of cloud mixing ratio is greater than or equal to zero, and at each node the value of cloud mixing ratio represents an average value in the grid cell, thus between a null value in the previous node and a positive value in the node considered, there is a positive increasing variation of cloud mixing ratio, and then a cloud concentration between them. For these reasons, calculated cloud base must be defined as the previous elevation in which the first value of cloud mixing ratio is located, starting at the ground level.

### *5.2.2 Cloud Base Calculation*

In this research the estimate of the cloud base was developed using a MATLAB program, where the input parameters are the GRADS file, provided by REVU, in the post processing of RAMS outputs. However, in Figure 5-9 through Figure **5-11** are presented the general flow chart to calculate the cloud base field, with or without considering the topography on the outputs calculation, i.e. it can be expressed in meters above the ground level (AGL) or meters above the sea level (ASL).

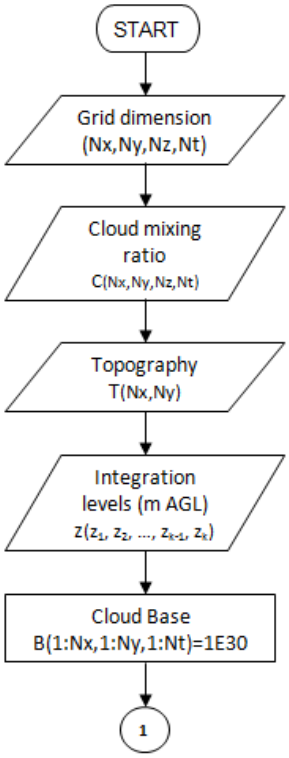


**Figure 5-9 Flow Chart to estimate Cloud Base.**

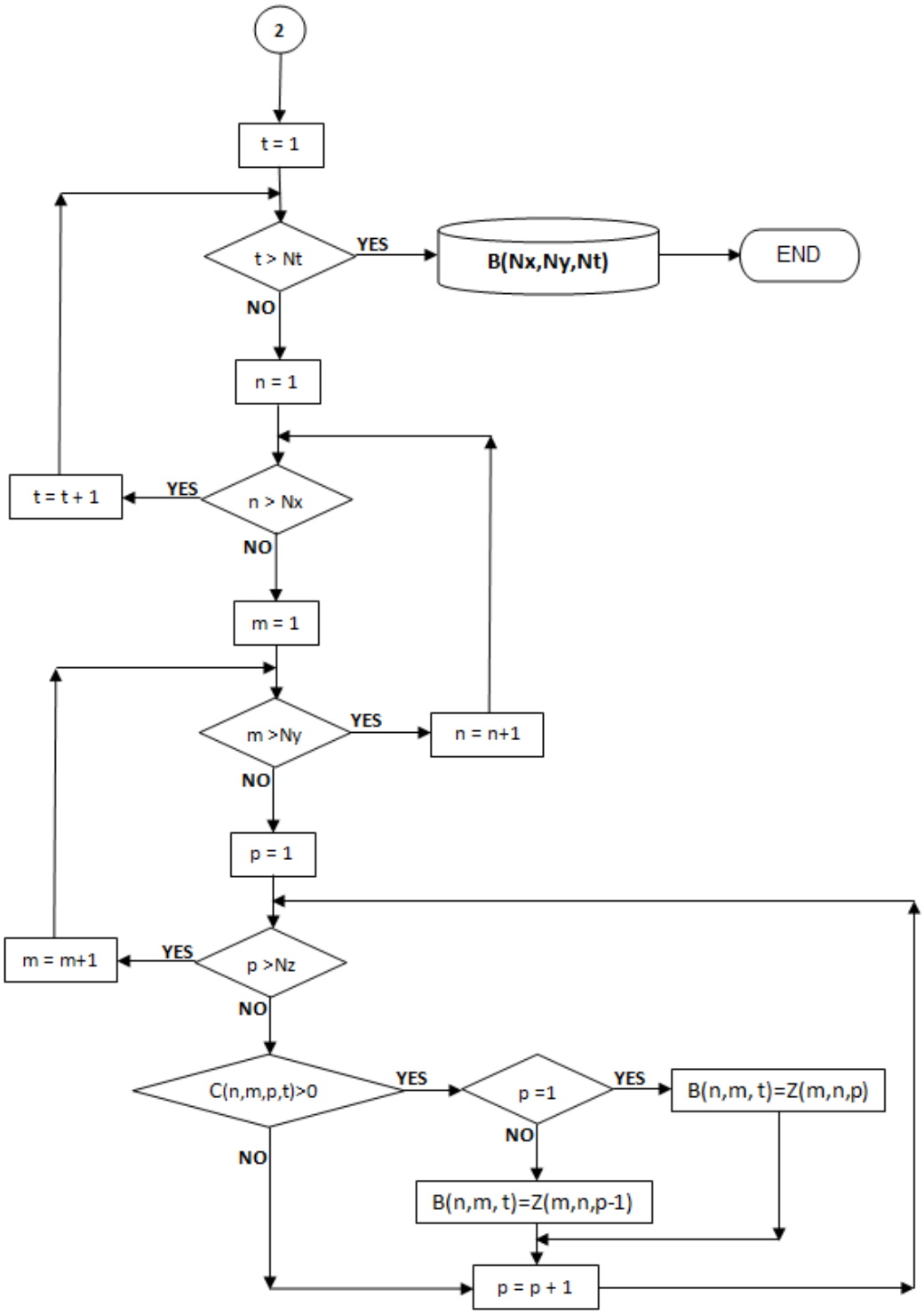


**Figure 5-10 Flow Chart to estimate Cloud Base (continuation).**

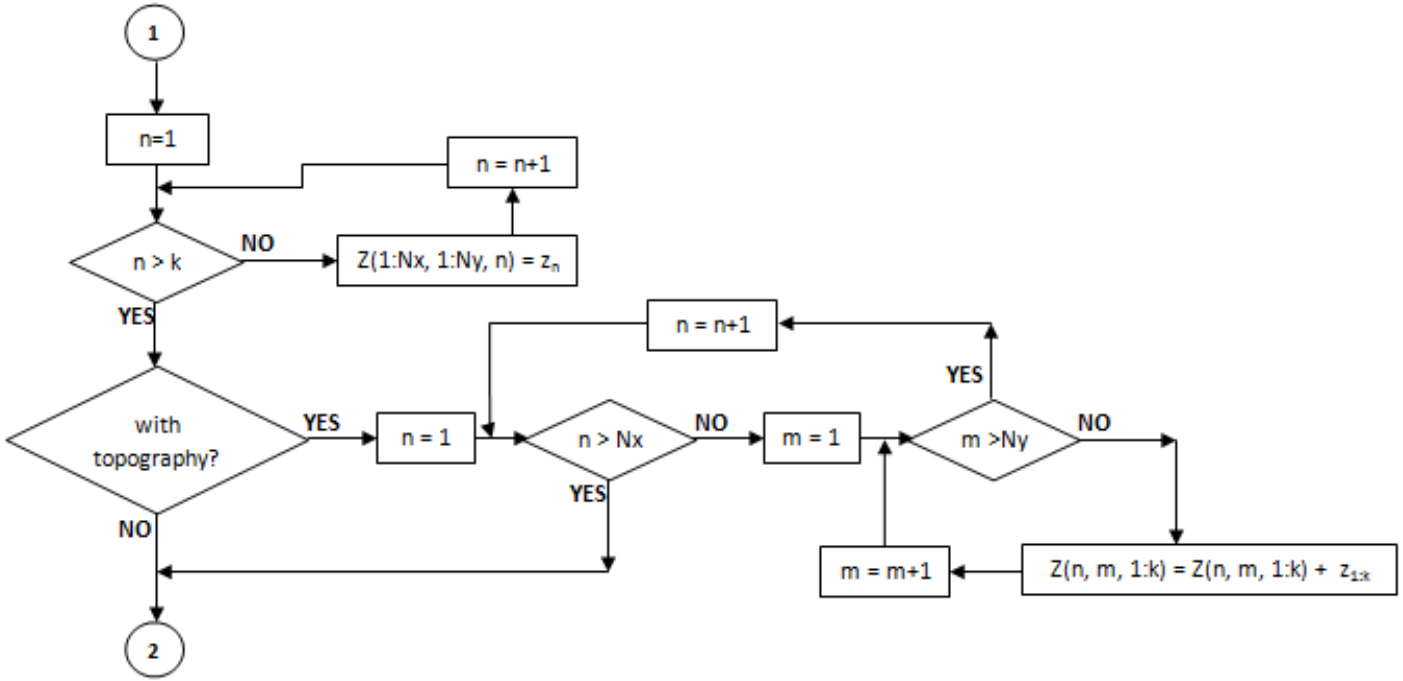


**Figure 5-11 Flow chart to estimate Cloud Base (continuation).**

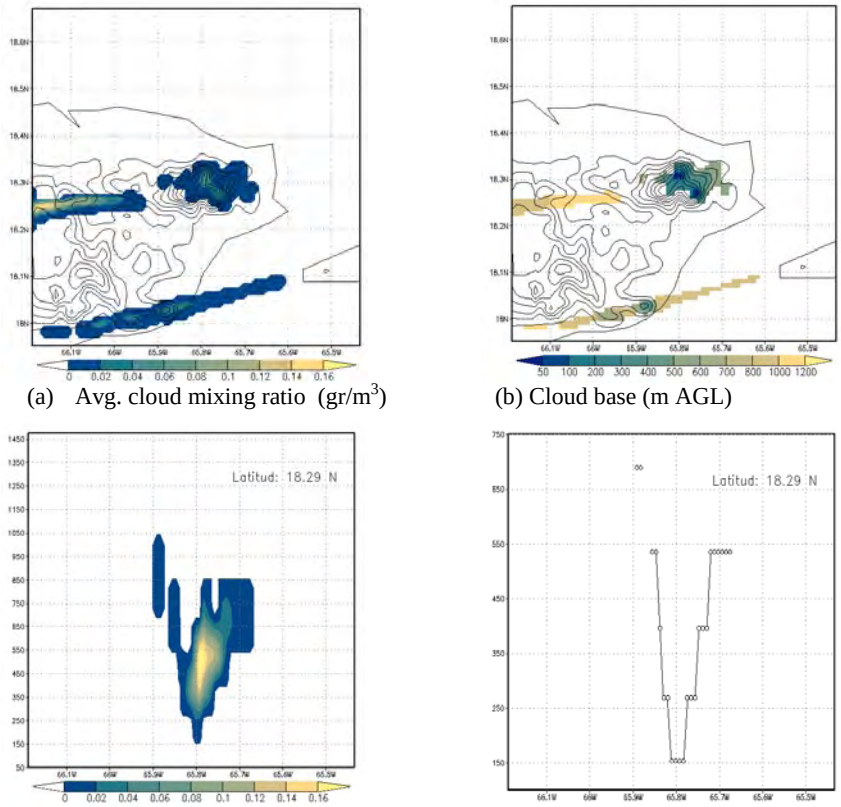


(a) Avg. cloud mixing ratio (gr/m$^3$) (b) Cloud base (m AGL)

(c) Cloud mixing ratio (gr/m$^3$) (d) Cloud base (m AGL)

**Figure 5-12 Simulated cloud mixing ratio (a) average from 50 to 1500 meters AGL and (c) at 18.25ºN. Cloud base (b) 2D field, and (d) at 18.29ºN at Feb/17/2004 16:00 local time.**

### *5.2.3 Cloud Base Comparison*

Since cloud base is calculated based on cloud mixing ratio, the comparison results must be done in conjunction with this field. With this in consideration, in Figure 5-12(a) it is shown the average of cloud mixing ratio between 50 and 1500 meters AGL at t=200 time step (Feb/17/2004 at 16:00 Local time) in the integration model; which represents the spatial distribution of the cloud in the grid of integration. Figure 5-12(b) indicates the cloud base (2D field) calculated following the methodology referred above. At the same time step "t" it

is depicted the cloud mixing ratio in the same grid at 18.29ºN (Figure 5-12(c)), showing the vertical variability of the cloud mixing ratio. The cloud base in the same latitude (18.29ºN) cross section is depicted in Figure 5-12(d). Base on comparison between cloud mixing ratio and cloud base in Figure 5-12, the calculated cloud base represents the exact behavior in the results of cloud mixing ratio field.

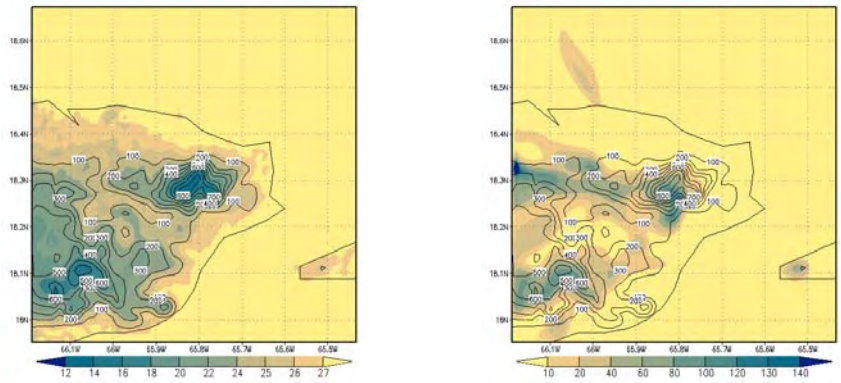


(a) Air temperature (ºC) (b) Precipitation (mm)

**Figure 5-13 Simulated average (a) temperature 2 meters AGL (ºC), and (b) accumulated precipitation (mm) for February 2004.**

## 5.3 Eastern Puerto Rico - February 2004 Simulation Results

The finer grid in the model covers the eastern part of Puerto Rico, thus monthly integration should provide the characteristic average monthly conditions and accumulated in the case of precipitation. From the average temperature 2 meters AGL on the eastern Puerto Rico (Figure 5-13(a)) is visible the orographic behavior of temperature, precipitation (Figure 5-13(b)), average cloud cover and cloud base (Figure 5-14). The cloud cover has high values in the windward areas of El Yunque, and lower values in the leeward areas, where the

windward areas are directly influenced by north-easterly trade winds (TMCF), which is also reflected in the average vertical wind velocity in this area (Figure 5-15).

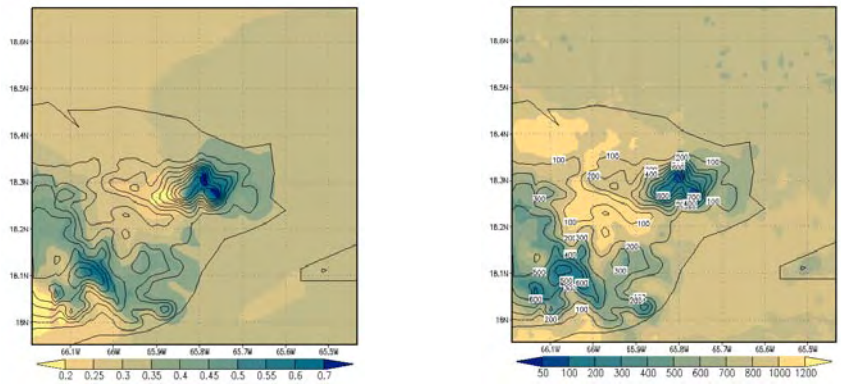


(a) Cloud cover (%) (b) Cloud base (m AGL)

**Figure 5-14 Simulated average (a) cloud cover (%), and (b) cloud base (m AGL) for February 2004.**

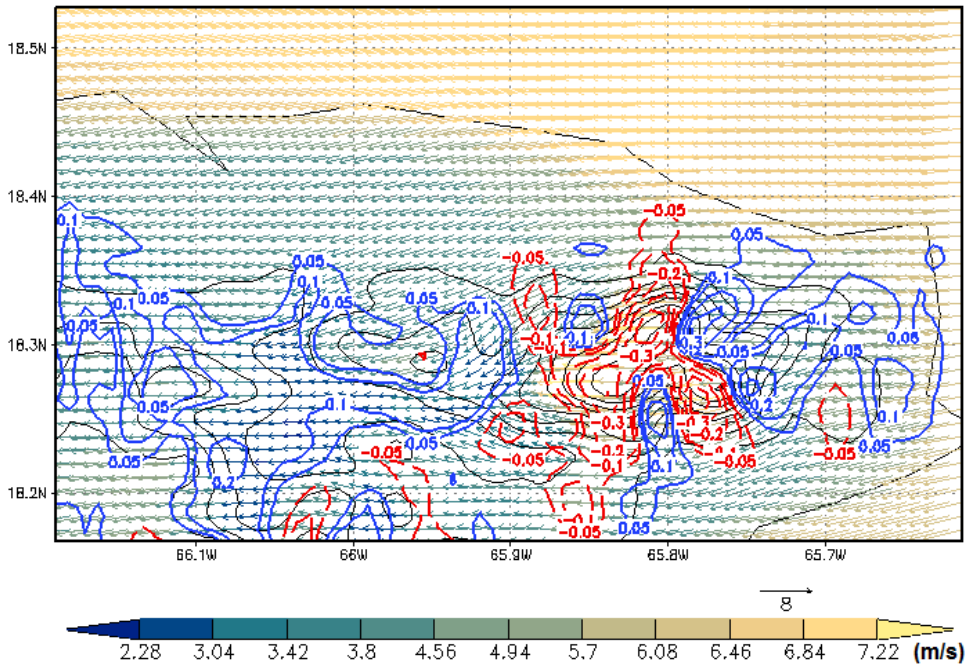


**Figure 5-15 Simulated average wind vector at 50 meters AGL and average vertical wind contours (m/s) at 700 meters AGL for February 2004 (blue means positive and red negative contour values).**

## 5.4 Results to Determine Impact of LULC Change and GHG

The analysis of separated effects, represented in the proposed ensemble simulations (TABLE 3-1) are presented as differences in the finer grid field, which is the analysis area of interest. For the synoptic conditions (first grid) it is analyzed the global warming effect, because the land use has changed only in the eastern region of Puerto Rico, and not in all non-water regions of the Caribbean domain. The fields will represent the difference between actual conditions and past conditions of GW or land use. Thus these differences represent the influence of these variables in the grid of analysis.

### *5.4.1 Synoptic Conditions*

Figure 5-16 and Figure **5-17** depict the simulated average conditions during February 2004 (blue curve) and average past conditions (black curve), where difference represents the GW effect in the Caribbean region. These results show that mean temperatures (Figure 5-16(a)) and GHT (Figure 5-16(b)) are increasing in the Caribbean region during dry season. GW effect is reflected in the increasing air and sea surface temperatures [5], generating more humid content in the low atmosphere (Figure 5-17(b)), which in turn is a consequence of the warmer sea (Figure 5-18) that generates more evaporation on the area. Between the 700 and 300 mbar with warmer air temperatures in the lower atmosphere there is a reduction of the humid content enclosed in the low levels of the atmosphere providing a first assessment to

explain the reduction in the cloud base and increased cloud cover in the area, as it will be shown later.

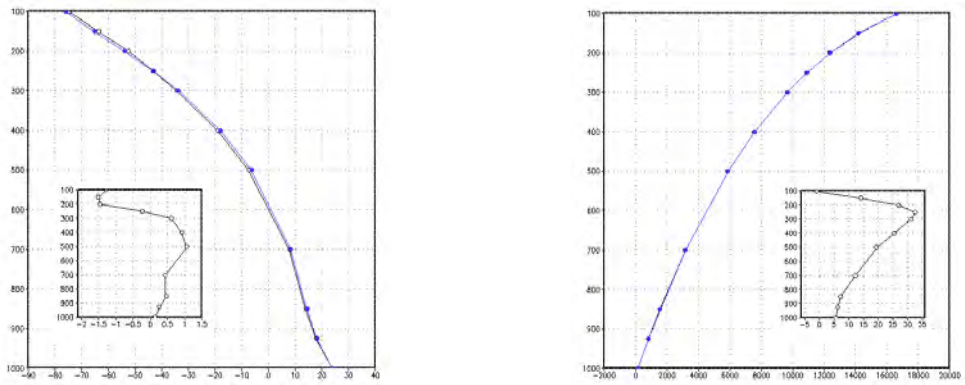

(a) Air temperature (ºC) (b) GHT (m)

**Figure 5-16 Simulated first grid average February 2004 (blue) and average past conditions (black) at different pressure levels (mbar) for (a) air temperature (ºC), and (b) GHT (m). The inserted plot represents the actual difference.**

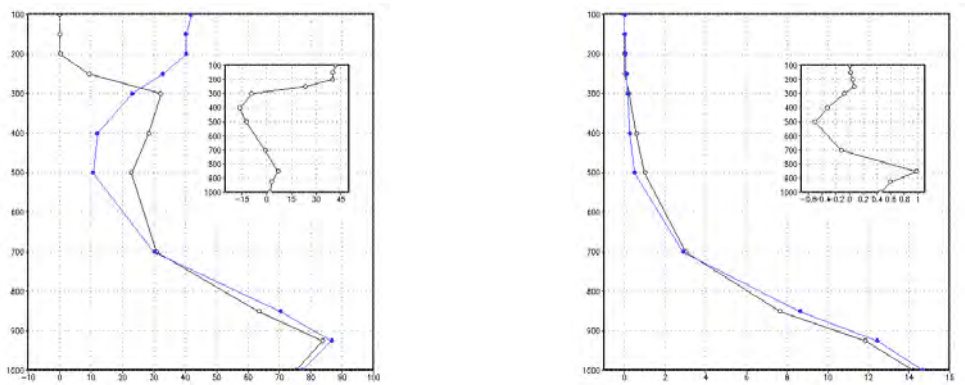

(a) Relative humidity (%) (b) Vapor mixing ratio (g/kg)

**Figure 5-17 Simulated first grid average February 2004 (blue) and average past conditions (black) at different pressure levels (mbar) for (a) relative humidity (%), and (b) vapor mixing ratio (g/kg). The inserted plot represents the actual difference.**

There is observed warmer air temperatures in the atmosphere and thus an increase in the saturation pressure. Additionally, increasing SSTs produce more vapor content in the lower atmosphere (1000-700 mb), but in the mid atmosphere (700-300 mb) there is a reduction in

vapor content, which coupled with the increasing saturation pressure generates a reduction in relative humidity at these pressure levels. This phenomenon do not appear at low pressure levels since the increasing vapor content and pressure produce greater values of relative humidity at these atmospheric levels.

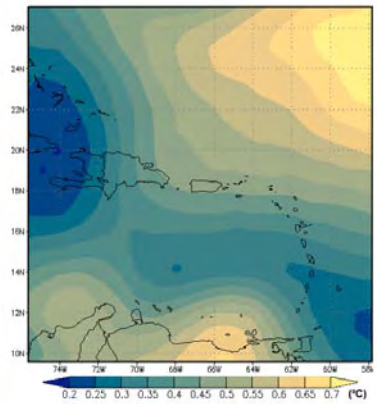


**Figure 5-18 Simulated SST difference (ºC) in the first grid of integration between average February 2004 and average past conditions.**

### *5.4.2 Average Temperatures at 2m AGL*

The global warming effects in the air temperature 2 meters AGL are depicted in Figure 5-19(a), where the actual increase in temperature near the surface is visible, with mean values of 1.5ºC warmer than similar average past conditions. SJMA clearly presents an increasing in local average temperatures, reaching maximum increases in the southwestern areas as a consequence of the heat transported from the high density urban areas along the north easterly trade winds (Figure 5-15). The land use change as well as the GW influence both the air temperature near the surface (Figure 5-19(b)). The land use change reduces the air temperature from the past agricultural and grass-land areas in about the same magnitude as the increase in temperature caused by GW effects. The coupled effect of GHG and Land use

change is shown in the Figure 5-19(c), presenting a total increased air temperature near the surface as result of GW effect and high density urban areas. The cooler areas are produced by the land use change which generates decreasing temperatures overriding the increasing effect by GW. Decreasing air temperatures in eastern Puerto Rico, around and inside El Yunque, mean that land use change is reducing the GW effect in this area since 1977-1978, which is the reference time for the past land use. This shows that emerging and recovery forests [34] and reduction in the agricultural zones [12], in the lowland areas are diminishing the increasing atmospheric average temperatures in the zone.

In SJMA the increase in average air temperatures do not reflect the same magnitude of as the reported by the UHI effect studies [47] [13]; this is because past land use has urbanized areas, however with lower density as the present conditions (Figure 3-7 and Figure **3-8**), for these reasons the warmer areas generated by the land use change are south of SJMA and in the direction of the trade winds. Past studies idealized the past land use by removing the cities entirely and possibly overestimated the effects of urbanization. However, the combined effects of LULC and GW may override any estimated extreme land use impact.

Since there is a variability in the response of average air temperatures under GW and LULC change, the discussion and results are separated into two areas: Lowland areas (<300 masl) and highland areas (>300 masl). Figure 5-20 shows the simulated mean variation, with time

interval of 2 hours for lowland and highland areas, where it is depicted the GW, LULC and the coupled effect along the daily hours.

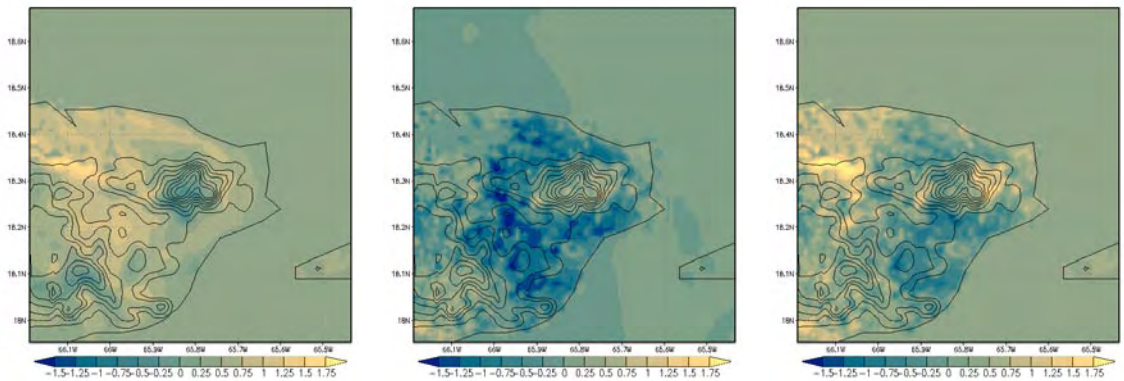


(a) GHGs effects - (ºC) (b) LULC effects - (ºC) (c) Coupled effects - (ºC)

**Figure 5-19 Average simulation air temperature difference at 2 meters AGL.**

In lowland areas (Figure 5-20(a)) it is produced an increase mean temperature of 0.373ºC near the surface (2 m AGL), where it is visible the greater influence of the GW, which produces a mean increase of 1.19ºC; however LULC change diminishes the effect of GW in the interval of analysis (1978 - 2004), reducing by 40% the mean effect of GW in the average air temperature. The reduction of air temperature due to GW effect by LULC change is greater during the early part of the day, where the reduction reaches 51% in the average maximum temperature (mean value between 12 – 14 hrs); however the average mean minimum temperatures are reduced by 36% (mean values between 04 – 06 hrs). Additionally, Figure 5-20(a) shows that the maximum increase is produced during the first hours of the morning, reaching a maximum increase value of 2.13ºC in the couple effect, as consequence of the reduction of 18.2% in GW effect by the LULC influence.

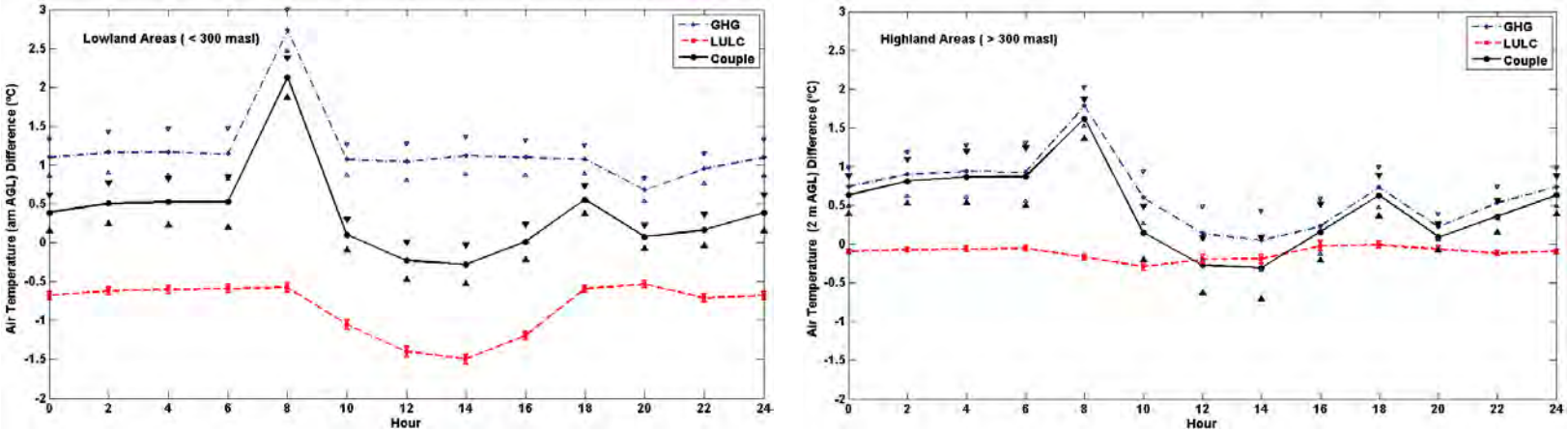


(a) Lowland areas (< 300 masl) (b) Highland areas (> 300 masl)

**Figure 5-20 Two-hourly average variation for simulated air temperature difference 2 meters AGL (ºC) for: (a) Lowland areas (< 300 masl) and (b) highland areas (> 300 masl). GHG effect, land use change effect and coupled effect are represented by blue, red and black curves, respectively. Color triangles represent the Standard Error (SE) for calculated mean value.**

In highlands areas (Figure 5-20(b)) the 2 hours time interval pattern is similar to the one presented by the lowlands, with reduction in the average maximum temperatures, and increasing in the minimum temperatures. However, GW produces larger influences in the increasing temperatures, reaching a mean value of 0.65ºC, where LULC reduces by 23.8% of these mean effects. The effect of LULC is greater in the maximum temperatures, producing a reduction of ~100% in the GW; however the average minimum temperature does not appear greater affected by the LULC, producing a reduction of 6% in the effect of increasing produced by GW.

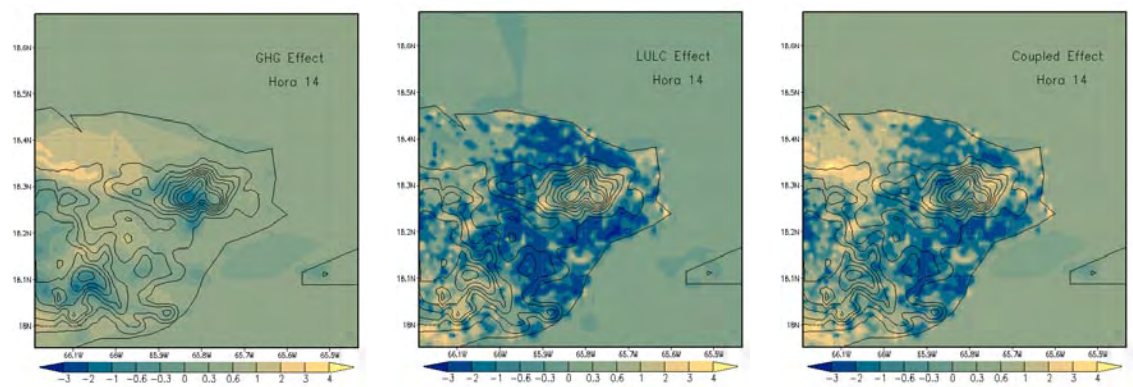


(a) GHGs effects - (ºC) (b) LULC effects - (ºC) (c) Coupled effects - (ºC)

**Figure 5-21 Average simulation maximum temperature differences at 2 meters AGL (ºC) at 14 hours.**

In Figure 5-21 it is depicted the separated effects produced in average air temperatures at 14 hours, or close to the maximum temperatures. It is visible that GW effects (Figure 5-21(a)) produce an increase in lowland air temperatures, where the most appreciable affect is in SJMA, produced by the increase scattering by water vapor content, transported by easterly trade winds; which is increased by the effect produced by LULC effect in the area (Figure

5-21(b)). This suggests that the increasing mean temperature in SJMA is a coupled LULC and GW effects. It can be noted that the net magnitude is close to 4ºC, which is consistent with reported works [47] [13].

In Figure 5-22 it is presented separated effects produced in average air temperatures at 06 hours, or close to the minimum temperatures. It can be observed that the coupled effect (Figure 5-22(c)) produces increasing average temperatures in the lowland areas; in highland areas it appear an asymmetric distribution, but the mean effect produces increasing results, as shown in Figure 5-20(b).

These results show that GW produces increasing air temperatures in lowland and highlands areas of the eastern Puerto Rico. Additionally, in lowland areas the land use change is reducing the increasing mean temperatures generated by GW; this effect is less pronounced at highland areas.

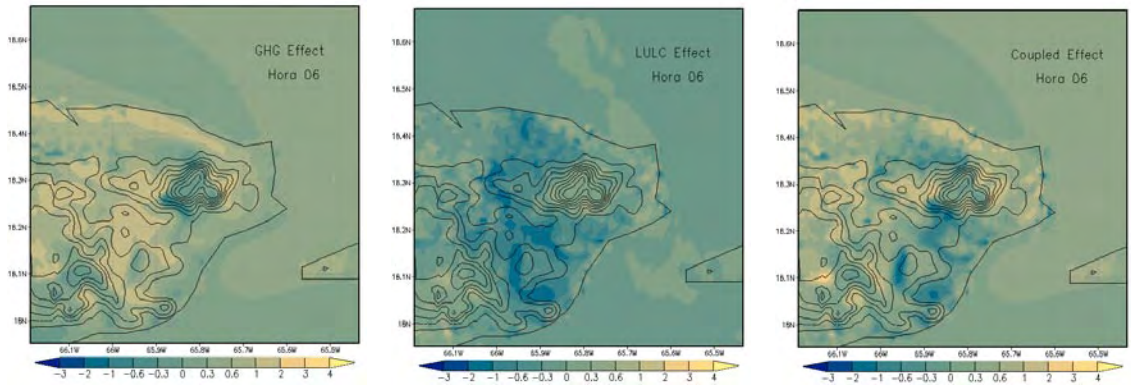


(a) GHGs effects - (ºC) (b) LULC effects - (ºC) (c) Coupled effects - (ºC)

**Figure 5-22 Average simulation minimum temperature differences 2 meters AGL (ºC).**

### *5.4.3 Average Cloud Base and Cloud Fraction*

The GW influence under mean cloud base height in eastern of Puerto Rico was calculated and it is depicted in Figure 5-23(a), showing that there is a large variation in the clouds, with cloud formation at low levels (reduction of cloud base) and increasing cloud cover at highlands (Figure 5-24(a)); the opposite effect is produced in most lowlands areas where there is a little increase in cloud base and reduction in cloud cover. Specific effects are produced in certain areas, such as the case SJMA and El Yunque, in the first case there is a reduction in cloud base, which is reflected in the small (increase) variation in cloud cover, because the cloud base is expressed in meters AGL, and around this area the cloud base is around 1000 meters AGL. In other hand, around El Yunque cloud base has lower values above the ground level (AGL), the variation in cloud base generates large variation in cloud cover resulting in an asymmetric behavior of cloud base, with an increasing cloud base in the entire area except in the eastern hills, where increased cloud base of 50 meters is reflected in a reduction in the cloud cover by about 10%. A large reduction in cloud base is produced in the north-western areas of El Yunque, around El Verde station, where there is an increase in average cloud cover, with a mean difference (reduction) in cloud base in about 200 meters. Land use change effects produce a local and reduced variation in cloud base (Figure 5-24(b)) and cloud cover (Figure 5-23(b)) around eastern Puerto Rico. The most important variation is above the SJMA with a localized increasing cloud base which generates a small variation in

the cloud cover. Another important effect is produced in El Yunque, where there is a small reduction in the cloud cover (small increase in the cloud base).

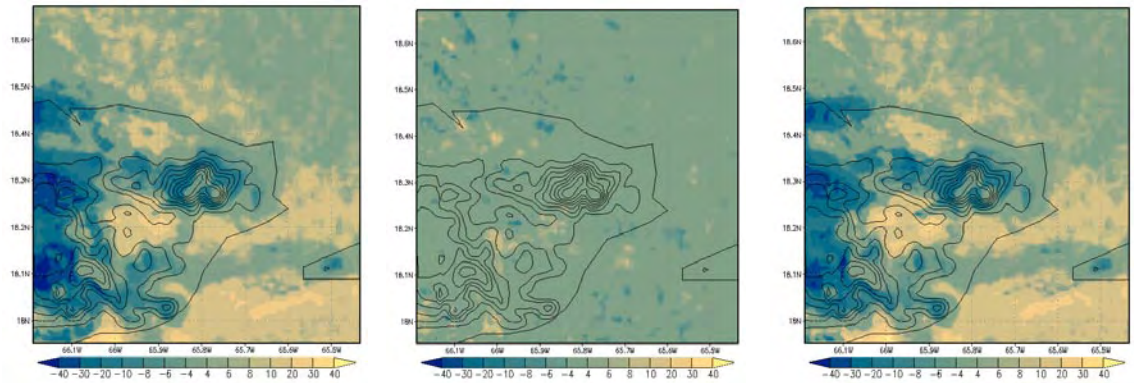


(a) GHGs effects - (x10m) (b) LULC effects - (x10m) (c) Coupled effects - (x10m)

**Figure 5-23 Average simulation Cloud Base difference (x10 m).**

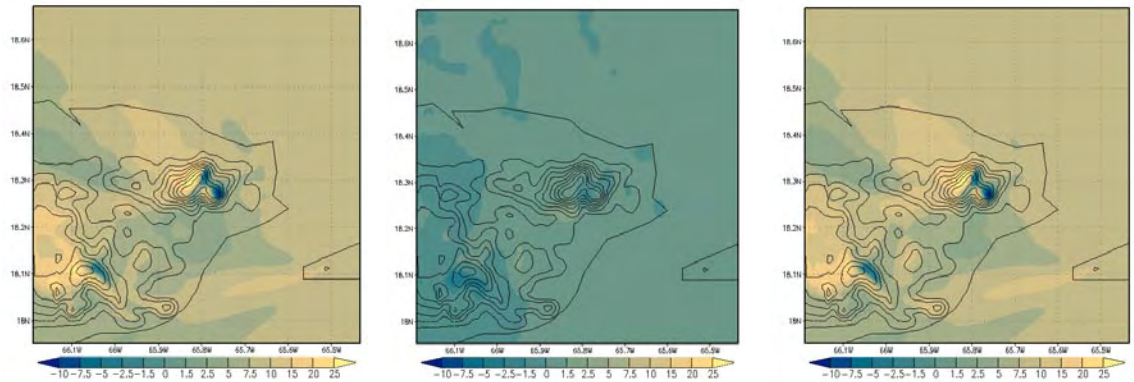


(a) GHGs effects (b) LULC effects (c) Coupled effects

**Figure 5-24 Average simulation Cloud Cover difference (%).**

Two hours mean cloud cover and cloud base profiles for the lowland areas (Figure 5-25 (a) & (c)) and highland areas (Figure 5-25 (b) & (d)), show that GW have larger effect in the cloud fraction.

In the lowland areas, during night hours (20 – 06 hr.), GW produces an increase in the mean cloud fraction by 0.085, that is associated with a reduction in cloud base by about 70 m. LULC modifies these values by less than 5% in the coupled effect, which means than the GW has the most important effect under cloud base height and cloud cover during night hours in lowland areas during the dry season. During daytime hours (08 – 18 hr.), mean values of increase cloud fraction by GW effect is 0.059, and in the coupled effect is 0.063, with the increase produced by the LULC effect in 7.8%, that is reflected in a low reduction in a cloud base, less than 50 meters (Figure 5-25(c)).

In highland areas the variations in cloud cover are greater than in lowland areas, because the low elevation at cloud is formed. In highlands there is a mean increase of 0.103 in cloud fraction, which is reduced in 6% from the individual effect that should have GW. i.e. GW produces a reduction in the average cloud base, and LULC produces increasing average cloud base in highlands (Figure 5-25(d)). However, considering that in the peaks, in both case are covered by clouds, have a null variation, but this does no imply that there is no any influence in this region, for this reason in Figure 5-26 is depicted the 2-hourly variation in cloud base in highland areas, without considering peaks of El Yunque.

In highlands areas, during the nighttime hours it is produced the major mean increase in cloud fraction, reaching a mean value of 0.123, that is affected (reduced) in 8.5% by the LULC effect (Figure 5-25(b)). Additionally, during nighttime hours GW produces a

predominant effect in the cloud base, generating a mean reduction by about 75 meters. However, during the daytime hours there is an increase in cloud fraction in 0.083, where LULC affects this increase in about 3%. In the same manner, cloud base during the early hours is more influenced by GW, generating a mean reduction in about 100 meters in highland areas (Figure 5-26). Thus cloud base is decreasing and cloud fraction is increasing in highland areas during the daytime in the dry season, with greater variations in cloud cover during nighttime hours, and greater variation in cloud base at noon hours, which suggests that the condensation level is diminished at this time.

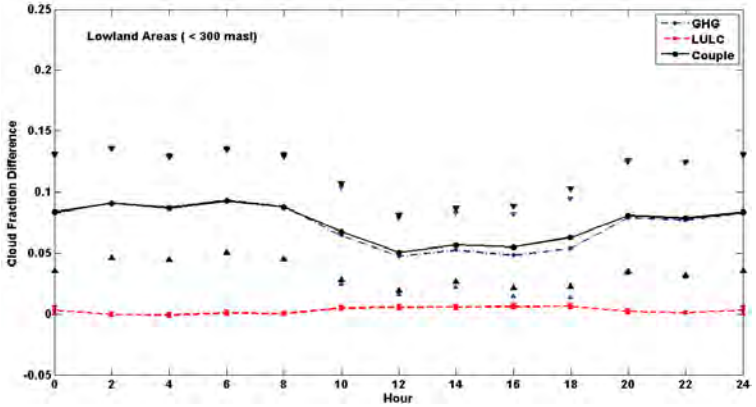


(a) Cloud fraction difference - Lowland areas (< 300 masl)

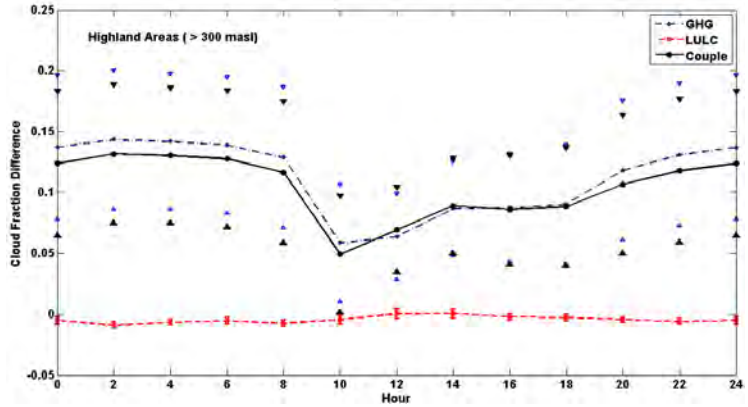


(b) Cloud fraction difference - Highland areas (> 300 masl)

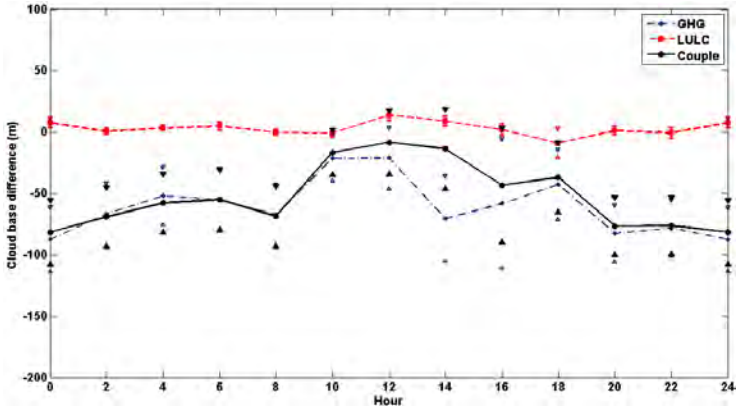


(c) Cloud base difference - Lowland areas (< 300 masl)

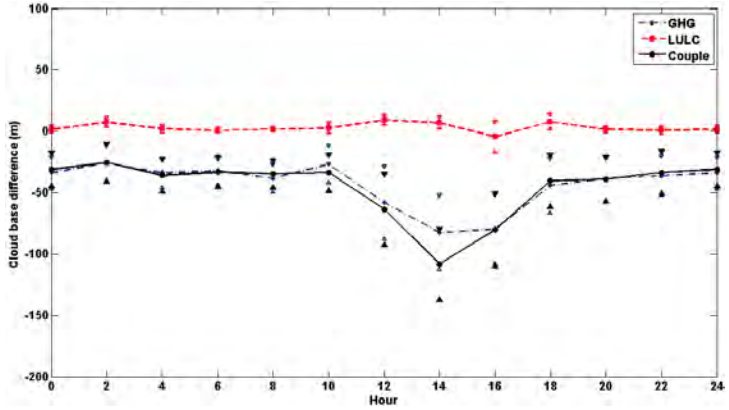


(d) Cloud base difference - Highland areas (> 300 masl)

**Figure 5-25 Two-hourly average variation for simulated cloud fraction difference for: (a) Lowland areas and (b) highland areas; and simulated cloud base variation for (c) Lowland areas and (d) highland areas. GW (or GHGs), LULC and coupled effects are depicted by blue, red and black curves, respectively. Color triangles represent the standard error (SE) for calculated mean values.**

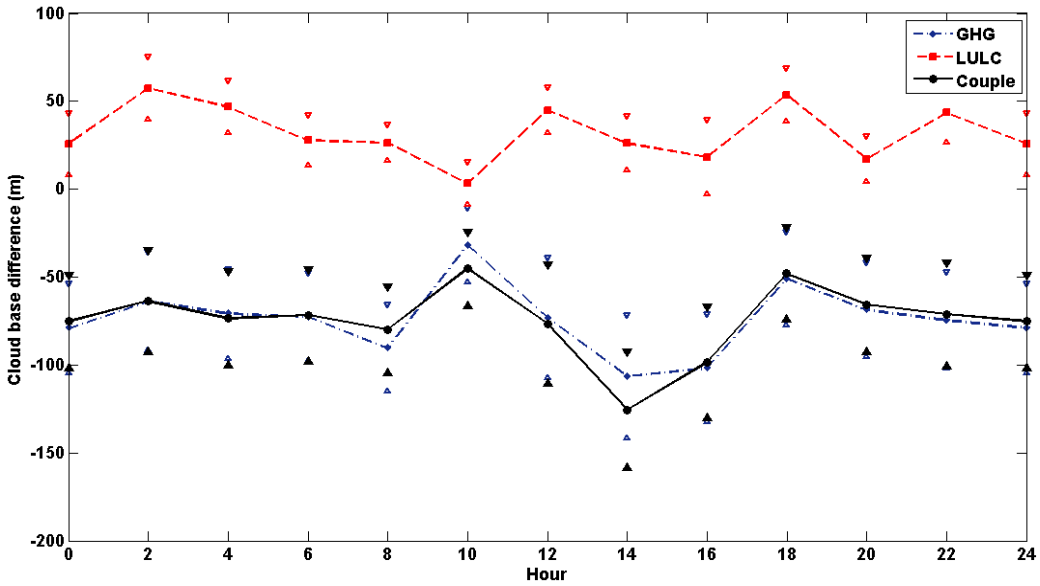


**Figure 5-26 Two-hours average variation for simulated cloud base variation for highland areas (>300m) without non variation areas at the peaks. GW (or GHGs), LULC and coupled effects are depicted by blue, red and black curves, respectively. Color triangles represent the standard error (SE) for calculated mean values.**

### *5.4.4 Sensible Heat Flux*

The spatial simulation results of the influence by GW, LULC change and coupled effects in sensible heat flux around El Yunque is presented in Figure 5-27, where GW produce a large variation around El Yunque, with increase in sensible heat fluxes in the windward areas. Similarly, land use change, (in this case) is generating increasing sensible heat fluxes in lowland areas and a reduction in highland areas; but in El Yunque an asymmetric variation results (Figure 5-27(b)); however land use produces lower effects than the GW in the area.

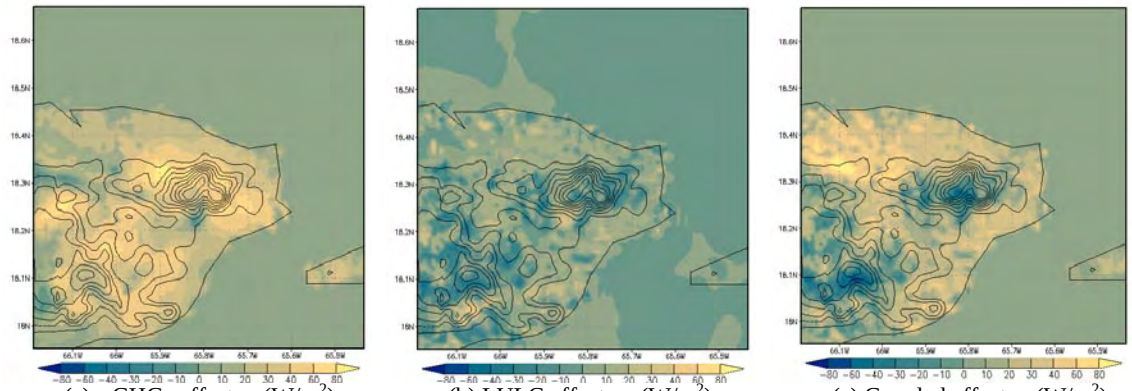

(a) GHGs effects - (W/m$^2$) (b) LULC effects - (W/m$^2$) (c) Coupled effects - (W/m$^2$)

**Figure 5-27 Average simulated sensible heat flux (W/m2).**

In Figure 5-28 it is shown the 2-hours mean variation of the GW, LULC change and coupled effects, for lowland and highland areas. As depicted, the major influence in mean sensible heat flux is produced at daytime hours (08 – 20 hr.) in eastern Puerto Rico. Then analysis of this variable will be centered in this time interval.

In lowland regions (Figure 5-28(a)), during the daytime hours there is an average sensible heat flux of 69 W/m$^2$ as a result of GW, which is reduced in 38.5% by the LULC change in the coupled effect.

In highland regions (Figure 5-28(b)), during the daytime hours there is a greater (than lowland region) mean value of sensible heat flux difference (76.7 W/m$^2$), however this larger value has a low influence in the coupled effect, where the LULC produce a dominant influence in the area, reducing the mean value of GHGs effect in 100%. As depicted (Figure 5-28(b)) land use has greater influence in highland areas in the sensible heat fluxes.

### *5.4.5 Average vector and vertical contour wind*

Individual and coupled GW and land use change effects on the average wind field in the eastern Puerto Rico is depicted in Figure 5-29, where part of the third grid is shown to depict a better representation of the difference vectors. It is noticed that GW produces important effects on the highlands and in coastal area of the Island (Figure 5-29(a)) which are in direct contact with the easterly trade winds. In these areas vector field variation in the direction of the winds that can imply that GW generates a variation in the average north easterly tradewinds (Figure 5-15). In addition, an increase in the vertical velocity at 700 meters AGL in the north coastal areas is noticed, and a reduction in the east side of El Yunque, which implies that the tradewinds coastal penetration is diminished by the GW effects.

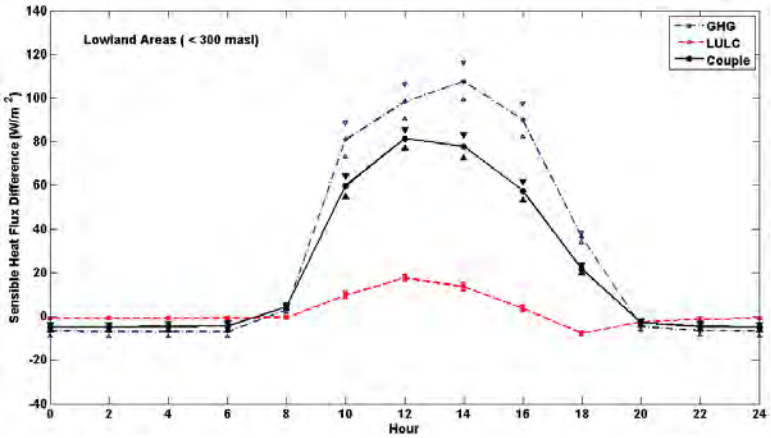


(a) Lowland areas (< 300 masl)

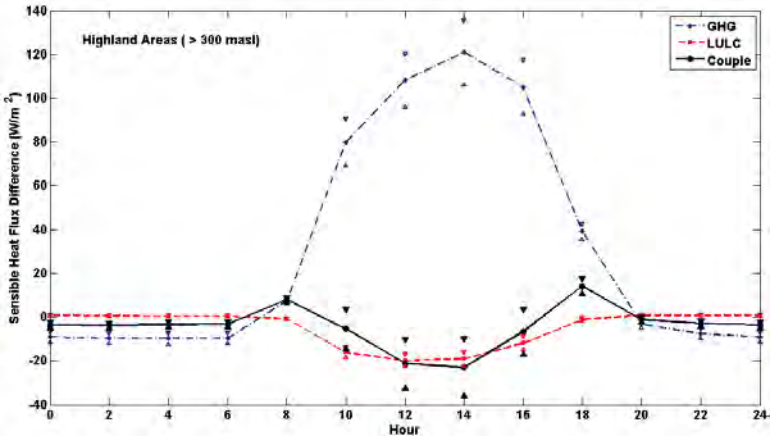


(b) Highland areas (> 300 masl)

**Figure 5-28 Two-hours average variation for simulated sensible heat flux (W/m$^2$) difference for: (a) Lowland areas (< 300 masl) and (b) highland areas (> 300 masl). GW (or GHGs) effects, land use change effects and coupled effects are represented by blue, red and black curves, respectively. Color triangles represent the standard error (SE) of mean values.**

In the other hand, the land use change effect is located inside the island (Figure 5-29(b)), but the magnitude of this field vector variation is less compared with the GW effect; the greater magnitudes are located in the areas that surround El Yunque, where the greater change in the vegetation cover is occurring. It is shown that vertical velocity contours have increasing differences in El Yunque, focused on the windward areas. The variation in wind field direction in the north eastern part of El Yunque generates diminishing vertical wind velocity on downwind areas of SJMA.

In summary, the coupled effect of GW and Land use change (Figure 5-29(c)) shows a similar trend as other variables analyzed, that the GW have a more significant influence on the total field effect. Vertical wind profile varies with increasing values in windward areas and reduced on inland lowland areas, as consequence of the influences produced by GW.

### *5.4.6 Accumulated precipitation*

Accumulated precipitation presents spatial variability (Figure 5-30(c)), with increasing tendency in highland areas and decreasing tendencies in lowland areas, where GW produces stronger effects than the LULC change, and these effects are spatially characterized and not depending only on local conditions such as Land use change.

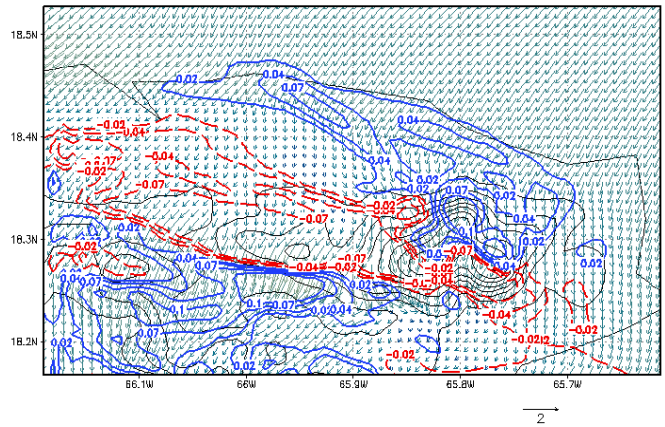


(a) GW effects - (m/s)

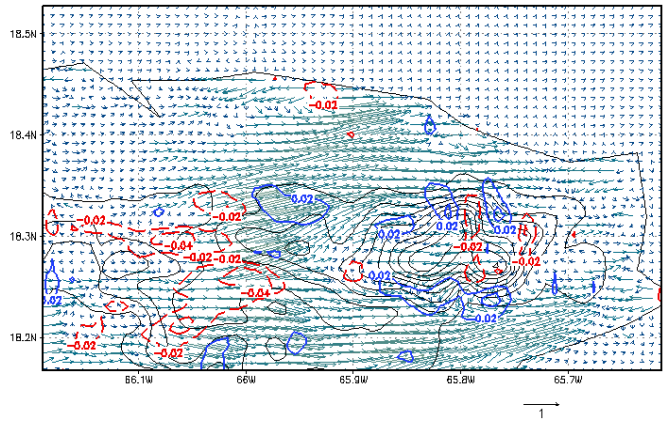


(b) LULC effects – (m/s)

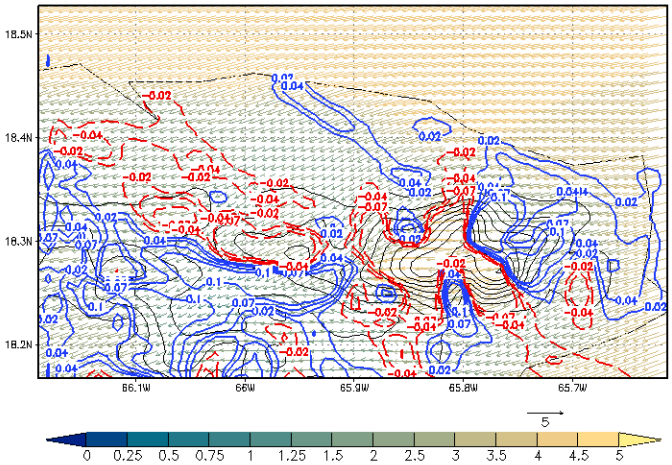


(c) Coupled effects – (m/s)

**Figure 5-29 Simulated average wind vector difference at 50 meters AGL (m/s) and average vertical wind difference contours (m/s). Blue are positive, red are negative.**

In Figure 5-30(a) it is depicted the effects of GW in accumulated precipitation during the complete simulation time frame, showing an increasing tendency in El Yunque, which corresponds to the trends of measured data presented in Figure 4-6. Land use change produces minimum effects in southern Puerto Rico. Above SJMA there is a precipitation reduction as consequence of GW but the difference in the accumulated precipitation generated by the land use change is lower in this area, because in the past LULC used (1977-1978) there is an urbanized area in SJMA (Figure 3-8), with lower extension and density than the present conditions (Figure 3-7).

In lowland areas (< 300 masl) there is a reduction in the average accumulated precipitation, 50% less than average precipitation generated by the GW in the eastern of Puerto Rico; i.e. LULC and GHG have similar effects in the lowland areas during the dry season.

Now, in highland areas (> 300 masl) there is a larger influence of GW in this region providing 97% of the total effect in the mountain regions; which means that LULC changes in the upwind lowland areas do not have significant effects in the precipitation in a TMCF.

This method to separate the effects of GHG and LULC in lowland and highland areas, quantifies the mean effects under and above the 300 masl, and does not take into account

spatial horizontal transport produced by the easterly trade winds; and then part of the increase tendency produced in highland can modify the average quantification in the lowland areas.

In summary, GW present larger influence in lowland and highland regions; but LULC generates more variation in the lowland precipitation, producing no significant effects in higher elevation, where it is dominated by the effects produced by GW, increasing the accumulated precipitation.

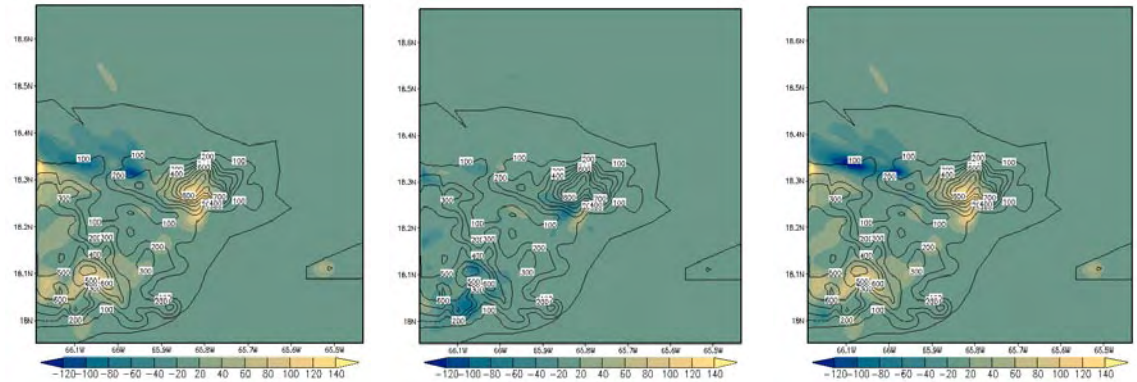


(a) GW effects - (mm) (b) LULC effects - (mm) (c) Coupled effects - (mm)

**Figure 5-30 Simulated accumulated monthly precipitation difference (mm).**

## 5.5 Summary of Results and Discussion

The results presented here represent the average conditions, or accumulated conditions in the case of precipitation, for 1 month simulation, where it is described the spatial pattern and, where it was needed, mean daily profiles to obtain the average maximum and minimum influences, and percentage of influence of the mean individual effects in the mean couple

results. The description of the separated effects of GW and LULC change in TMCFs, represented by El Yunque is one of the main objectives of this research, thus the analysis of the results will be focused in highlands, i.e. zones with elevations greater than 300 masl.

Based on the synoptic analysis (Figure 5-16 and Figure **5-17**) it is shown that there is an increasing vapor content in the low atmosphere, under 700 mbar, as consequence of the increase in SSTs, which generates larger evaporation and then increasing air temperatures in the low atmosphere, produced by greater scattering generated by the elevated GHGs. The larger increase in sea surface temperature occurs in the Atlantic Ocean as consequence of GHE (Figure 5-18), the vapor content generated in this areas, added to warm air is transported by the northeasterly trade winds, generating increasing air temperatures near the ground surface in the north eastern areas of El Yunque (Figure 5-19). In these areas of El Yunque, LULC change has greater effect in the maximum temperatures, as consequence of the reduction in the sensible heat fluxes produced at this time. However, increase in the maximum temperatures produced by the GW effect in a TMCF is lower than the one produced in the lowlands. Additionally, it appears that the maximum increase in air temperatures is produced in the first hours of the morning, which represents the minimum temperatures. During the nighttime hours (20 – 06 am) it is reflected a mean increase 0.6ºC in air temperature, and greater increase (0.87ºC) in the minimum temperatures. Thus, mean effects show a reduction in the maximum temperatures in a TMCF based of GW influences,

but in El Yunque it is shown an asymmetric behavior produced by the heat transported by the trade winds in the northeastern areas.

Clouds base and fraction are influenced with more complexity in the highlands by the GW, where the maximum mean influence produced by LULC change in the couple effect reaches 8.5% during the nighttime hours (20 – 06 hr.) in cloud fraction. Then, GW produces a mean increase in the cloud fraction by about 10% (Figure 5-25), and a reduction in the cloud base height.

From the description of the spatial mean patterns of variables in eastern Puerto Rico, it can be conclude that reduction in cloud base height is consequence of most vapor content in the atmosphere transported by easterly trade winds, and upwind elevated with highest vertical velocities (Figure 5-29) in the north-eastern areas of El Yunque, generating lower cloud formation in the area. In leeward areas of El Yunque there is a reduction in the mean vertical velocities, which generates lower increase of warmer and humid air masses that producing lower cloud base height in these areas, which is reflected in a lower cloud fraction increase (Figure 5-24). This suggests a possible explanation for the reduction in the accumulated precipitation, because the cloud probably is not reaching the condensation level at this pressure level.

Previous studies in the area of Puerto Rico [2] [3] present that the cloud base is reduced in the areas around El Yunque under a lowland forest replaced by pastures, where the average reduction reached about 200 meters. This past simulations replaced totally the lowland forest areas by grass land, but did not quantify the realistic processes of the historical land use changes in the area. In the past land use, during 1977-1978 [44] [45], there is presence of deforested lowland zones, by agriculture and grassland areas, and at the present there is recovery forest in the lowland [34], which implies that the land use is generating an increase in cloud base, in this extreme change, by about 200m in eastern Puerto Rico. This tendency of reduction in the cloud base and increase in cloud fraction (Figure 5-25) is presented as a result of changes in the lowland areas, however the magnitude of the impact is relatively low when compared with GW. The variation in differences presented in [3] [2], was in the same magnitude as the reported in [5] in the cloud base increase as consequence of the increasing $CO_2$ in the atmosphere, but in the opposite directions. The case presented in this work provides similar magnitudes and directions as in [5].

In the studies of Costa Rica, the land use change appears as a variable with significant influence in the cloud base in a TMCF [15] [16] [14] [17] [49], but there the magnitude of land use change is in upwind areas that have greater dimensional scales than the similar areas of El Yunque, which is located very close to the coastal areas. This suggests that the magnitude of land use change in the upwind areas affect strongly the analysis of the TMCF.

# 6 CONCLUSIONS AND RECOMENDATIONS

## 6.1 CONCLUSIONS

The main objective of this research project was to determine and quantify the mean impacts of the individual effects of land use changes and global warming on the coastal tropical mountain cloud forest (TMCF), through the formulation of a methodology based on the analysis of three relevant variables namely surface temperature, precipitation, and cloud cover and base. These variables were investigated for the dry season in the Caribbean region and for the specific case of El Yunque, a TMCF located in the eastern side of the Island of Puerto Rico.

The following general statements can be concluded from this research:

1. A TMCF is very sensitive to increases of sea surface temperatures caused may be by increases in green house gases in the atmosphere. This global warming reflected in increases in sea surface temperatures produces the most significant changes in the upper air variables within a TMCF. The sensitivity of the TMCF is associated to the orographic cloud formation and air temperatures. This study estimated increases in minimum surface temperatures by about 1ºC, linked directly to global warming.
2. The increase in the air temperature near the surface as consequence of the UHI is augmented by the global warming effects, producing a warmer air in the area a

possible consequence of the combination of sensible heat flux due to the land use modification, and warmer air masses advected from the adjacent warmer ocean. For the case investigated here, the UHI was estimated in 2ºC while the total effects in 4ºC.

3. The analysis presented in this thesis supports the argument that global warming generate a reduction in the cloud base in about 100 meters due mostly to additional moisture in the lower atmosphere.
4. The extension of the land use changes in the upwind areas affect a TMCF, since the variation in the sensible and latent heat fluxes, consequence of deforestation, or forest recovery, or urbanization, are transported to the highland areas by the easterly winds, varying the cloud base height, and consequently the TMCF productivity reflected in fresh water production. This study found 32% increase precipitation in the highlands, which is attributed to the influences of GHGs.

Focused on the specific case of El Yunque, a TMCF in eastern Puerto Rico, the following statements can be concluded:

1. During the Caribbean dry season there are increasing air temperatures and increasing SSTs generating more humid content in the lower atmosphere. Sea surface temperatures were found to have increased by 1ºC between 1976 and 2004.

2. The past average conditions during the Caribbean dry season are determined only by the ENSO index 3, because the SSTs and GHGs are currently monotonically increasing functions.
3. The increasing precipitation in El Yunque and other highlands (TMCF), in Puerto Rico is an effect mostly of global warming, as consequence of more vapor content and warmer air in the atmosphere transported through the northeasterly trade winds to the windward areas of El Yunque, producing a low cloud base (high cloud cover and warmer areas).
4. The land use changes effect generate influences in the air variables near the surface, and can produce important effects in a TMCF when the change is produced on it or in windward areas. It was found that LCLU can contribute in a reduction of 0.11ºC at the top of the mountain, may rise the cloud base by 100 meters, and may induced additional 30% precipitation.
5. The methodology proposed to separate the effects of global warming (as reflect in sea surface temperatures and a warmer atmosphere) and land use changes is unique and reflects very good results during dry season in the Caribbean region, which can help to understand the individual influences of these variables on a TMCF, a sensitive bio-system of many different species.

## 6.2 RECOMENDATIONS

To continue further research in the way presented here, it is recommended to take into account the following suggestions:

1. The methodology of separating the individual effects of global warming and local land use should be followed and further expanded to a complete dry season time, to obtain the extremes (maximum and minimum) variations at this time.
2. The methodology of separating the effects global warming and local land use changes should be expanded for futures scenarios, including an increase of the urban development around El Yunque. This may require the use of global circulation models.
3. The methodology should be expanded to the rainy season in the Caribbean, adding the influencing global and local variables for this time.
4. Separate and quantify the effects of the global warming and land use change, growth urban areas, for the analysis of the UHI effects for cities across the Caribbean.

# REFERENCES


[1] IPCC. *Climate Change - Fourth Assessment.* Intergovernmental Panel of Climate Change, 2007.

[2] Van der Molen M.K., Dolman A.J., Waterloo M.J., and Bruijinzeel L.A. "Climate is affected more by Maritime than by Continental Land Use Change: A multiple scale analysis." *Global and Planetary Change.* 16 (2006): 128-149.

[3] Van der Molen, M.K. *Meteorological Impacts of Land Use Change in the Maritime Tropics.* PhD thesis, Amsterdam, Netherlands: Vrije Universiteit, 2002, 262.

[4] Melendez-Colom, E.C. "Regression Relationships of Air Temperature and Elevation along an Elevation Gradient in the Luquillo Experimental Forest (LEF), Puerto Rico." LTERNET. 2004. http://luq.lternet.edu/data/temp/bistempdata/Bistemp.htm.

[5] Still C.J., Foster P.N., Schneider S.H. "Simulating the effects of Climate Change on Tropical Montane Cloud Forest." *Nature.* 398 (April 1999): 608-610.

[6] Aldrich Mark, Bubb Philip, Hostettler Silvia, and Van de Wiel Han. "Tropical montane Cloud Forests." WWF International / IUCN, 2000.

[7] IPCC. *Land Use, Land-Use Chane, and Forestry.* Summary fro Polyicymakers., IPCC, 2000.

[8] Polcher J. and Laval K. "The impact of African and Amazonian deforestation on Tropical Climate." *Journal of Hydrology.* 155 (1994): 389-405.

[9] Karl Thomas R. and Jones Philip D. "Urban Bias in Area-Average Surface Air Temperature Trends." *Bulletin American Meteorological Society.* 70(3) (March. 1989): 265-270.

[10] Shepherd J. Marshall and Burian Steven J. "Detection of Urban-Induced Rainfall Anomalies in a Major Coastal City." *Earth Interactions.* 7 (2003): 1-17.

[11] Grabowski, Wojciech W. "Cloud Microphysics and the Tropical Climate: Cloud-Resolving Model Perspective." *Journal of Climate.* 13 (July. 2000): 2306-2322.

[12] FAO. *Global Forest Resources Assessment 2005.* Forestry Paper 147., Rome: Food and Agricultural Organization of the United Nations., 2005.

[13] Velazquez-Lozada Alexander, Gonzalez Jorge E., and Winter Amos. "Urban Heat Island effect analysis for San Juan, Puerto Rico." *Atmospheric Environment.* 40 (2006): 1731-1741.

[14] Oke T.R., Spronken Smith R.A., Jauregui E., and Grimmond C.S.B. "The Energy Balance of central Mexico City during the Dry Season." *Atmospheric Environment.* 33 (1999): 3919-3930.

[15] Lawton R.O., Nair U.S., Pielke R.A., and Welch R.M. "Climatic Impact of Tropical Lowland Deforestation on Nearby Montane Cloud Forest." *Science.* 294 (October, 2001): 584-597.

[16] Nair U.S., Lawton R.O., Welch R.M., and Pielke R.A. "Impact of Land Use on Costa Rican Tropical Montane Cloud Forests: Sensitivity of Cumulus Cloud field characteristics to Lowland Deforestation." *Journal of Geophysical Research.* 108(D74206) (2003): 1-13.

[17] Ray Deepak K., Nair Udaysankar S., Lawton Robert O., Welch Ronald M., and Pielke Roger A. "Impact of Land Use on Costa Rican Tropical Montane Cloud Forests: Sensitivity of Orographic Cloud Formation to Deforestation in the Plains." *Journal of Geophysical Research* 111(D02108) (2006): 1-16.

[18] Folkins Ian and Brown Christopher. "Tropical Rainfall and Boundary Layer Moist Entropy." *Journal of Climate.* 16 (June. 2003): 1807-1819.

[19] Lanzante, Jhon R. "Lag Relationships Involving Tropical Sea Surface Temperatures." *Journal of Climate.* 9 (October 1996): 2568-2578.

[20] Goldenberg Stanley B., Landsea Christopher W., Mestas-Nuñez Alberto M., and Cray William M. "The Recent Increase in Atlantic Hurricane Activity: Causes and Implications." *Science* (ProQuest Biology Journals) 293 (July 2001): 5529.

[21] Chikamoto Yoshimitsu and Tanimoto Youichi. "Role of Specific Humidity Anomalies in the Caribbean SST Response to ENSO." *Journal of the Meteorological Society of Japan.* 83(6) (2005): 959-975.

[22] Pielke R.A., Cotton W.R., Walko R.L., Tremback C.J., Lyons W.A., Grasso L.D., Nicholls M.E., Moran M.D., Wesley D.A., Lee T.J., and Copeland J.H. "A Comprehensive Meteorological Modeling System - RAMS." *Meteorology and Atmospheric Physics.* 49 (1992): 69-91.

[23] Tremback Craig J., Walko Robert L. "The Regional Atmospheric Modeling System (RAMS): Development for Parallel Processing Computer Architectures." http://65.57.243.56/docs/parallel.pdf.

[24] Wu Wei, Hall C.A., Scatena F.N., and Quackenbush L.J. "Spatial Modeling of Evapotranspiration in the Luquillo Experimental Forest of Puerto Rico using remotely-sensed data." *Journal of Hydrology.* 328 (2006): 733-752.

[25] Kottek M., Grieser J., Beck C., Rudolf B., Rubel F. "World Map of the Kvppen-Geiger Climate Classification Updated." *Meteorol. Z.* 15 (2006): 259-163.

[26] Peel M.C., Finlayson B.L., McMahon T.A. "Updated World map of the Koppen-Geiger Climate Classification." *Hydrol. Earth Syst. Sci. Discuss.* 4 (2007): 429-473.

[27] Scatena, F.N. "Climate and hydrology." *LTERNET.* 2006. http://luq.lternet.edu/research/projects/climate_hydrology_description.html.

[28] Daly Christopher, Helmer E.H., and Quiñones Maya. "Mapping the Climate of Puerto Rico, Vieques and Culebra." *International Journal of Climatology.* 23 (May. 2003): 1359-1381.

[29] Malmgren Bjorn A. and Winter Amos. "Climate Zonation in Puerto Rico Based on Principal Components Analysis and an Artificial Neural network." *Journal of Climate.* 12 (April. 1999): 977-985.

[30] Waide Robert C., Angeles Moises, Gonzalez Jorge E., Hall Charles A., Lugo Ariel, Murphy David J., Ortiz-Zayas Jorge R., Ramirez Nazario D. "Factors influencing the Changing Climate of the Luquillo Mountains, Puerto Rico." *Caribbean Climate Symposium.* University of Puerto Rico at Mayaguez, 2006.

[31] Wu Wei, Hall Charles, and Zhang Lianjun. "Predicting the Temporal and Spatial Probability of Orographic Cloud Cover in the Luquillo Experimental Forest in Puerto Rico using Generalized Linear (Mixed) Models." *Ecological Modelling.* 192 (2006): 473-498.

[32] Thomlinson John R. and Rivera Lyaned Y. "Suburban Growth in Luquillo, Puerto Rico: Some Consequences of Development on Natural and Semi-Natural Systems." *Landscape and Urban Planning.* 49 (2000): 15-23.

[33] Martinuzzi Sebastián, Gould William, Ramos Gonález Olga. "Land Development, Land Use, and Urban Sprawl in Puerto Rico integrating Remote Sensing and Population Census data." *Landscape and urban planning.* 79 (2007): 288-297.

[34] Lugo Ariel E. and Helmer Eileen. "Emerging Forest on Abandoned Land: Puerto Rico's New Forests." *Forest Ecology and Management.* 190 (2004): 145-161.

[35] Birdsey Richard A. and Weaver Peter L. *Forest Area Trends in Puerto Rico.* Research Note, SO-331, USDA, Forest Service, 1987.

[36] Del Mar Lopez Tania, Aide T. Mitchell, and Thomlinson John R. "Urban Expansion and the Loss of Prime Agricultural Lands in Puerto Rico." *Ambio.* 30 No.1 (2001).

[37] ATMET. "Regional atmospheric modeling system - technical description." 2003. www.atmet.com/html/docs/rams/rams_techman.pdf.

[38] Walko Robert L., Tremback Craig J. "Regional Atmospheric Modeling System - introduction to RAMS 4.3/4.4." 2003. www.atmet.com/html/docs/rams/ug44-rams-intro.pdf.

[39] Angeles Malaspina, Moises. *An Assessment of Future Caribbean Climate Change using Business and Usual Scenario by Coupling GCM data and RAMS.* Master's thesis, Department of Mechanical Engineering, Mayaguez: University of Puerto Rico, Mayaguez Campus, 2005.

[40] Smith Thomas, Reynolds Richard. "Extended Reconstructed of Global Sea Surface Temperatures based on COADS data (1854 - 1997)." *Journal of Climate.* 16 (2003): 1495-1510.

[41] Smith Thomas, Reynolds Richard. "Improved Extended Reconstruction of SST (1854 - 1997)." *Journal of Climate.* 17 (2004): 2466-2477.

[42] Briscoe, C.B. *Weather in the Luquillo Mountains of Puerto Rico.* Technical Report 3, Intitute of Tropical Forestry, Forest Service - U.S. Department of Agriculture, 1966.

[43] Kanamitsu M., Ebisuzaki W., Woollen J., Yang S-K, Hnilo J.J., Fiorino M., and Potter G.L. "NCEP-SEO AMIP-II Reanalysis (R-2)." *Bul. Of the Atmos. Met. Soc.*, Nov. 2002: 1631-1643.

[44] Helmer, Eileen. "Forest Conservation and Land Development in Puerto Rico." *Landscape Ecology.* 19 (2004): 29-40.

[45] Kennaway T. and Helmer Eileen. "The Forest Types and Ages Cleared for Land Development in Puerto Rico." *GIScience & Remote Sensing.* 44(4) (2007).

[46] Giannini Alessandra, Chang John C., Cane Mark A., Kushnir Yochanan, and Seager Richard. "The ENSO Teleconection to the Tropical Ocean: Contributions the remote and local SSTs to rainfall variability in the Tropical Americas." *Journal of Climate* 14 (2001): 4530-4544.

[47] Edwards A.L. (1967) Statistical Analysis. (Second ed.). New York, United States. Hold, Rinehart and Winston, INC. (252-253).

[48] González Jorge E., Luvall Jeffrey, Rickman Douglas, Comarazamy Daniel, Picón Ana, Harmsen Erick, Parsiani Hamed, Ramírez Nazario, Vásquez Ramón, Williams Robin, Waide Robert, and Tepley Craig. "Urban Heat Island developing in Coastal Tropical Cities." *EOS* 86(42) (2005): 397-412.

[49] Ray Deepak K., Welch Ronald M., Lawton Robert O., and Nair Udaysankar S. "Dry Season Clouds and Rainfall in Northern Central America: Implications for the Mesoamerican Biological Corridor." *Global and Planetary Change.* 54 (2006): 150-162.

[50] Pielke, R.A. *Mesoscale Meteorological Modeling.* Orlando, Florida: ACADEMIC PRESS INC, 1984.

# APPENDIX A
# RAMS – SOLVED EQUATIONS

Equations of motion

$$\frac{\partial u}{\partial t} = -u\frac{\partial u}{\partial x} - v\frac{\partial u}{\partial y} - w\frac{\partial u}{\partial z} - \theta\frac{\partial \pi'}{\partial x} + fv + \frac{\partial}{\partial x}\left(K_m\frac{\partial u}{\partial x}\right) + \frac{\partial}{\partial y}\left(K_m\frac{\partial u}{\partial y}\right) + \frac{\partial}{\partial z}\left(K_m\frac{\partial u}{\partial z}\right) \quad \textbf{A-1}$$

$$\frac{\partial v}{\partial t} = -u\frac{\partial v}{\partial x} - v\frac{\partial v}{\partial y} - w\frac{\partial v}{\partial z} - \theta\frac{\partial \pi'}{\partial y} - fu + \frac{\partial}{\partial x}\left(K_m\frac{\partial v}{\partial x}\right) + \frac{\partial}{\partial y}\left(K_m\frac{\partial v}{\partial y}\right) + \frac{\partial}{\partial z}\left(K_m\frac{\partial v}{\partial z}\right) \quad \textbf{A-2}$$

$$\frac{\partial w}{\partial t} = -u\frac{\partial w}{\partial x} - v\frac{\partial w}{\partial y} - w\frac{\partial w}{\partial z} - \theta\frac{\partial \pi'}{\partial z} - \frac{g\theta_v}{\theta_0} + \frac{\partial}{\partial x}\left(K_m\frac{\partial w}{\partial x}\right) + \frac{\partial}{\partial y}\left(K_m\frac{\partial w}{\partial y}\right) + \frac{\partial}{\partial z}\left(K_m\frac{\partial w}{\partial z}\right) \quad \textbf{A-3}$$

Thermodynamic equation

$$\frac{\partial \theta_{il}}{\partial t} = -u\frac{\partial \theta_{il}}{\partial x} - v\frac{\partial \theta_{il}}{\partial y} - w\frac{\partial \theta_{il}}{\partial z} + \frac{\partial}{\partial x}\left(K_h\frac{\partial \theta_{il}}{\partial x}\right) + \frac{\partial}{\partial y}\left(K_h\frac{\partial \theta_{il}}{\partial y}\right) + \frac{\partial}{\partial z}\left(K_h\frac{\partial \theta_{il}}{\partial z}\right) + \left(\frac{\partial \theta_{il}}{\partial z}\right)_{rad} \quad \textbf{A-4}$$

Water species mixing ratio continuity equation

$$\frac{\partial r_n}{\partial t} = -u\frac{\partial r_n}{\partial x} - v\frac{\partial r_n}{\partial y} - w\frac{\partial r_n}{\partial z} + \frac{\partial}{\partial x}\left(K_h\frac{\partial r_n}{\partial x}\right) + \frac{\partial}{\partial y}\left(K_h\frac{\partial r_n}{\partial y}\right) + \frac{\partial}{\partial z}\left(K_h\frac{\partial r_n}{\partial z}\right) \quad \textbf{A-5}$$

Mass continuity equation

$$\frac{\partial \pi'}{\partial t} = -\frac{R\pi_0}{c_v\rho_0\theta_0}\left(\frac{\partial \rho_0\theta_0 u}{\partial x} + \frac{\partial \rho_0\theta_0 v}{\partial y} + \frac{\partial \rho_0\theta_0 w}{\partial z}\right) \quad \textbf{A-6}$$

Hydrostatic option in RAMS replaces the vertical equation and mass continuity equation with:

Hidrostatic equation

$$\frac{\partial \pi}{\partial z} = -\frac{g}{\theta_v} + g\left(r_T - r_v\right) \quad \textbf{A-7}$$

$$\frac{\partial \rho u}{\partial x} + \frac{\partial \rho v}{\partial y} + \frac{\partial \rho w}{\partial z} = 0 \quad \textbf{A-8}$$

**TABLE A-1 Description of the symbols used in the conservation equations resolved by RAMS.**

| Symbol | Description |
|---|---|
| u | east-west wind component. |
| v | north-south wind component. |
| w | vertical wind component. |
| f | Coriolis parameter. |
| $K_m$ | eddy viscosity coefficient for momentum. |
| $K_h$ | eddy viscosity coefficient for heat and moisture. |
| $\theta$ | ice-liquid water potential temperature. |
| r | water mixing ratio species of total water, rain, pristine, crystal, aggregates, and snow. |
| $\rho$ | density |
| con | subscript denoting tendency from convective parameterization. |
| rad | subscript denoting tendency from radiation parameterization. |
| res | subscript denoting tendency from resolvable scale microphysical parameterization. |
| g | gravity. |
| $r_t$ | total water mixing ratio. |
| $r_v$ | water vapor mixing ratio. |
| $\pi$ | total Exner function. |
| $\pi'$ | perturbation Exner function. |
| $\theta_v$ | virtual potential temperature. |
| p | pressure. |
| $z_g$ | Topography height |
| H | Height of the top of the grid |

Terrain following $\sigma_z(x^*,y^*,z^*)$ coordinate modifies the vertical structure of the grid, generating a top of the domain is flat and the bottom follows the terrain, under the next coordinate transformation:

$$x^* = x \qquad \textbf{A-9}$$

$$y^* = y \qquad \textbf{A-10}$$

$$z^* = H\left(\frac{z - z_g}{H - z_g}\right) \qquad \textbf{A-11}$$

**TABLE A-2 Options in RAMS configurations [22].**

| Configuration | Option |
|---|---|
| Basic Equations | Hydrostatic or Incompressible. |
| | Nonhydrostatic; compressible |
| Dimensionality | 2-Dimensional |
| | 3-Dimensional |
| Vertical Coordinates | Cartesian Coordinates |
| | Terrain-following $\sigma_z$ |
| Horizontal Coordinates | Cartesian Coordinates. |
| | Stereographic tangent plane. |
| Grid Structure | Arakawa C grid, single grid. |
| | Arakawa C grid, multiple nested grid. |
| Time Differencing | Leapfrog. |
| | Forward. |
| | Hybrid Scheme. |
| Turbulent Closure | Smagorinsky deformation K. |
| | Mellor – Yamada. |
| | Deardorff. |
| Cloud Microphysics | Warm microphysics. |
| | Ice microphysics, specified nucleation. |
| | Ice microphysics, predicted nucleation. |
| Radiation | Chen and Cotton. |
| | Mahrer and Pielke. |
| Lower Boundary | Specified air-surface temperature and moisture difference. |
| | Diagnosed surface temperature and moisture fluxes based on a prognostic soil model. |
| Upper Boundary | Rigid lid. |
| | Gravity wave radiation condition. |
| Lateral Boundary | Radiative boundary Condition I, Orlansky |
| | Radiative boundary Condition II, Klemp and Wilhelmson |
| | Radiative boundary Condition II, Klemp and Lilly |
| | Large scale boundary forcing conditions |
| | Large scale nudging boundary conditions |

# APPENDIX B.
# MAIN FLAGS OPTIONS CONFIGURED IN RAMSIN

| | | |
|---|---|---|
| TIMMAX | 694 (hr) | Time of simulation |
| NGRIDS | 3 | Number of grids to run. |
| NNXP | 100,62,82, | Number of x gridpoints. |
| NNYP | 100,62,82, | Number of y gridpoints. |
| NNZP | 40,40,40, | Number of z gridpoints. |
| NZG | 10,10,10, | Number of soil layers. |
| | | |
| NSTRATX | 1,4,5, | x-direction |
| NSTRATY | 1,4,5, | y-direction |
| NNDTRAT | 1,4,5, | time |
| | | |
| CENTLAT | 18.45,18.23,18.32, | Center latitude and longitude of grids, |
| CENTLON | -66.66,-66.30,-65.80, | may or may not be same as pole point. |
| | | |
| NUDLAT | 5, | Number of points in lateral boundary region. |
| TNUDLAT | 3600., | Nudging time scale(s) at lateral boundary. |
| TNUDCENT | 21600., | Nudging time scale(s) in center of domain. |
| TNUDTOP | 0., | Nudging time scale(s) at top of domain. |
| | | |
| FRQHIS | 3600., | History file frequency (seconds) |
| FRQANL | 7200., | Analysis file frequency (seconds). |
| | | |
| ITOPTFLG | 1,1,1, | 2 - Fill data in "rsurf" |
| ISSTFLG | 1,1,1, | 0 - Interpolate from coarser grid |
| IVEGTFLG | 1,1,1, | 1 - Read from standard Lat/Lon data file |
| ISOILFLG | 2,2,2, | Soil files not yet available: avoid |
| | | |
| Isoilflg = | 1 | |
| | | |
| IUPDSST | 0, | 0 - No update of SST values during run |
| | | 1 - Update SST values during run |
| IZ0FLG | 0,0,0, | 0 = Based of vege, bare soil and water surface |
| | | 1 = Subgrid scale orograhic roughness |
| MKCOLTAB | 1, | Make table: 0 = no, 1 = yes |
| COLTABFN | './ct2.0', | Filename to read or write |
| | | |
| ICORFLG | 1, | Coriolis flag/2D v-component |
| | | 0 = off, 1 = on |
| IBND | 2, | Lateral boundary condition flags |
| JBND | 2, | 1-Klemp/Wilhelmson, 2-Klemp/Lilly, 3-Orlanski, 4-cyclic |
| ISWRTYP | 2, | Shortwave and Longwave radiation type |
| ILWRTYP | 2, | 0-none, 2-Mahrer/Pielke, 1-Chen |
| | | |
| NPATCH | 4 | Number of patches per grid cell (min=2) |

| | | |
|---|---|---|
| SLZ | -.50,-.40,-.30,-.25,-.20,-.16,-.12,-.09,-.06,-.03,-.01, | |
| | Soil grid levels | |
| SLMSTR | 0.45,0.45,0.45,0.45,0.45,0.45,0.45,0.45,0.45,0.45,0.45, | |
| | Initial soil moisture | |
| STGOFF | 5.,4.9,4.8,4.7,4.6,4.5,4.4,4.2,4.0,3.5,3.1, | |
| | Initial soil temperature offset from lowest atmospheric level | |
| IDIFFK | 1,1,1, | K flag: |
| | | 1 - Horiz deform/Vert Mellor-Yamada |
| | | 2 - Anisotropic deformormation (horiz & vert differ) |
| | | 3 - Isotropic deformation (horiz and vert same) |
| | | 4 - Deardorff TKE (horiz and vert same) |